8-2009

Seismic Evaluation Of Clark County Critical Bridges Using Nonlinear Static Procedures

Ahmad Said Saad
University of Nevada, Las Vegas

SEISMIC EVALUATION OF CLARK COUNTY CRITICAL BRIDGES USING NONLINEAR STATIC PROCEDURES

by

Ahmad Said Saad

Bachelor of Engineering
Ain Shams University, Cairo, Egypt
2004

A thesis submitted in partial fulfillment
of the requirements for the

Master of Science in Engineering
Department of Civil and Environmental Engineering
Howard R. Hughes College of Engineering

Graduate College
University of Nevada, Las Vegas
August 2009

UNLV
UNIVERSITY OF NEVADA LAS VEGAS

THE GRADUATE COLLEGE

We recommend that the thesis prepared under our supervision by

Ahmad Said Saad

entitled

Seismic Evaluation of Clark County Critical Bridges Using Nonlinear Static Procedures

be accepted in partial fulfillment of the requirements for the degree of

Master of Science
Civil and Environmental Engineering

ALY M. SAID, Committee Chair

BARBARA LUKE, Committee Member

SAMAAN LADKANY, Committee Member

WANDA TAYLOR, Graduate Faculty Representative

Ronald Smith, Ph. D., Vice President for Research and Graduate Studies
and Dean of the Graduate College

August 2009

ABSTRACT

Seismic Evaluation of Clark County Critical Bridges Using Nonlinear Static Procedures

by

Ahmad Said Saad

Dr. Aly M. Said, Examination Committee Chair
Assistant Professor of Civil Engineering
University of Nevada, Las Vegas

Bridges are vital connective elements in community transportation systems. In the past, bridges have been severely damaged by earthquakes. However, with proper mitigation techniques, such as bridge retrofit, severe earthquake damage to bridges can be avoided. Since the 1970's, design codes underwent major changes with regard to seismic analysis and design provisions of structures and bridges. Meanwhile, one third of the nation's 600,000 inventoried highway bridges are considered as either structurally deficient or functionally obsolete.

This study is a part of the "Earthquakes in Southern Nevada" project. Earlier in this project, buildings and bridges in southern Nevada were studied in order to prioritize their need for rehabilitation. This prioritization was based on a risk assessment that combines both vulnerability and importance. In this study, bridges with the highest risk scores were structurally evaluated against earthquake loads using performance-based approach. Performance-based approach was chosen for the evaluation process of the bridges as it

had been recognized as an efficient and practical procedure to perform analysis and evaluation of structures. A nonlinear static procedure, specified by the Federal Emergency Management Agency, was used in the evaluation process. This procedure was modified by AlAyed (2002) for the applicability to bridges rather than buildings.

The Maximum Considered Earthquake (MCE) level was used for the evaluation of five bridges. Seismic loads were applied in two horizontal directions of each bridge: transverse and longitudinal directions. Nonlinear behavior of the bridge substructure components (columns) were evaluated and compared to the acceptance criteria. The acceptance criteria of the bridges set in this study was the Immediate Occupancy performance level, as these bridges are of high importance and are expected to be fully operational maintaining the pre-earthquake strength and stiffness of their components. Most of the evaluated bridges violated the acceptance criteria under the aforementioned level of earthquake in one or more of the analysis cases. The main two deficiencies identified in these five bridges were: (1) the insufficient flexural capacity of some columns at the plastic hinge regions and (2) the inadequate development lengths provided in the longitudinal reinforcement of the columns, either at the lap splice locations or at the beam-column joints.

TABLE OF CONTENTS

LIST OF TABLES

LIST OF FIGURES

ACKNOWLEDGEMENTS

All praise and thanks to Allah (God) for giving me the strength to complete this work.

I would like to express my gratitude to my advisor, Dr. Aly Said, for the teaching, support and friendship provided during the study.

As part of the Earthquakes in Southern Nevada project, I would like to thank Dr. Barbara Luke and Mr. Suchan Lamichhane for providing the seismic site classifications of the soil underneath the studied bridges.

Thanks to Mr. Mohamed Zeidan for his help in the final stage of this work.

I thank my parents for their continuous support and prayers to me. My mother, you are the best ever. My father, you are my mentor and everything I know is because of you. I thank my wife for her support and patience during difficult times of my studies. I thank my brother and sisters for their continuous support and encouragement.

CHAPTER 1

INTRODUCTION

1.1. Introduction

An earthquake is a sudden, rapid shaking of the earth's crust that can cause severe damage to structures to the extent of their collapse. Preventing the occurrence of earthquakes is impossible, whereas it is possible to mitigate their destructive effects. Seismic design aims at producing structures that can resist certain levels of ground shaking without excessive damage. Codes and specifications are continuously developing to improve structures' performance during seismic events.

In highway systems, bridges are considered the most critical component that may be affected by earthquakes. In addition to being the most vulnerable and costly component of the highway, its damage can severely disrupt the traffic. This disruption may have a great impact on the economy of the region as well as post-earthquake emergency response, repair, and reconstruction operations. A large number of bridges were designed and constructed according to codes that had inadequate or no seismic design provisions. In recent earthquakes (in California, Japan, Central and South America), a number of bridges did not perform adequately under seismic loads. Despite the fact that they were designed for earthquake resistance, some of them suffered severe damage or even collapse due to lack of ductility or poor detailing (Priestly *et al.,* 1996).

The first step in mitigating earthquake losses in transportation systems is identifying bridges that are likely to fail and cause disruption to these systems. This identification is

usually done based on bridges' vulnerability and importance. Seismic evaluation of these bridges is the second step and is considered as an essential part of the rehabilitation process. As defined in FEMA-356 (2000), four different analytical procedures can be used for the evaluation process of structures in general and can be extended to bridges. These procedures are: linear static, linear dynamic, nonlinear static (pushover), and nonlinear dynamic procedures. A brief description of the four analysis methods is presented in Chapter 2.

Performance-based approach has been recognized among structural engineers as an efficient approach for evaluation purposes. Since most of the structures are expected to respond beyond their elastic limits under moderate to high magnitudes of earthquake ground shaking, it is impractical to implement the performance-based design without a nonlinear analysis procedure.

1.2. Project background

The Federal Emergency Management Agency (FEMA) lists Clark County, Nevada as a region of high seismicity. Slemmons *et al.* (2001) showed that there are eight faults in Clark County capable of producing earthquakes of magnitude (M_w) between 6.5 and 7.0. Based on these facts, a proposal was prepared by researchers from UNLV, Department of Civil and Environmental Engineering and Department of Geoscience in early 2004. Later that same year the grant was awarded to the UNLV team. Seismic risk assessment for essential infrastructures located in Clark County was performed. Keller (2006) performed the seismic risk assessment for buildings of high importance (i.e. hospitals, police stations, fire stations and schools). Seismic risk assessment of the bridges was performed

by Ebrahimpour *et al.* (2007) and compared to the prioritization of Nevada bridges by Sanders *et al.* (1993).

A comprehensive and accurate database for the bridges in Clark County was established for the classification purpose. The National Bridge Inventory (NBI), a database maintained by the Federal Highway Administration (FHWA), along with the Nevada Department of Transportation (NDOT) provided the essential information needed for bridges' prioritization. The prioritization process was done based on a risk assessment that combines (1) the vulnerability assessment and (2) the importance assessment of the bridges. Table 1.1 lists the top 20 high risk bridges (Ebrahimpour *et al*., 2007). It also shows the vulnerability and importance scores in addition to the final combined risk score.

Some of the ranked bridges were exempted from the seismic evaluation process for one of the following three reasons:

1- Having a single span. According to the seismic specifications of the AASHTO (2007), seismic analysis is not required for a single span bridge, regardless of its seismic zone.

2- The bridge is exactly similar to another bridge which is already evaluated. This is common in the case of having two typical bridges holding the same route or highway in the two opposite directions.

3- The bridge is considered in a widening, retrofit or replacement process by the Nevada Department of Transportation (NDOT) in their present or near future plans and accordingly there is no need to consider them in the evaluation.

Table 1.1 Top 20 high risk bridges

Rank	Bridge	Latitude	Longitude	Vulnerability score	Importance score	Risk score
1	H-942S	36.1771694	-115.1509944	0.985	0.964	0.973
2	H-1443	36.1661056	-115.0966611	0.993	0.952	0.968
3	H-948	36.1883556	-115.1432278	1	0.945	0.966
4	G-1064	36.1439861	-115.1659139	0.979	0.958	0.967
5	H-942N	36.1771694	-115.1509944	0.952	0.966	0.961
6	H-1460	36.0584972	-115.0286917	0.943	0.913	0.925
7	G-947	36.1755056	-115.1450361	0.806	1	0.923
8	G-805N	36.1221278	-115.1803806	0.918	0.923	0.921
9	G-805S	36.1216667	-115.1800000	0.918	0.923	0.921
10	B-1448	36.1421056	-115.0912000	0.893	0.912	0.904
11	I-1449	36.1358278	-115.0903194	0.846	0.934	0.899
12	I-956	36.2402194	-115.1017750	0.995	0.812	0.885
13	B-1455	36.0889750	-115.0679083	0.814	0.908	0.87
14	H-946	36.1748222	-115.1491361	0.689	0.99	0.87
15	I-947	36.1755667	-115.1437500	0.667	0.973	0.851
16	I-937	36.1741944	-115.1547889	0.667	0.968	0.848
17	H-1446	36.1462444	-115.0913167	0.685	0.953	0.846
18	H-1211	36.1812139	-115.2442944	0.618	0.995	0.844
19	G-953	36.2034083	-115.1347167	0.797	0.873	0.843
20	I-2139	36.17347222	-115.1576889	0.771	0.89	0.842

Table 1.2 represents the bridges that are exempted from the evaluation process in addition to the reason of exemption. Out of the 12 remaining bridges, 5 were chosen in this study for the evaluation. These bridges were chosen to represent diversity in their number of spans and columns cross sections.

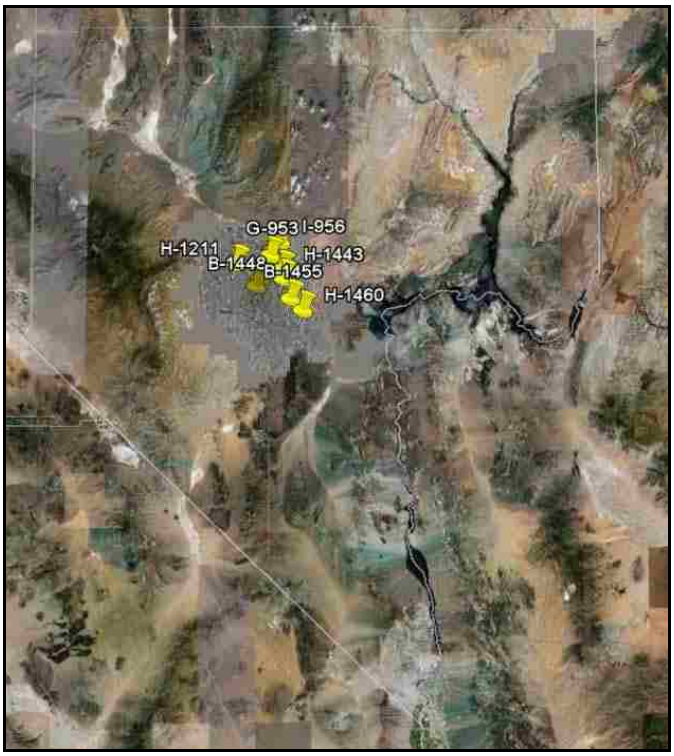

Figure 1.1 Locations of the 20 ranked bridges on Clark County map, using Google earth

Table 1.2 Exempted bridges from the evaluation process

Bridge	Rank	Reason for Exemption
H-942S	1	Will be replaced
H-942N	5	Will be replaced
G-805N	8	Widening, retrofit (NDOT, 2007)
G-805S	9	Widening, retrofit (NDOT, 2007)
B-1448	10	Single span bridge
B-1455	13	Single span bridge
H-946	14	Widening, retrofit (NDOT, 2007)
I-937	16	Widening, retrofit (NDOT, 2007)

1.3. Objective of this study

The main objective of this study is to evaluate the seismic performance of critical bridges in Clark County using a nonlinear static procedure introduced by the FEMA-356 (2000). This procedure has been developed for the assessment of buildings and was modified by AlAyed (2002) for applicability to bridges. The assessment of the bridges in this work is focused only on the behavior of bridge columns under high earthquake levels.

1.4. Organization of this work

The presented thesis consists of five chapters. The current chapter presents an overview of the study, the project background along with the objectives of the study. A literature review is presented in Chapter 2; it includes a presentation of damages that occurred to bridges in recent earthquakes, a review of the principles of nonlinear analysis, previous work done in nonlinear static pushover analysis, and an overview of the performance-based approach. The theoretical approach used in the evaluation process in this work is described in Chapter 3. The detailed description of the evaluated bridges along with calculations and evaluation results are presented in Chapter 4. Summary and conclusions are presented in Chapter 5, in addition to the proposed future research.

CHAPTER 2

LITERATURE REVIEW

2.1. Introduction

This chapter presents an extensive survey of previous work done by various researchers in the field of nonlinear analysis alongside with seismic evaluation of bridges. It begins with an overview of the potential damage of bridge components by earthquake loads and the factors affecting them and then discusses different techniques for seismic analysis of bridges which can also be used for evaluation purposes. Furthermore, a description of the theoretical background of the nonlinear static analysis procedures and a review to the performance based approach are presented.

2.2. Potential damage to bridge components due to earthquake loads

In this section two main aspects are briefly discussed to present the possible damage that can occur to bridges under earthquake ground shaking. These aspects are: (1) factors affecting seismic damage to bridges and (2) damage observed in bridge components in recent earthquakes.

2.2.1. Factors affecting seismic damage to bridges

Damage to bridges caused by earthquakes can be categorized into the following two classes (Chen and Duan, 2003): (1) *Primary Damage* caused by earthquake ground shaking or deformation that was the primary cause of damage to the bridge, and that may have triggered other damage or collapse; and (2) *Secondary Damage* caused by redistribution of internal actions for which the structure was not designed. This

redistribution is the result of structural failures elsewhere in the bridge. However, the controlling factors that affect the seismic behavior of the bridge can be classified into the following categories:

2.2.1.1. Effect of site conditions

Performance of a bridge structure during an earthquake is likely to be influenced by the bridge proximity to faults and their characteristics. In addition to that, the soil types underneath bridge substructure components greatly affect the intensity of ground shaking and ground deformation. Variability of those effects along the length of the bridge may have higher influences than in the case of buildings because bridges are extended horizontally.

2.2.1.2. Bridge construction era

Seismic design practices for structures generally and for bridges specifically have evolved over years, largely reflecting lessons learned from structures' performance in past earthquakes (Chen and Duan, 2003). Therefore, the construction era of a bridge is a good indicator of the likelihood of poor performance with higher damage levels expected in older construction than in newer construction.

2.2.1.3. Change in bridge condition

Changes in the condition of a bridge can significantly affect its seismic performance. This factor includes two aspects: (1) deterioration of the bridge components (superstructure, substructure, bearings, etc.) which reduces the seismic performance of this component and consequently the overall performance of the bridge; and (2) construction modifications either during the original construction or during the service life of the bridge. An example of the latter aspect is illustrated in Figure 2.1, where the

bridge columns were restrained with the construction of the wall for the channel, which shortened the effective length of the columns causing an increase in columns' shear force and shifting the nonlinear response from the region of heavy confinement upward to a zone of light transverse reinforcement where the ductility capacity was inadequate (Chen and Duan, 2003).

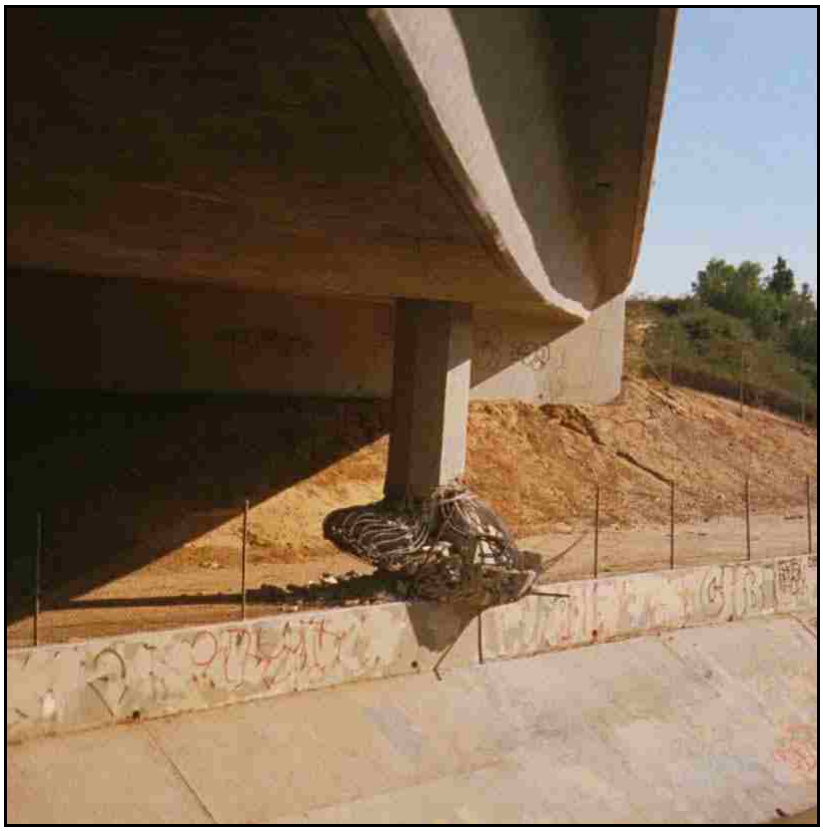

Figure 2.1 Damage to bridge column caused by post-construction change in boundary condition (Caltrans, 2003)

2.2.1.4. Structural configuration

Generally, structures with regular configurations perform better under earthquake loads than structures that contain irregularities in their structural systems. This is due to the fact that regular structures contain even distribution of forces and masses which

prevents stress concentrations under abnormal loads, and the inelastic energy dissipation is promoted in a large number of readily identified yielding components. However, in practice, bridges with certain configurations are more vulnerable to earthquakes than others. Experience indicated that a bridge is most likely to be vulnerable if (1) excessive deformation demands occur in a few brittle elements; (2) the structural configuration is complex; or (3) the bridge lacks redundancy (Chen and Duan, 2003).

The main points that define the structural configuration are:

a- Structural irregularity such as non-uniform column length or irregular deck structural system.

b- Long span bridges, where non-uniform soil condition exists along the bridge length and causes variation in ground excitation at different bridge supports.

c- Bridge layouts (curved, skewed …)

2.2.2. Damage to bridges observed in recent earthquakes

In reviewing bridge damage caused by recent earthquakes, three basic design deficiencies were identified by Priestly *et al.* (1996): (1) underestimating seismic deflections based on the specified lateral load level; (2) incorrect ratio of gravity load to lateral force, as the design seismic loads were low, and accordingly the envelopes of the load combinations were different from the actual ones; and (3) not considering the inelastic structural actions and the associated concepts of ductility and capacity design in the elastic design process. This last deficiency may lead to inadequate detailing of the plastic hinge locations preventing it from sustaining large inelastic deformations. These three deficiencies tend to be consequences of the elastic design philosophy used in the

seismic design of bridges prior to 1970 and is still used in some countries (Priestly *et al.*, 1996).

In this section, most of the bridge damage modes due to seismic loading are presented, and each of them can be attributed to any of the aforementioned three deficiencies (Priestly *et al.*, 1996).

2.2.2.1. Seismic displacements

The underestimation of seismic displacement in the design process may be attributed to any of the following reasons: (1) elastic theory was used in the analysis/design of the bridge; (2) the gross section stiffnesses were used in the analysis and not the actual cracked ones; and (3) the lateral force levels used in the analysis were lower than the actual ones. The following are three failure modes due to underestimating the seismic displacements in the design process (Priestly *et al.*, 1996).

a- *Span failure due to unseating at movement joints:* This kind of failure is mainly caused by the relative movement of bridge spans in the longitudinal direction exceeding the seating widths, resulting in unseating at unrestrained movement joints as shown in Figure 2.2. Skew bridges are particularly vulnerable to such failure due to their tendency to rotate in the direction of increasing the skew, thus tending to drop off the supports at the acute corners; see Figure 2.3.

Figure 2.2 Spans slipped off narrow support seats, 1971 San Fernando earthquake (Caltrans, 2003)

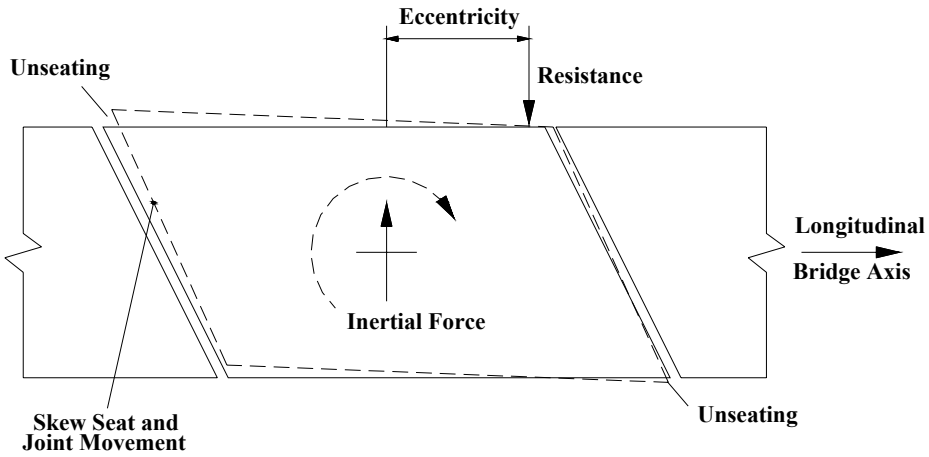

Figure 2.3 Unseating due to bridge skew - plan view of bridge deck (after Priestly *et al.*, 1996)

b- *Amplification of displacements due to soil effects:* This amplification is mainly due to constructing the bridge on soft or liquefiable soils. These kinds of soil generally result in an amplification of structural vibrational response, which increases the probability of unseating. When bridges are supported on piles that have either silty sand or sandy silt soil underneath; liquefaction may occur

causing a loss of piles support, with excessive vertical and/or lateral displacements unrelated to vibrational response.

c- *Pounding of bridges:* This is always caused by insufficient separation between adjacent structural elements that have the potential to shake freely during earthquake loading. This mode of damage is common in older construction where the clearance between adjacent structures was designed to accommodate only thermal expansion or under-predicted seismic displacements. This may cause a global failure and jeopardize the safety of the bridge.

2.2.2.2. Abutment slumping

This kind of failure is related to the response of soft (or poorly consolidated) soil types to the vibration. Due to seismic accelerations, earth pressure on the abutments is induced because of the longitudinal movement of the deck. When such soil types are located behind or underneath the abutments, slumping of abutment fill and rotation of abutments may occur, as shown in Figure 2.4 (Priestly *et al.*, 1996).

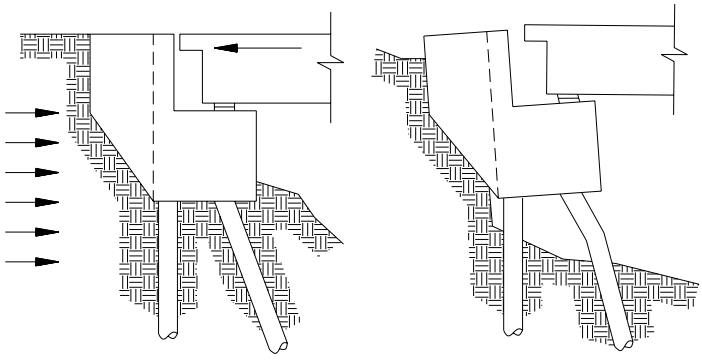

(a) Before Failure (b) After Failure

Figure 2.4 Abutment slumping and rotation
(after Priestly *et al.*, 1996)

2.2.2.3. Column failure

2.2.2.3.1. Flexural strength and ductility failure

The main reason for bridge column failures in recent earthquakes is the unawareness of the designers, in the past, of the need to build ductility capacity into potential plastic hinge regions. Four particular deficiencies can be identified in this kind of failure (Priestly *et al.*, 1996):

a- *Inadequate flexural strength:* This deficiency is mainly due to the low seismic force levels that were used to characterize the seismic actions in the design phase.

b- *Undependable column flexural strength:* Lap splices for longitudinal bars of columns were often taken immediately above the foundation, with an inadequate splice length to develop the strength of the bars. Prior to 1971, lap-splice as short as 20 bar diameters was commonly provided at the column bases in bridges of California. Recent earthquakes indicated that this is insufficient to enable the flexural strength of the column to develop. Inadequate flexural strength may also result from butt welding of longitudinal reinforcement close to maximum moment locations.

c- *Inadequate flexural ductility:* In such a deficiency, the flexural strength of bridge columns is less than the required strength for elastic response to the expected seismic intensities. Accordingly, structures must possess ductility to survive under intense seismic events. The term ductility describes the ability of the components to deform through several cycles of displacements much larger than the yield displacements, without significant strength degradation. One

important key element that increases ductility of the bridge columns is the proper confinement using the transverse reinforcement. Figure 2.5 shows a flexural plastic hinge failure due to the low level of transverse reinforcement at the plastic hinge region.

Figure 2.5 Confinement failure at column top
(Caltrans, 2003)

d- *Premature termination of column reinforcement:* Usually the location of bars termination is based on the design moment envelope. However, due to diagonal shear cracking, tension shift may occur and the location of maximum moment will change. As a consequence, failure at the column mid-height may develop during earthquakes; such failure is considered a flexure-shear failure.

2.2.2.3.2. Column shear failure

Unlike flexural failure, shear failure is a complex failure mechanism. It results from a combination of mechanisms involving concrete compression shear transfer, aggregate interlocking, arching action sustained by axial forces and others. If yield is reached in the transverse reinforcement of a column, flexure-shear crack widths increase rapidly,

reducing the shear strength of concrete provided by aggregate interlock. As a consequence, rapid strength degradation takes place and therefore shear failure is considered to be brittle. Thus, shear failure is unsuitable for ductile seismic response (Priestly *et al.*, 1996).

In older column designs, especially if they are designed on the basis of elastic theory, flexural strength design was conservative. However, shear strength equations for column design were less conservative than flexural strength design. Accordingly, when high values of shear/moment ratio develop, generally in short columns, columns will be more susceptible to shear failure.

Shear failure of bridge columns occurred extensively in recent major earthquakes (e.g. 1971 San Fernando earthquake, 1994 Northridge earthquake, and 1995 Kobe earthquake) for various reasons and design deficiencies as mentioned (Priestly *et al.*, 1996). Figure 2.6 illustrates two of the column failure modes that occurred in the Northridge earthquake in California, 1994 (Caltrans, 2003).

(a) (b)

Figure 2.6 Examples of column shear failures (a) within the plastic hinge region and (b) outside the plastic hinge region (Caltrans, 2003)

2.2.2.4. Cap beam failure

Three main deficiencies were observed to be the causes of failure in cap beams under seismic loading: (1) insufficient shear capacity, particularly where seismic and gravity shears are additive; (2) premature termination of cap beam negative moment reinforcement; and (3) insufficient anchorage of cap beam reinforcement into joint regions. The first two deficiencies are encountered in the outrigger cap beams, while the third prevails in multi-column bents (Priestly *et al.*, 1996).

2.2.2.5. Joint failure

Transfer of shear forces through connections between cap beams and columns may result in horizontal and vertical joint shear forces far exceeding the shear forces in the connected members. Joint shear failure is considered to be the major contributor to the collapse of a 1-mile length of the Cypress Viaduct during the 1989 Loma Prieta earthquake, with the tragic loss of 43 lives (Priestly *et al.*, 1996). Joint shear forces were not generally considered part of the bridge design, and accordingly joint shear reinforcement was inadequate (Priestly *et al.*, 1996). Figure 2.7 illustrates an example of joint shear failure that occurred in four bent of the Southern Freeway Viaduct in the 1989 Loma Prieta earthquake.

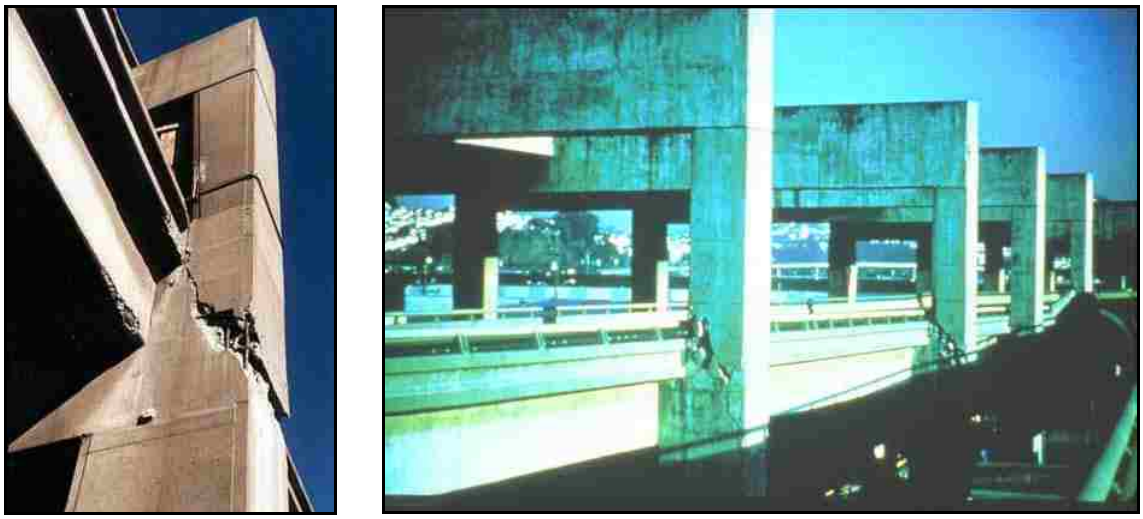

(a) (b)

Figure 2.7 Joint shear failure (a) Cypress Street Viaduct and (b) Southern Freeway Viaduct, 1989 Loma Prieta earthquake (Caltrans, 2003)

2.2.2.6. Footing failure

Footing failure, caused by seismic actions, has comparatively small number of reported incidences. The following are the deficiencies in footing design that may cause seismic failure: (1) footing flexural strength; (2) footing shear strength, as shear reinforcement is rarely provided; (3) joint shear strength in the region immediately below the column (subjected to high shear stresses); (4) column reinforcement anchorage and development in the footing (as in Figure 2.8); and (5) inadequate connection between tension piles and footing.

Figure 2.8 Pullout failure, 1971 San Fernando earthquake
(Caltrans, 2003)

2.2.2.7. Failure of steel bridge components

There is a general perception that steel bridge components are less susceptible to bridge damage than concrete components. Although steel bridge components are lighter than equivalent concrete ones, they may still sustain damage. The main two deficiencies that occur to steel bridges are (Priestly *et al.*, 1996): (1) buckling of steel I-beam bridge girders as a result of inadequate bracing and (2) buckling of steel columns, which significantly reduce ductility capacity.

2.3. Seismic analysis approaches for bridges

Various methods were introduced by different researchers, codes, specifications, and guidelines to deal with seismic analysis of bridges. To choose the appropriate method, users need be knowledgeable about these methods and their limitations. This can provide the required accuracy within reasonable computational efforts. Three levels can be used to perform seismic evaluation for bridges (Mehta, 1999):

- Level 1 is a simple screening using flowcharts based on bridge characteristics previously known to be vulnerable to seismic activity. It is not necessary to perform computer modeling or calculations at this level. Buckle *et al.* (1987) outlined this procedure, which can be used to quickly screen several "regular" bridges as defined in the AASHTO Standard Specifications.
- Level 2 evaluation is a schematic assessment. Simple and approximate models are used to evaluate the applied seismic demand against the capacity of bridge components. The results are conservative for "regular" structures. However, for "irregular" structures, this assessment may not be conservative. Irregular structures may have different forms of irregularity. This includes unusual geometries, abrupt changes in components stiffnesses, varying soil conditions and foundations, etc.
- Level 3 evaluation is an in-depth seismic evaluation. This is usually employed for bridges that cannot be conservatively assessed by a Level 2 evaluation and for bridges that serve as very critical links in transportation systems. Global and local 3-D finite element models are developed to compute the seismic demands. Foundations are modeled considering soil-structure interaction. A site-specific response spectrum may be developed for seismic input in the case of a very important bridge.

After determining the appropriate level of evaluation, the seismic analysis is performed using one of several methods. Four distinct procedures can be used to perform the analysis for existing structures: linear static, nonlinear static, linear dynamic and

nonlinear dynamic procedures (FEMA-273, 1997). Each one of these procedures is briefly discussed below:

- Linear Static Procedure (LSP): Under this procedure, design seismic forces, their distribution over the structure, and the resulting internal forces and displacements are determined using linear (elastic) static analysis. This procedure may give accurate results when the structure is expected to respond elastically to the ground shaking, which means the ductility demands are suitably low. However, this procedure is not recommended for irregular structures. To determine the applicability of this procedure, FEMA-356 (2000) listed a method using the demand capacity ratio (DCR). If all the computed DCRs for a component are less than 1.0, then the evaluated component is expected to respond elastically to earthquake loads. If all DCRs computed for all critical actions of all components of the primary elements are less than 2.0, then linear procedures are still applicable. Various codes and guidelines proposed different methods and empirical formulas to estimate the lateral forces distribution and the structure's natural periods.
- Linear Dynamic Procedure (LDP): Under this procedure, design seismic forces, their distribution over the structure, and the resulting internal forces and displacements are determined using linear elastic dynamic analysis. It is similar to the LSP with the advantage of considering higher modes in the analysis. The main difference between the two procedures is that, in the LDP, the response calculations are carried out using either modal spectral or time-history analysis. Modal spectral analysis is carried out using linear elastic response spectra that

are not modified to account for anticipated nonlinear response. This procedure should be allowed only in case of structures that are expected to respond elastically under the earthquake loading. This is more applicable in case of high buildings or when higher modes play a significant role. The number of modes required to be included in the analysis, as a requirement by FEMA-356 (2000), is the number that can satisfy at least 90% of the participating mass of the structure in each of the principal horizontal directions.

- Nonlinear Static Procedure (NSP): This procedure, often called "pushover analysis", applies simplified static nonlinear techniques to estimate the seismic structural deformations. It can be used for the estimation of the dynamic demand imposed on the structures by earthquake loads. A static lateral load pattern, equivalent to the seismic load, is applied to the structure in the direction under consideration. The structure is then displaced (pushed over) incrementally to the required level of deformation expected by the evaluated earthquake (target displacement) while the applied load pattern is kept the same. A pushover curve is then built as the relation between the base shear and the corresponding displacement. The nonlinear load-deformation relation for each component in the structure should be defined to account for the possibility of exceeding elastic limits. NSP can be used for any structure and it is recommended by FEMA-356 (2000) for irregular structures. This procedure should not be used for structures in which higher modes are significant unless LDP evaluation is also performed to capture the effect of higher modes. Because the main objective of this study is to perform seismic evaluation of bridges using this procedure, principles of

nonlinear analysis as well as researchers' previous work in NSP will be discussed later in this chapter.

- Nonlinear Dynamic Procedure (NDP): This procedure is often called the nonlinear time-history analysis. It is considered to be the most accurate procedure, among the four presented procedures, to represent the effect of earthquake load on structures. It is applicable to any kind of structure except wood frame structures (FEMA-356, 2000). The main difference between this procedure and the NSP is in the input, as the NDP uses earthquake records in form of time vs. acceleration that is applied at the base of the structure. The structure's response is incrementally calculated and the stresses and deformations are considered as an initial condition in the analysis for the next step. As this procedure is considering the ground motion of the earthquake in the form of the acceleration vs. time, the target displacement concept is no longer used. Instead, the design displacements are directly determined from the analysis. Material inelastic response is considered in the NDP which results in reasonable calculated internal forces. It is considered as a realistic procedure as it contains the structure's full mass participation in the analysis. The main disadvantage of this method is its high computational efforts, especially with the uncertainty in the earthquake records, where many time-history records should be used. Increasing the number of records used in the analysis increases its computational effort in addition to the increase in the results accuracy. FEMA-356 (2000) specifies at least 3 time-history records to be used in the analysis to account for the uncertainty in the time-history records. In this case, the

maximum response of the parameter of interest shall be used for design or evaluation purposes. However, if seven or more records are used for the time-history, the average response of the parameter of interest may be considered. A special computer program with nonlinear material and hysteresis model is required to perform this type of seismic analysis.

2.4. Principles of nonlinear analysis

This section is intended to give a background of the NSP. The NSP described in FEMA-356 (2000) is based on the capacity spectrum method which was originally developed by Freeman *et al.* (1975) and Freeman (1978). Because pushover analysis is essential for NSP, its theoretical background will be presented next.

2.4.1. Theoretical background for pushover analysis

Static pushover analysis is based on the assumption that the response of the multiple degrees of freedom (MDF) structure is governed by a single mode that remains constant through the time-history analysis (Dutta, 1999). The governing equation of motion for linear MDF system subjected to horizontal earthquake ground motion (single excitation) is:

$$m\{\ddot{q}\} + c\{\dot{q}\} + k\{q\} = -m\{i\}\ddot{q}_g(t) \qquad \text{Eq. 2.1}$$

where m, c, and k are the mass, classical damping, and lateral stiffness matrices of the system, respectively, and $\{i\}$ is the unity vector corresponding to the translational degrees of freedom (DOF) in the direction under consideration and zeros corresponding to rotational DOFs. In the modal analysis approach, for linear static systems, the displacements vector relative to ground q is represented as a truncated series in the form

of a coordinate transformation. Specifically, q is written as the product of the mode shape matrix Φ and a vector of generalized modal coordinates p

$$q(t) = \sum_{r=1}^{N} \phi_r p_r(t) = \Phi p(t) \qquad \text{Eq. 2.2}$$

where

$$\Phi = [\phi_1 \quad \phi_2 \quad \ldots \phi_m \quad \ldots \phi_N] \qquad \text{Eq. 2.3}$$

$$p = [p_1(t) \quad p_2(t) \quad \ldots p_m(t) \quad \ldots p_N(t)]^T \qquad \text{Eq. 2.4}$$

where $\phi_1 \quad \phi_2 \quad \ldots \phi_m \quad \ldots \phi_N$ are N mode shape vectors and $p_1(t)\ p_2(t)\ \ldots p_m(t)\ \ldots p_N(t)$ are N modal coordinates . By substituting Eq. 2.2 into Eq. 2.1, it can be rewritten as

$$\sum_{r=1}^{N} m\phi_r \ddot{p}_r(t) + \sum_{r=1}^{N} c\phi_r \dot{p}_r(t) + \sum_{r=1}^{N} k\phi_r p_r(t) = -m\{i\}\ddot{q}_g(t) \qquad \text{Eq. 2.5}$$

Pre-multiplying each term in this equation by ϕ_n^T gives

$$\sum_{r=1}^{N} \phi_n^T m\phi_r \ddot{p}_r(t) + \sum_{r=1}^{N} \phi_n^T c\phi_r \dot{p}_r(t) + \sum_{r=1}^{N} \phi_n^T k\phi_r p_r(t) = -\phi_n^T m\{i\}\ddot{q}_g(t) \qquad \text{Eq. 2.6}$$

Because of the orthogonal relationship between different modes, all terms in each of the summations vanish, except the $r = n$ term, reducing this equation to

$$(\phi_n^T m\phi_n)\ddot{p}_n(t) + (\phi_n^T c\phi_n)\dot{p}_n(t) + (\phi_n^T k\phi_n)p_n(t) = -(\phi_n^T m\{i\})\ddot{q}_g(t) \qquad \text{Eq. 2.7}$$

The above equation can be rewritten as

$$M_n\ddot{p}_n(t) + C_n\dot{p}_n(t) + K_n p_n(t) = -L_n\ddot{q}_g(t) \qquad \text{Eq. 2.8}$$

The above equation is similar to the equation of motion for SDF system with the consideration of the n^{th} mode only and can be rewritten as

$$\ddot{p}_n(t) + 2\zeta_n\omega_n\dot{p}_n(t) + \omega_n^2 p_n(t) = -\Gamma_n\ddot{q}_g(t) \qquad \text{Eq. 2.9}$$

where $(\phi_n^T m \phi_n) = M_n$ = generalized n^{th} modal mass, ζ_n = generalized nth modal damping, ω_n = generalized n^{th} modal frequency, L_n = n^{th} modal excitation factor, and $\Gamma_n = (L_n / M_n)$. Eq. 2.9 is the standard modal equation (Chopra and Goel, 2001). The right side of Eq. 2.1 can be interpreted as effective inertia forces resulting from earthquake excitation:

$$Q_{eff}(t) = -m\{i\}\ddot{q}_g(t) \qquad \text{Eq. 2.10}$$

The spatial distribution of these forces over the structure (building or bridge) is defined by the vector $s = m\ \{i\}$ and the time variation $\ddot{q}_g(t)$. The contribution of the nth mode to s and $Q_{eff}(t)$ are:

$$s_n = \Gamma_n m \phi_n \qquad Q_{eff,n}(t) = -s_n \ddot{q}_g(t) \qquad \text{Eq. 2.11}$$

For linear systems, the response of the MDF system to $Q_{eff,n}(t)$ is entirely in the n^{th} mode, with no contribution from other modes.

The solution to Eq. 2.9 can be obtained by comparing this equation to the equation of motion for an elastic SDF system with natural frequency ω_n and damping ratio ζ_n, both for the n^{th} mode of the MDF system. If a SDF is subjected to $\ddot{u}_g(t) = \ddot{q}_g(t)$, the equation of motion will be

$$\ddot{u}_n(t) + 2\zeta_n \omega_n \dot{u}(t) + \omega_n^2 u_n(t) = -\ddot{u}_g(t) \qquad \text{Eq. 2.12}$$

Comparing Eq. 2.9 and Eq. 2.12 gives

$$p_n(t) = \Gamma_n u_n(t) \qquad \text{Eq. 2.13}$$

and substituting Eq. 2.13 in Eq. 2.2 gives the floor displacements due to the n^{th} mode.

$$q_n(t) = \Gamma_n \phi_n u_n(t) \qquad \text{Eq. 2.14}$$

Any response quantity *r(t)* such as story drift, internal element forces, etc., can be represented as (Chopra and Goel, 2001)

$$r_n(t) = r_n^{st} A_n(t) \qquad \text{Eq. 2.15}$$

where r_n^{st} denotes the modal static response, the static value of *r* due to external forces s_n, and $A_n(t) = (\omega_n^2 u_n(t)/g)$ is the pseudo-acceleration response of the n^{th}-mode SDF system (Chopra, 2001).

Eq. 2.14 and Eq. 2.15 represent the response of the MDF system to the total excitation $Q_{eff}(t)$. Therefore, the response of the system to the total excitation $Q_{eff}(t)$ is

$$q(t) = \sum_{n=1}^{m} q_n(t) = \sum_{n=1}^{m} \Gamma_n \phi_n u_n(t) \qquad \text{Eq. 2.16}$$

$$r(t) = \sum_{n=1}^{m} r_n(t) = \sum_{n=1}^{m} r_n^{st} A_n(t) \qquad \text{Eq. 2.17}$$

The first *m* modes are considered in the above two equations where *m*<<*N*. Equations 2-14 and 2-15 define the contribution of the n^{th}-mode to the response, and equations 2-16 and 2-17 reflect the combination of the response contributions of *m* modes. The modal expansion of the spatial distribution of the effective earthquake forces, s_n was used in the derivation of these standard equations, which provides a rational basis for the modal pushover analysis procedure (Chopra and Goel, 2001).

The peak value r_0 of the total response $r(t)$ can be estimated directly from the response spectrum of the ground motion. In such a response spectrum analysis (RSA), the peak value r_{n0} of the n^{th}-mode contribution $r_n(t)$ to response $r(t)$ is determined from

$$r_{n0} = r_n^{st} A_n \qquad \text{Eq. 2.18}$$

where A_n is the ordinate $A_n(T_n, \zeta_n)$ of the pseudo-acceleration response (or design) spectrum for the n^{th}-mode single degree of freedom (SDF) system, and $T_n = 2\pi / \omega_n$ is the natural vibration period of the n^{th}-mode of the MDF system. The modal peak responses are combined according to the Square-Root-of-Sum-of-Squares (SRSS) or the Complete Quadratic Combination (CQC) rules. The SRSS rule provides an estimate of the peak value of the total response

$$r_0 = \sqrt{\sum_{n=1}^{m} r_{n0}^2} \qquad \text{Eq. 2.19}$$

It can be noticed that in a static analysis of a structure subjected to lateral forces

$$f_{n0} = \Gamma_n m \phi_n A_n \qquad \text{Eq. 2.20}$$

which will provide the same value of r_{n0}, the peak n^{th}-mode response as in Eq. 2.18 (Chopra, 2001). Alternatively, this response value can be obtained by static analysis of the structure subjected to lateral forces distributed over the structure according to

$$s_n^* = m \phi_n \qquad \text{Eq. 2.21}$$

and the structure is pushed until the roof displacement reaches q_{rn0}, the peak value of the roof displacement (or the control node displacement) due to the n^{th}-mode, which comes from Eq. 2.14 is

$$q_{rn0} = \Gamma_n \phi_{rn} u_n \qquad \text{Eq. 2.22}$$

where $u_n = A_n g / \omega_n^2$. Obviously, u_n and A_n are available from the response (or design) spectrum (Chopra and Goel, 2001).

The peak modal responses, r_{n0}, each determined by one pushover analysis, can be combined according to Eq. 2.19 to obtain an estimate of the peak value r_0 of the total response. This is the basis for the modal pushover analysis (MPA), which was developed by Chopra and Goel (2001). The MPA for linearly elastic systems is equivalent to the well-known RSA.

A similar approach, with few differences, was used by Dutta (1999) with the capacity spectrum method (CSM) to derive the basis for pushover analysis. From Eq. 2.13, the maximum p_{m0}, which is the response due to the m^{th} mode, can be rewritten as

$$q_{rn0} = \Gamma_m S_d(\omega_m, \zeta_m) \qquad \text{Eq. 2.23}$$

where $S_d(\omega_m, \zeta_m)$ is the spectral displacement corresponding to damping ζ_m and natural frequency ω_m. Multiplying both sides of the above equation by ϕ_{nm} (the magnitude of the m^{th} mode at the n^{th} location) yields

$$q_{nm} = \phi_{nm} p_{m0} = \phi_{nm} \Gamma_m S_d(\omega_m, \zeta_m) \qquad \text{Eq. 2.24}$$

where q_{nm} is the displacement at the nth location due to the m^{th} mode shape. It is clear that the above equation is similar to Eq. 2.22. Using Eq. 2.24 the spectral displacement can be solved as

$$S_d = \frac{q_{nm}}{\phi_{nm}\Gamma_m} = \frac{q_{nm}}{PF_1 \phi_{nm}} = \Delta^* \qquad \text{Eq. 2.25}$$

This can also be defined as the effective displacement $(\Delta^* = S_d)$

$$PF = \frac{\sum_{i=1}^{N}(w_i \phi_{im})}{\sum_{i=1}^{N}(w_i \phi_{im}^2)} \qquad \text{Eq. 2.26}$$

where w_i is the tributary weight at location i varying from 1 to N being the total number of discrete weights for pushover mode-shape locations.

The base shear for the m^{th} mode can be calculated from the force vector

$$F_m = \Gamma_m m \phi_m S_a(\omega_m, \zeta_m) \qquad \text{Eq. 2.27}$$

where $S_a(\omega_m, \zeta_m)$ is the spectral acceleration corresponding to frequency ω_m and damping ζ_m. The base shear capacity can be obtained by adding all the terms of the force vector. Therefore

$$V = \sum_{i=1}^{N} F_{im} = \alpha_1 S_a W \qquad \text{Eq. 2.28}$$

where S_a in the above equation is the normalized spectral acceleration. This can be used to define normalized base shear capacity as follows (ATC, 1996 and Dutta, 1999):

$$C_c^* = S_a = \frac{V/W}{\alpha_1} \qquad \text{Eq. 2.29}$$

where

$$\alpha = \frac{\left[\sum_{i=1}^{N}(w_i \phi_{im})/g\right]^2}{\left[\sum_{i=1}^{N} w_i/g\right]\sum_{i=1}^{N}(w_i \phi_{im}^2)/g} \qquad \text{Eq. 2.30}$$

and $\sum_{i=1}^{N} w_i = W$ = total effective weight considered in seismic analysis.

From the above formulation it can be concluded that if the base shear vs. displacement relation at any location in a MDF system subjected to any arbitrary distribution of lateral forces is given, it is possible to convert them to Δ^* and C_c^* capacity

as a companion to the S_d vs. S_a demand format by using the transformation mentioned in Eq. 2.25 and Eq. 2.29, respectively.

Creating a pushover curve includes the application of a force (applied laterally on the structure) or a lateral displacement incrementally to build the base shear-displacement curve which can be converted to a C_c^* vs. Δ^* curve. The intersection of this curve with the S_a vs. S_d response spectrum is the performance point which gives the demand displacement. However, the conventional response spectrum (S_a vs. T) can be converted to acceleration-displacement response spectrum (S_a vs. S_d).

It also becomes clear that the pushover mode acts like a SDF system if PF and α are assumed to be equal to unity in Eq. 2.25 and Eq. 2.29. In this case, the shear force vs. displacement curve can be used synonymously with the spectral acceleration vs. displacement (S_a vs. S_d). It can be argued that most of the commonly encountered multi-span standard bridges under large displacement essentially behave like MDF systems with a single governing mode (Dutta, 1999). This argument is considered to be the basis of the CSM. Thus, using PF and α, the transformation can be used to convert the pushover curve to the capacity spectrum curve.

2.5. Previous work on NSP

Most of the research performed within the last 2 decades focused on applying the NSP for buildings (i.e. COLA (1995); ATC (1996); FEMA-273 (1997); FEMA-356 (2000); Fajfar (2000); and Chopra and Goel (2001)). Only a few studies were published about using the NSP for seismic analysis of bridges (AlAyed, 2002). NSP is generally based on pushover analysis, which started in the early 1990s through experimental work

(Priestly and Seible, 1991). Priestly and Seible (1994) developed their procedure by applying it to a number of real assessment and retrofit situations.

In 1995, the City of Los Angeles (COLA) presented a nonlinear static procedure using what they referred to as the secant method, which uses substitute structure and secant stiffness. In this method, pushover curves are developed for each element or component in the structure. The associated element secant stiffness is determined. The force-displacement behavior of the elements at the assumed displacement level is represented by that secant stiffness. An elastic model considering the element secant stiffness is analyzed using the elastic response spectrum. If the analysis predicts a displacement different than the one used to calculate element stiffness, iteration is performed using the new displacement to calculate element stiffnesses. Iterations continue untill the displacement used to calculate the element secant stiffnesses reasonably matches the displacements predicted by the computer model.

The Applied Technology Council (ATC) (1996) published a report presenting the Capacity Spectrum Method (CSM). It was presented as nonlinear static procedure to evaluate performance of reinforced concrete buildings subjected to seismic loadings. This procedure used the pushover analysis to (1) represent the structure's lateral force-resisting capacity; (2) determine the displacement demand produced by the earthquake intensity on the structure; and (3) verify the acceptable performance level. The structure's performance is generally accepted when the structural capacity is larger than the demand required to satisfy a proper performance level. CSM was adopted by ATC (1996) to determine the demand displacement, which is defined as the maximum expected response of the building during the ground motion. In CSM, the demand displacement occurs at a

point on the pushover (capacity) curve called the performance point. This performance point is defined as the point where the seismic capacity of the structure is equal to the seismic demand imposed on the structure by the specified ground motion. Determination of the performance point requires a trial and error search. The main steps for applying the CSM method are briefly described here:

1. Develop the pushover (capacity) curve. Using nonlinear computer analyses, the structure is pushed and the relation between the base shear V and the roof displacement Δ (Figure 2.9 (a)) is plotted. This relation is named the pushover curve and can be built without iterations. However, using linear methods require iterations and many steps for developing the pushover curve.
2. Convert the pushover curve to the capacity spectrum curve (Figure 2.9 (b)) using the equation previously mentioned in NSP principles in section 2.4 (Eq. 2.25 and Eq. 2.29).
3. Convert the elastic response spectrum from its standard format (S_a vs. T) to Acceleration Displacement Response Spectrum (ADRS) format (S_a vs. S_d) (Figure 2.9(c)).
4. Determine the displacement demand. This is defined as the intersection of the capacity spectrum curve and the spectral demand curve, reduced from the elastic 5% damped design spectrum (Figure 2.9 (d)). The point of intersection represents the nonlinear demand at the same structural displacement. Iterations are needed in this step, where each iteration includes calculating updated values of the natural period T_{eq} and the effective damping β_{eff}. Based on the shape of the capacity

curve, the estimated displacement demand, and the resulting hysteretic loop, an approximate effective damping is calculated (Figure 2.10).

5. Convert the displacement demand determined from the previous step back to global roof displacement.
6. Evaluate the deformations of individual components corresponding to demand displacement with the capacity of the component. Generally, if the deformation demand in deformation-controlled components exceeds the permissible values, then the component is deemed to violate the performance criteria.

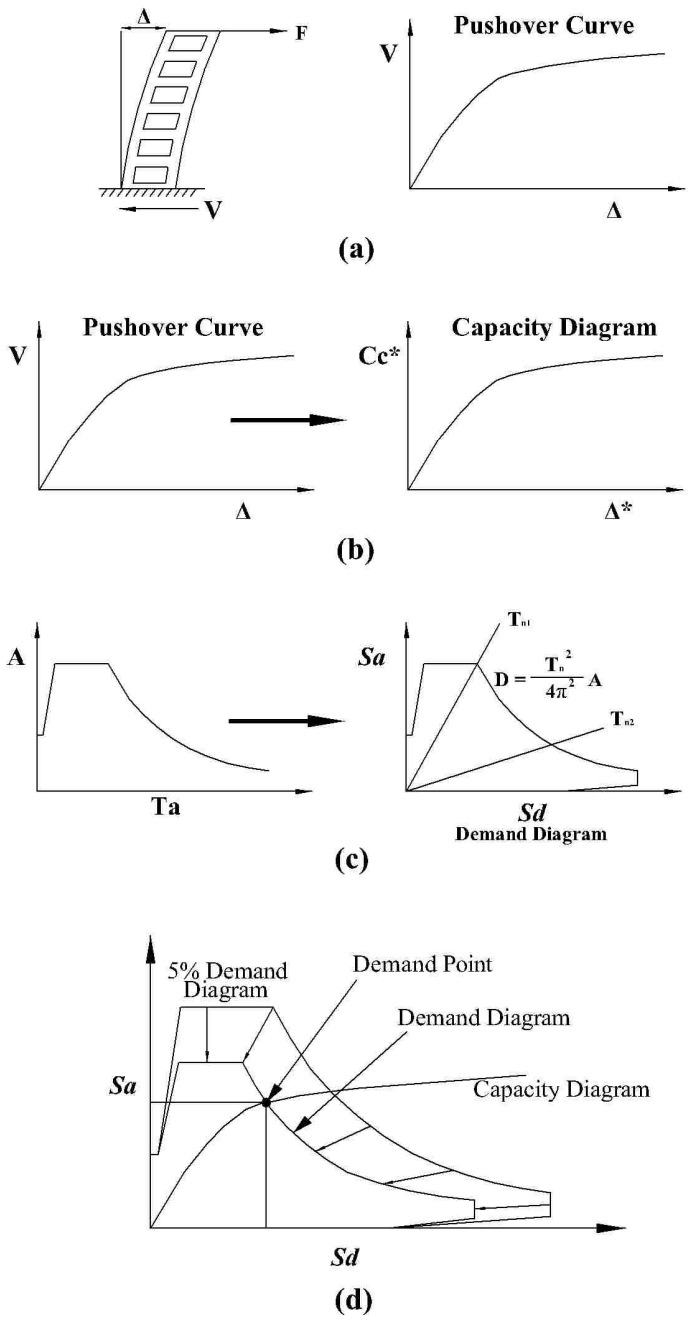

Figure 2.9 Capacity Spectrum Method (a) development of pushover curve; (b) conversion of pushover curve to capacity spectrum diagram; (c) conversion of elastic response spectrum to ADRS format; and (d) determination of the displacement demand (Chopra and Goel, 2000)

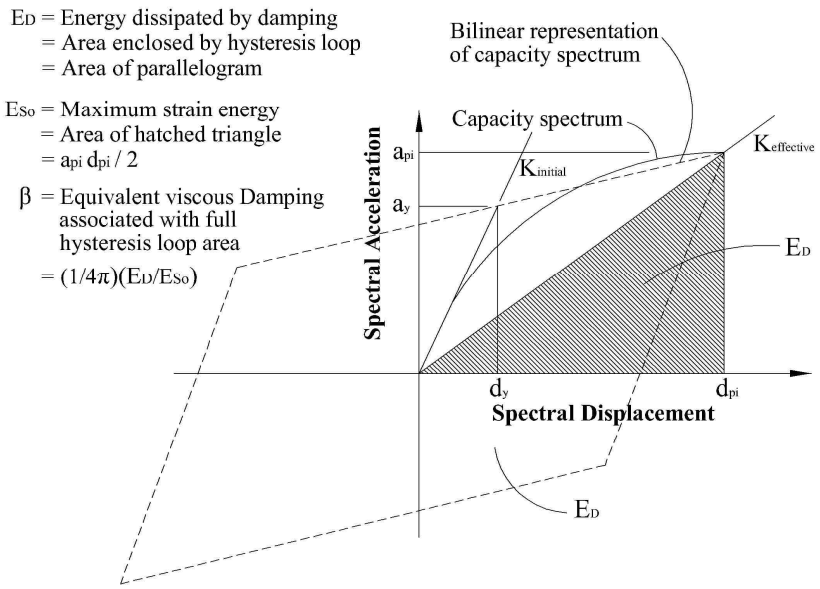

Figure 2.10 Derivation of damping for spectral reduction (ATC, 1996)

Chopra and Goel (2000) criticized the iterative method in the CSM (introduced in ATC, 1996) as it requires a sequential analysis of equivalent linear systems. They stated several deficiencies in the ATC-40 procedure (A) since this iterative procedure did not converge for some of the systems analyzed in the study. They also stated that Procedure (A) converged in many cases resulting into deformations much different than dynamic nonlinear analysis of inelastic system. The CSM procedure (B) gives the same value determined by Procedure (A) if it converges. It was stated in the study that these approximate procedures significantly underestimate the deformation for a wide range of periods and ductility factors with errors up to 50% (the estimated value is about half of the exact one). It was also mentioned that the elastic design spectrum could be used to estimate the peak deformation of an inelastic system using the well-known equal displacement rule without recourse to an iterative procedure.

FEMA-273 (1997) introduced the NEHRP Guidelines for Seismic Rehabilitation of Buildings. In those guidelines, nonlinear static procedure was presented as a simplified and efficient procedure to evaluate the seismic nonlinear response of buildings. It was stated in the guidelines that NSP may be used for any structure and any rehabilitation objective, with few exceptions. The NSP method presented there was named as the Displacement Coefficient Method (DCM). DCM was intended to be used for the evaluation of buildings only. It uses the pushover analysis and a modified version of equal displacement approximation to estimate maximum displacement demand. DCM is presented in more detail in the next chapter as it is the basis for the theoretical approach used in this study for the evaluation of the bridges.

Chopra and Goel (2001) developed a procedure based on the structural dynamics theory; they referred to this procedure as Modal Pushover Analysis (MPA) procedure. The lateral force-distribution over the building height used in the MPA is proportional to the modal shape of the elastic system as

$$s_n^* = m\phi_n \qquad \text{Eq. 2.31}$$

where s_n^* is the modal inertia force distribution, m is the mass matrix of the system, and ϕ_n is the modal shape vector for the nth mode shape. To estimate the peak response r_{n0} due to the individual modal terms $Q_{eff,n}(t) = -s_n \ddot{q}_g(t)$, pushover analysis was used, where $s_n = \Gamma_n m \phi_n$ and Γ_n is defined in Eq. 2.9. Considering the nonlinear analysis of the structure subjected to lateral forces distributed over the building height in accordance with s_n^*; then the structure is pushed to a roof displacement of u_{rn0}. The value of the roof displacement can be calculated as:

$$q_{rn0} = \Gamma_n \phi_{rn} u_n \qquad \text{Eq. 2.32}$$

where u_n is the peak value of $u_n(t)$ that can be determined by solving the equation of motion for the inelastic system or from the inelastic response (design) spectrum (Chopra, 2001). At this roof displacement, the pushover analysis provides an estimate of the peak value r_{n0} of any response $r_n(t)$. The response value r_{n0} is an estimate of the response peak value of the inelastic system to $Q_{eff,n}$ governed by the equation of motion or response spectrum for inelastic system. The total demand r_0 is obtained by the combination of the $r_{n0}(n = 1,2,3,....)$ according to an appropriate modal combination rule.

Whittaker *et al.* (1998) performed a study, after the development of the DCM by FEMA-273 (1997), for the purpose of evaluating the validity of this method to predict the demand (target) displacement. The authors studied the effect of different modification factors implemented in the DCM to modify the target displacement as shown in Eq. 3.4. They concluded that the assumption of having the mean inelastic displacement of the bilinear system equal to the mean elastic displacement is reasonable when the period T_e is greater than T_S (where T_e and T_S are defined in Eq. 3.3 and Eq. 3.7, respectively). When $T_e > T_0$, the factor C_1 (Eq. 3.7 & Eq. 3.8) is used by FEMA-273 (1997) to account for the possibility that the mean inelastic displacement exceeds mean elastic displacement.

Chopra *et al.* (2001) performed an important study in which they investigated the basic premise of determining the roof displacement of a multistory building from the deformation of a SDF system. This assumption was used with some modifications by the FEMA-273 (1997) for the estimation of the target displacement (as will be thoroughly

discussed in the next chapter). In this study, the authors concluded that the previous method is biased in the estimation of the median roof displacement. The nature and magnitude of that bias is based on how far the structure has gone into the inelastic range, characterized by the overall ductility demand. For larger ductility demands, that assumption (which is determining the roof displacement of a multistory building from the displacement of a SDF system) overestimates the median roof displacement and this bias increases for longer-period systems. The situation is reversed for small ductility demands. The authors also concluded that the bias in the SDF estimate of roof displacement increases when the P-Δ effects, due to gravity loads, are included.

A procedure was proposed by Bracci *et al.* (1997) to evaluate the seismic performance and retrofit of existing low-to-mid rise concrete buildings. This procedure was based on developing a range of site-specific demand curves and comparing them to the computed pushover capacities at each story level of the structure. In this method, pushover curves are plotted for each story level as the story shear vs. drift of that story and this is considered as the main difference between this method and other aforementioned methods such as CSM, DCM and MPA introduced by ATC (1996), FEMA-273 (1997) and Chopra and Goel (2001), respectively.

Elnashai (2001) presented a study where he explored possible development ways that may improve the applicability of the NSP to predict the nonlinear response of structures. He stated that no one load pattern distribution is capable of representing the dynamic response throughout the full displacement range. He proposed an adaptive load pattern to improve the current representation of the seismic inertia force by static loadings. He referred to the current methods of load pattern application as the conventional method

and the adaptive method as the advanced method. The results of his adaptive method, which implemented an incremental updating for the force vector, were closer to the NDP than the constant force vector. However, the constant force vector is easier and directly applicable.

CSM was implemented by Shinozuka *et al.* (2000) in the analysis of girder bridges to develop fragility curves. Their study is considered as one of the first that applied the nonlinear static procedure to bridges instead of buildings. They applied lateral forces in proportion to the fundamental mode shape as

$$F_i = \left(\frac{w_i \phi_i}{\sum_{i=1}^{N} w_i \phi_i} \right) V \qquad \text{Eq. 2.33}$$

Where F_i is the lateral force of node $i (i = 1,2,....,N)$; w_i is the dead weight assigned to node i; ϕ_i is the amplitude of the fundamental mode at node i; V is the base shear ; and N is the number of nodes. The results of this method were compared to the nonlinear time-history analysis method in the form of fragility curves. The comparison of fragility curves developed using both methods shows an excellent agreement at least for minor damage states. For major damage states, because the nonlinearity plays a main role in this stage, the agreement between the two methods was low. Considering the number of assumptions in the fragility curves development, they considered that the agreement is adequate even for the major damage state. Despite the importance of this study in the contribution for the NSP application on bridges, it does not show any comparison between different key points such as base shear, plastic hinge rotations, or displacements.

Nonlinear static procedures were also implemented in a study by Fenves and Ellery (1998). In this study, pushover analysis was used to estimate the capacity of the piers. They were able to define the performance level for each component and accordingly determined the most likely cause of failure. They found that before reaching the target displacement produced by the earthquake, the shear capacity curve intersects with the capacity (pushover) curve. This, in turn, causes the failure of that pier. Their pushover curves were plotted for each pier individually rather than plotting one pushover curve for the entire bridge.

A methodology to perform seismic fragility analysis of structures and produce fragility curves was proposed by Hwang and Huo (1998). They used the displacement-based approach, which can be considered as an equivalent approach to pushover analysis. In this approach, displacement demand is compared to the displacement capacity, which can be represented by the pushover curve.

Dutta (1999) adopted the nonlinear static analysis using the CSM. Given the complete capacity curve obtained from the pushover analysis, he applied the capacity demand spectral approach to evaluate the magnitude of the ground acceleration. He also applied uncertainty to this approach to develop fragility curves.

Pushover analysis was also used for the development of fragility curves for buildings and bridges by Barron (2000). He estimated the capacity of the structures using static pushover analysis and compared that with the dynamic pushover analysis. In dynamic pushover analysis, capacity is estimated for increasing inertia forces. The dynamic pushover analysis can approximately be obtained from the dynamic analysis using increasing amplitudes of time-history accelerations. In his study, to account for inelastic

response of the structure, Barron implemented updating stiffness of the structure after each yield point and modal distribution of forces based on the updated mode shape.

Fu and AlAyed (2003) implemented the nonlinear static analysis on a bridge using the Displacement Coefficient Method (DCM) and compared its results to the nonlinear dynamic analysis. They applied three different load patterns in the NSP to represent the inertia forces resulting from earthquakes, and used nine different time-histories to perform the NDP. They also used two levels of earthquakes in the analyses, the Design Earthquake Level and the Maximum Considered Earthquake (MCE) level. Their comparison showed that the nonlinear static analysis gives conservative results compared to the nonlinear dynamic analysis in the Design Earthquake level and even more conservative results in the MCE level.

2.6. Performance-based approach

There is a strong relationship between performance-based design and pushover analysis. Pushover analysis is an important tool to perform performance-based design (AlAyed, 2002). Accordingly, this section is intended to discuss the performance-based approach.

Performance-based approach is a general design philosophy in which the design criteria are expressed in terms of achieving stated performance objectives when the structure is subjected to stated levels of seismic hazard. The performance targets may be a level of stress not to exceed, a load, a displacement, a limit state or a target damage state (Ghobarah, 2001).

The current requirements are based on the importance of the structure, the level of deformation imposed on the structure, soil conditions, and the ductility of its structural

members, especially piers and supports. Performance-based design is focused on meeting a performance objective, which corresponds to the desired level of service. A performance level can be defined as the expected behavior of the structure under the application of the design earthquake; it consists of a combination of damage states to structural and non-structural components (FEMA-356, 2000). Unlike buildings, bridges contain fewer nonstructural elements, thus the nonstructural damage may not be included in choosing the performance level. The performance-based approach has been recently implemented widely across the United States. Different levels of performance, ranging from "fully operational" to "near collapse" can be used to meet post-earthquake conditions.

The Structural Engineering Association of California (SEAOC) (1995), Vision 2000 committee, defined the performance-based engineering as "*consisting of the selected design criteria appropriate structural systems, layout, proportioning and detailing for a structure and its nonstructural components and contents, and the assurance and control of construction quality and long term maintenance, such that at specified levels of ground motions and with defined levels of reliability, the structure will not be damaged beyond certain limiting states or other usefulness limits*". Four performance levels for buildings subjected to earthquake design levels were introduced by the SEAOC (1995). Performance levels can be described as fully operational, operational, life safety, and near collapse. These performance levels correspond to earthquake design levels that can be expressed as frequent, occasional, rare, and very rare, respectively. Each of these design levels is based on a specific recurrence period of 43, 72, 475, and 970 years, respectively. Performance-based seismic design criteria were proposed by different researchers.

Saiidi (1997) proposed three performance levels for bridge seismic design. These levels are: (1) operational without interruption to traffic flow; (2) operational with minor damage; and (3) near collapse.

AASHTO (2007) specifications categorized bridges into three categories according to the bridge importance, these categories are: (1) critical bridges, which must remain open to all traffic after the design earthquake (which is defined as a 475-year return-period event) and be usable by emergency vehicles and for security/defense purposes after a large earthquake (which is defined as a 2500-year return-period event); (2) essential bridges, which should, as minimum, be open to emergency vehicles and for security defense purposes immediately after the design earthquake; and (3) other bridges, which have lower importance than critical and the essential ones, and accordingly lower performance standards.

ATC-18 (1997) presented two levels of design earthquakes and ground motions, based on them, two levels of service were recommended. The two levels of earthquakes are: (1) functional-evaluation ground motion, which is defined as an event having a probability of occurrence of 30-50% during the design life of the structure; (2) safety-evaluation ground motion, which is defined as an event having the probability of occurrence of 10% during the design life of the structure. The first recommended level of service is the immediate service level, which corresponds to the first ground motion level. It requires full access of normal traffic almost immediately after the earthquake. The second is the limited service level, which corresponds to the second ground motion level. It permits reducing access due to lane closures or restriction of emergency traffic only, while full service is restorable within months.

The California Department of Transportation (Caltrans) (1999) categorized bridges according to their desired level of performance into ordinary and important bridges. Two levels of earthquake loading were introduced:

1- Functional-evaluation ground motion, which may be assessed either deterministically or probabilistically, where the determination of this event is to be reviewed by a Caltrans consensus group.

2- Safety-evaluation ground motion, which may be assessed either deterministically or probabilistically. The deterministic assessment corresponds to the Maximum Credible Earthquake. The probabilistic ground motion for the safety evaluation typically has a long return period (approximately 1000-2000 years).

Two service levels were defined as Immediate and Limited. Immediate service level requires full access to normal traffic almost immediately following the earthquake. The Limited service level permits lane closure and access reduction or restrictions to emergency traffic only and full service is restorable after months. Three damage levels were also defined as minimal, repairable and significant.

Floren and Mohammadi (2001) proposed three levels of performance in seismic design of bridges. They can be described as (1) immediate service (operational without interruption to traffic flow), where minimal damage has occurred, minor inelastic response may occur, damage is restricted to narrow flexural cracking in concrete and permanent deformations are not apparent; (2) limited service (operational with minor damage), where some structural damage has occurred, concrete cracking, reinforcement yield, and minor spalling of concrete cover is evident due to inelastic response; (3) collapse prevention, where significant damage has occurred, concrete cracking,

reinforcement yield, and major spalling may require closure for repair. They categorized the bridges as critical, important, and ordinary. They also used the same earthquake design levels presented by the SEAOC Vision 2000 committee.

Hwang and Hou (1998) used previous work done by other researchers to define limit states. They proposed four damage states for buildings. Their damage states are defined by implementing the displacement-based approach using the inter-story drift ratio (δ) as:

1- No damage state, when δ is less than 0.2%.

2- Insignificant damage state, for δ ranging between 0.2 and 0.5%.

3- Moderate damage state, for δ ranging between 0.5 and 1%.

4- Heavy damage state, when δ is more than 1%.

FEMA-356 (2000) presented many performance levels for buildings, including structural and nonstructural components. Four levels were presented for damage control and performance as: (1) operational; (2) immediate occupancy; (3) life safety; and (4) collapse prevention. Only three levels were concerned with structural elements performance. These levels are (1) immediate occupancy; (2) life safety; and (3) collapse prevention. A damage state description for each structural element is presented, depending on the element (being primary or secondary element in the structural system), in addition to the plastic hinge rotation, the percentage of the drift, or the strain reached by the element deformation. Other tables are presented for the non-structural elements. A more detailed description for the FEMA-356 (2000) performance levels and evaluation procedures is presented in the next chapter as the NSP of this document is used for the evaluation of the bridges in this work.

CHAPTER 3

THEORETICAL APPROACH

3.1. Introduction

FEMA-356 (2000) presented the "Prestand and Commentary for the Seismic Rehabilitation of Buildings", which included a nonlinear static procedure and presented it as a simplified and efficient procedure to evaluate seismic nonlinear response of buildings. The DCM was first introduced in the FEMA-273 (1997) then was developed and applied for bridges by AlAyed (2002). In this bridge evaluation process, the DCM presented in FEMA-356 (2000) will be used with the same modification used by AlAyed (2002). DCM uses pushover analysis and a modified version of the equal displacement demand; it needs no iterations to determine the displacement demand as it implements coefficients to modify the elastic displacement.

In the pushover analysis concept, a model incorporating the inelastic response of the structural elements is developed. The load-deformation characteristics of individual components and elements are directly defined in the model. The structure is then displaced under monotonically increasing load or displacement, through a specific load pattern, until either the target displacement is exceeded or the structure becomes unstable. The resulting internal deformations and forces are determined and compared to the acceptance criteria for the nonlinear procedures presented in the FEMA-356 (2000). The target displacement is intended to represent the maximum displacement likely to be experienced by the structure under the considered earthquake intensity. Because the

mathematical model accounts directly for effects of material inelastic response, the calculated internal forces are assumed to be a reasonable approximation of those expected during the earthquake. The target displacement may be calculated by any procedure that accounts for the effects of nonlinear response on displacement amplitude. FEMA-356 (2000) presented a procedure that can be used to calculate the target displacement for buildings.

3.2. Lateral Load Patterns

FEMA-356 (2000) specified the applied lateral load to the building model in profiles that approximately simulate the likely distribution of the inertia forces in an earthquake. For all analyses, at least two vertical distributions of lateral load shall be applied. One pattern shall be selected from the following two groups (FEMA-356, 2000):

1. A model pattern selected from the following:
    a. Equivalent lateral force (ELF) pattern: Using the vertical distribution factor (defined in equation (3-12) in FEMA-356 (2000)) then distributing the force on the different floors. This pattern may be used if more than 75% of the total mass participates in the fundamental mode of the direction under consideration.
    b. A distribution proportional to the shape of the fundamental mode in the direction under consideration. Use of this distribution shall be permitted only when more than 75% of the total mass participates in this mode.
    c. A distribution proportional to the story shear distribution calculated by combining modal responses from a response spectrum analysis of the

building, including sufficient modes to capture at least 90% of the total building mass, and using the appropriate ground motion spectrum.

2. A second pattern selected from the following (FEMA-356, 2000):
    a. A uniform distribution of lateral forces at each level proportional to the total mass at each level.
    b. An adaptive load distribution that changes as the structure is displaced. The adaptive load distribution shall be modified from the original load distribution using a procedure that considers the properties of the yielded structure.

For each evaluated bridge, two load patterns were selected from the aforementioned ones. The first pattern is (a) in the second group. It is based on lateral forces that are proportional to the total mass assigned to each node with accordance to the deck mass distribution. The equation used in the force distribution on the nodes is:

$$F_i = m_i \times g \qquad \text{Eq. 3.1}$$

where F_i is the lateral force at node $i(i = 1,2,...,N)$, N is the number of nodes, m_i is the mass assigned to node i, and g is the ground acceleration. It is considered as the primary load pattern and is intended to emphasize the base shear rather than giving high moments or deformations (AlAyed, 2002). This pattern will be referred to as the "Uniform Load Pattern".

The second pattern is (b) in the first group. It represents the deformation of the structure (or the bridge) in its fundamental mode. The equation on which the distribution is based is given as:

$$F_i = \left(\frac{m_i \delta_i}{\sum_{i=1}^{N} m_i \delta_i} \right) V \qquad \text{Eq. 3.2}$$

where F_i, m_i and N are the same as defined in the first load pattern, Eq. 3.1, and V can be taken as an optional value since the distribution of the forces is the important part, while the value is increased incrementally until it reaches the prescribed target displacement or collapse occurs. This process should be done using the fundamental mode shape, which has 75% or more of the total mass participating in it. The fundamental mode is considered to have the highest contribution of all modes to the final deformation of the structure (or the bridge) under the earthquake load. In the analyses of this work, this pattern will be referred to as the "Modal Pattern".

3.3. Estimation of Target Displacement

The effective fundamental period in the direction under consideration is based on the idealized force-displacement curve described in Figure 3.1. The nonlinear force-displacement relationship between the base shear and displacement of the control node is replaced with an idealized relationship to calculate the effective stiffness, K_e, and effective yield strength, V_y, of the structure. This relationship is bilinear, with initial slope K_e and post yield slope α. The effective lateral stiffness, K_e, is taken as the secant stiffness calculated at a base at a base shear force equal to 60% of the effective yield strength of the structure. The post yield slope, α, shall be determined by a line segment that passes through the actual curve at the calculated target displacement and the effective yield strength shall not be taken the maximum base shear force at any point along the actual curve. The effective fundamental period, T_e, will be calculated as:

$$T_e = T_i \sqrt{\frac{K_i}{K_e}} \qquad \text{Eq. 3.3}$$

where T_i is the elastic fundamental period (in seconds) in the direction under consideration calculated by elastic dynamic analysis, K_i is the initial slope of the original pushover curve, K_e is as defined before. K_e and K_i are shown in Figure 3.1.

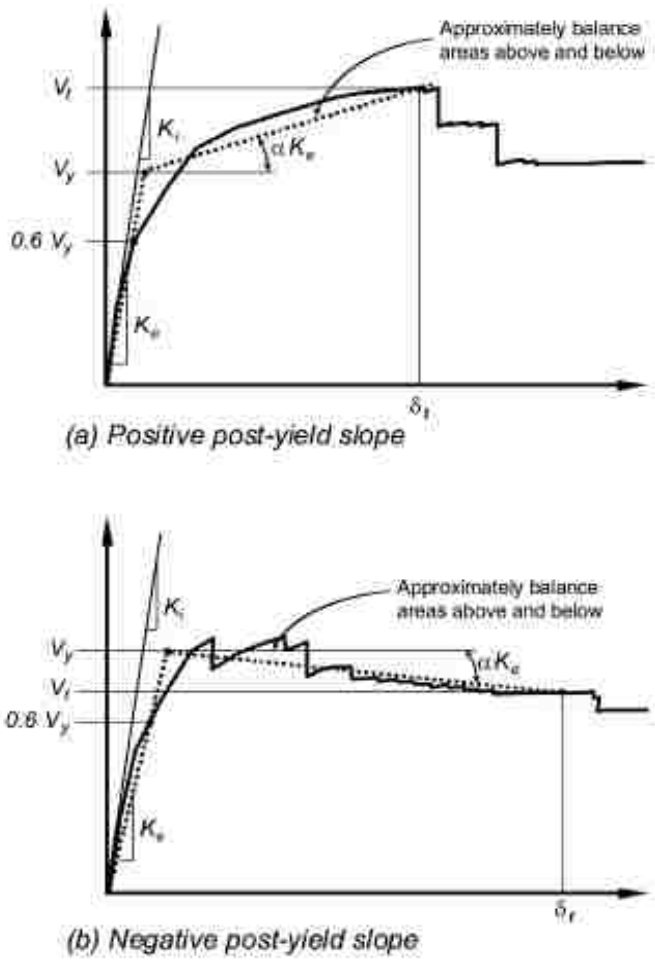

Figure 3.1 Idealization of force-displacement curves (FEMA-356, 2000)

The relation between the base shear and the displacement of the control node shall be established for the displacement of control node ranging between zero to 150% of the

target displacement, δ_t. The target displacement formula used in the FEMA-356 (2000) procedures is as follows:

$$\delta_t = C_0 C_1 C_2 C_3 S_a \frac{T_e^{\,2}}{4\pi^2} g \qquad \text{Eq. 3.4}$$

where:

T_e = effective fundamental period of the structure for the direction under consideration as defined in Eq. 3.3

C_0 = modification factor to relate spectral displacement of an equivalent SDOF system to the roof displacement of the building MDOF system. It is calculated using one of the following procedures:

a. The first modal participation factor at the level of control node

$$C_0 = PF_1 \times \phi_{CN,1} = \left(\frac{\sum_{i=1}^{N} (w_i \phi_{i,1}) / g}{\sum_{i=1}^{N} (w_i \phi_{i,1}^{\,2}) / g} \right) \times \phi_{CN,1} \qquad \text{Eq. 3.5}$$

where w_i is the tributary weight at the location i varying from the 1 to N being the total number of discrete weights for the pushover mode shape locations, $\phi_{i,1}$ is the amplitude of node i for mode 1, and $\phi_{CN,1}$ is the amplitude of mode 1 at the control node.

b. The modal participation factor at the level of control node calculated using a shape vector corresponding to the deflected shape of the building at the target displacement.

$$C_0 = \left(\frac{\sum_{i=1}^{N} (w_i \delta_{i,1}) / g}{\sum_{i=1}^{N} (w_i \delta_{i,1}^{\ 2}) / g} \right) \times \delta_{CN,1} \qquad \text{Eq. 3.6}$$

where w_i is the same as the previous step, $\delta_{i,1}$ is the amplitude of the shape vector at joint i, and $\delta_{CN,1}$ is the amplitude of the shape vector at the control node.

c. The appropriate value from Table 3.1.

Table 3.1 Values for the modification factor C_0 (FEMA-356, 2000)

Number of stories	1	2	3	5	10
Modification factor C_0	1.0	1.2	1.3	1.4	1.5

C_1= modification factor to relate expected maximum inelastic displacements to displacements calculated for linear elastic response

$= 1.0$ for $T_e \geq T_s$ Eq. 3.7

$= [1.0 + (R - 1)\, T_s / T_e] / R$ for $T_e < T_s$ Eq. 3.8

T_s = characteristic period of the response spectrum, defined as the period associated with the transition from the constant acceleration segment of the spectrum to the constant velocity segment of the spectrum (Figure 3.4).

The factor C_1 is intended to account for the difference in peak displacement response amplitude for nonlinear response as compared to linear response, as observed for

buildings with relatively short initial vibration periods. The short initial vibration period is defined as the time periods that are less than T_s as shown in Eq. 3.8.

R = ratio of elastic strength demand to calculated yield strength coefficient, it is calculated as

$$R = \frac{S_a}{V_y / W} C_m \qquad \text{Eq. 3.9}$$

where C_m is the effective mass factor to account for the higher mode mass participation effects obtained from Table 3.2 and shall be taken as 1 if the fundamental period, T_e, is greater than 1.0 second.

Table 3.2 Values for Effective Mass Factor C_m (FEMA-356, 2000)

No. of stories	Concrete Moment Frame	Concrete Shear Wall	Concrete Pier-Spandrel	Steel Moment Frame	Steel Concentric Braced Frame	Steel Eccentric Braced Frame	Other
1-2	1.0	1.0	1.0	1.0	1.0	1.0	1.0
3 or more	0.9	0.8	0.8	0.9	0.9	0.9	1.0

Eq. 3.9 was changed in the FEMA-356 (2000) from the equation used in the older version (FEMA-273, 1997) as it used to have the factor $(1/C_0)$ instead of the factor C_m. AlAyed (2002) proposed a modification to this equation (the older version of the equation) to be:

$$R = \frac{S_a}{V_y / W} \frac{1}{C_0} \leq \frac{S_a}{V_y / W} \qquad \text{Eq. 3.10}$$

The reason for such modification is that C_0 is the only factor that is affected by the location of the control node. When the control node is far from the maximum

displacement point and has a smaller displacement value, the value of C_0 will be small, which may amplify the value of R many times. A higher value of R may amplify the values of C_1 and C_3. As a preliminary estimation, values of C_0 range from 1.0 to 1.5 (Table 3.1). Based on this fact, AlAyed (2002) added the condition in Eq. 3.10 to prevent the unnecessary amplification of the R factor. Unlike buildings, bridges don't have a defined control node (which is defined in buildings as the center of mass of the roof level), and accordingly, this modification is very important in case of bridges. In the current bridge evaluation process the modified equation of AlAyed (2002) (Eq. 3.10) will be used because he included a numerical example that illustrated the estimation of target displacement when the control node is different from the point of maximum displacement.

S_a = response spectrum acceleration, g, at the effective fundamental period and damping ratio of the structure in the direction under consideration. The value of S_a will be discussed later as well as the earthquake level used in the evaluation process.

V_y = yield strength calculated using results of the NSP for the idealized nonlinear force-displacement curve developed for the structure (Figure 3.1).

W = effective seismic weight of the structure (discussed in section 4.2.3).

C_2 = modification factor to represent the effect of pinched hysteretic shape, stiffness degradation and strength deterioration on maximum displacement response. Values of C_2 for different framing systems are presented in the FEMA-356 (2000) as shown in Table 3.3.

Table 3.3 Values for modification factor C_2 (FEMA-356, 2000)

Performance Level	T = 0.1 second *		$T \geq T_0$ second *	
	Framing Type 1[1]	Framing Type 2[2]	Framing Type 1[1]	Framing Type 2[2]
Immediate Occupancy	1.0	1.0	1.0	1.0
Life Safety	1.3	1.0	1.1	1.0
Collapse Prevention	1.5	1.0	1.2	1.0

1 Structures in which more than 30 % of the story shear at each level is resisted by components or elements whose strength and stiffness may deteriorate during the design earthquake.
2 All frames not assigned to framing type1.
* Linear interpolation may be used for periods between 0.1 and T_0.

C_3 = modification factor to represent increased displacements due to dynamic P-Δ effects, for buildings with positive post-yield stiffness, C_3 shall be taken as 1.0. For buildings with negative post-yield stiffness, C_3 shall be calculated using Eq. 3.11. Values for C_3 have an upper limit set in section 3.3.1.3 of FEMA-356 (2000)

$$C_3 = 1.0 + \frac{|\alpha|(R-1)^{3/2}}{T_e} \qquad \text{Eq. 3.11}$$

where R and T_e as defined above and α is the ratio of post-yield stiffness to effective elastic stiffness, where the nonlinear force-displacement relationship shall be characterized by a bilinear relation as shown in Figure 3.1.

g = gravitational acceleration.

3.3.1. Control node

Control node for buildings is defined as the center of mass of the roof level (FEMA-356, 2000). There is no precise definition for the control node in the ATC (1996) as it considered the roof floor to be moving as a rigid body. In general, the roof displacement for the building is known to be the maximum displacement. This is not applicable for bridges as bridges extend horizontally while buildings extend vertically. This means that

the important dimension for buildings is the vertical dimension; as its main restraint is at the base. However, for bridges, the important dimension is the horizontal one as its main restraints are at the abutments (AlAyed, 2002).

Control node is defined as the node used to monitor the displacement of the structure. Its displacement versus the base shear forms the capacity (pushover) curve of the structure. Two conditions shall be satisfied in the selection of the control node: (1) its location is expected to have the maximum displacement; (2) its displacement is reflecting the behavior of the structure (AlAyed, 2002). These two conditions mean that the control node displacement is affected by the inelastic behavior of any member that contributes to the stiffness of the structure in the direction under consideration. The second condition is an essential one and it may cause significant error if it is not satisfied. However, the first condition seems to be more flexible.

In bridge analysis, two horizontal directions should be considered in the earthquake load application, longitudinal and transverse directions. In the longitudinal direction, the bridge usually moves as a rigid body, which gives the same displacement value for all bridge nodes, if neglecting axial deformations. Accordingly, the selection of the control node is straightforward.

In the transverse direction, the boundary conditions of the bridge at the abutments are the main factors that affect its final deformed shape. When the bridge is restrained at both ends, it will deform in the shape of a simply supported beam. In this case the control node will be the center of mass of the bridge. However, if the bridge is non-symmetric, the point of maximum displacement will be shifted. Accordingly, it is necessary to use the

modification of the equation of the *R* ratio that was previously explained in the estimation of the target displacement.

3.4. Performance level

The main objective of performance-based design is the performance evaluation. A component or an action is considered satisfied if it meets a prescribed performance level. The deformation demands are compared to the maximum permissible values for the components for the deformation-controlled actions. For the force-controlled actions, the force demand is compared to the strength capacity. If either the deformation demand in a deformation-controlled element, or force demand in a force-controlled element, exceeds the permissible values, then the element is deemed to violate the performance criteria.

As mentioned in the previous chapter, FEMA-356 (2000) introduced three structural performance levels of evaluation to the structural components. These levels are: (1) Immediate Occupancy (IO), which is defined as the post-earthquake damage state that remains safe to occupy, essentially retains the pre-earthquake design strength and stiffness of the structure. In this level of performance, only limited structural damage occurs. (2) Life Safety, which is defined as the post-earthquake damage state that includes damage to structural components but retains a margin against onset of partial or total collapse. In this level of performance, significant damage to structural components may occur, injuries may take place during the earthquake. However, the overall risk of life threatening injury is expected to be low. Reoccupying the structure is not guaranteed immediately after the earthquake. Some structural repairs may need to be implemented or some bracing members may need to be installed. (3) Collapse Prevention, which is defined as the post-earthquake state that includes damage to structural components such

that the structure continues to support gravity loads but retains no margin against the collapse. In this level of performance, substantial damage to structure occurs, including significant degradation in the stiffness and strength of the lateral resisting system. Nonetheless, all significant components of the gravity-load-resisting system must continue to support their gravity load demands. Significant risk of injury due to falling structural debris may exist. The structure may not be safe to reoccupy and technically impractical to be repaired.

The choice of the required level of performance is based on the choice of the rehabilitation objective. FEMA-356 (2000) presented three rehabilitation objectives defined as the Basic, Enhanced and Limited objectives. The Basic Safety Objective (BSO) is a rehabilitation objective that achieves the dual rehabilitation goals of life safety level performance for the Basic Safety Earthquake-1 (BSE-1) hazard level and the collapse prevention level performance for the Basic Safety Earthquake-2 (BSE-2) hazard level. These two levels of earthquake will be defined in the next section of this chapter. The Enhanced Rehabilitation Objective is the term that is used for rehabilitation objective exceeding the BSO. It shall be achieved using one or a combination of the following two methods (FEMA-356, 2000):

1- Designing for target building performance levels that exceed those of the BSO at either the BSE-1 or BSE-2 hazard levels, or both.
2- Designing for the target building performance levels of the BSO using an earthquake hazard level that exceeds either the BSE-1 or BSE-2 hazard levels, or both.

The Limited Rehabilitation Objective is the term used for rehabilitation that provides building performance less than that of the BSO. Limited rehabilitation objective shall be achieved using either reduced rehabilitation or partial rehabilitation. Reduced rehabilitation addresses the entire building structural and nonstructural elements, but with lower seismic hazard. However, partial rehabilitation objective addresses a portion of the building without considering the complete lateral-force-resisting system (FEMA-356, 2000).

FEMA-356 (2000) also introduced different performance levels for non-structural components of the buildings. Bridges, unlike buildings, contain fewer nonstructural elements. Accordingly, the performance levels for nonstructural damage may be neglected (AlAyed, 2002). In the bridges evaluation process of this study, due to the high importance of the bridges, the Enhanced Rehabilitation Objective was chosen. A target performance level of immediate occupancy at BSE-2 was selected. These bridges, in accordance with its high importance, should be fully operational without interruption to traffic flow and without lane closure. The performance level will be applied only to the bridge substructures (piers or columns), where the plastic hinges are defined. However, the bridge superstructure (bridge deck) is assumed to behave elastically under earthquake loads (AlAyed, 2002).

3.5. Seismic loading (Design response spectrum)

To perform the NSP analysis of structures using the DCM, design response spectra should be available to estimate the factor S_a (spectral acceleration). This factor is an essential step in the calculation of the target displacement as it represents the level of earthquake used in the evaluation in addition to the structure location effect and site

condition (soil effects). FEMA-356 (2000) implements hazard maps to estimate parameters used to develop design response spectrum. Two earthquake levels are defined in FEMA-356 (2000); the first one is the Basic Safety Earthquake-1 (BSE-1) which has a 10% probability of exceedance in 50 years. The second level of earthquake is the Basic Safety Earthquake-2 (BSE-2) which has a 2% probability of exceedance in 50 years (It can also be expressed as 10% probability of exceedance in 250 years). This level is also referred to as the Maximum Considered Earthquake (MCE). The two levels of earthquake correspond to motions that are expected to occur, on average, about once every 500 and 2500 years respectively (FEMA-356, 2000).

In the bridge evaluation process of this investigation, only the BSE-2 level is used as mentioned, for the implementation of the Enhanced Rehabilitation Objective. Approved seismic hazard maps for the conterminous United States, provided by the United States Geological Survey (USGS), were used in this work in obtaining the short (0.2 second) and long (1.0 second) period mapped spectral acceleration for each level of earthquake. Parts of the two maps (contains only Clark County area) are presented in Figure 3.2 and Figure 3.3.

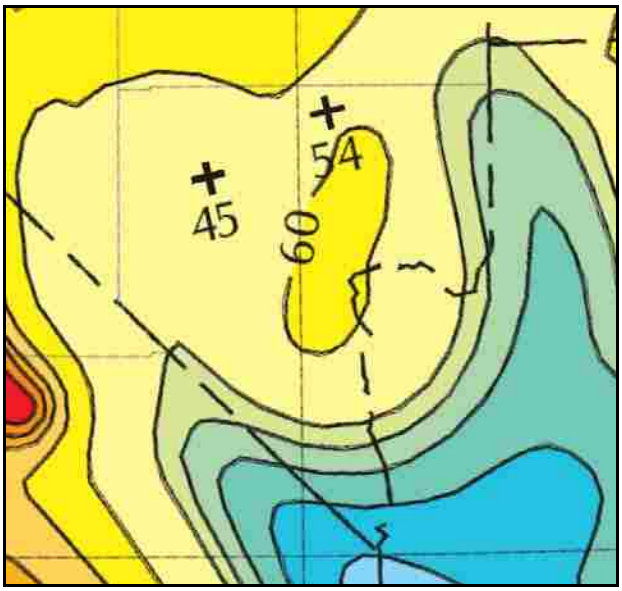

Figure 3.2 MCE's Spectral Response Acceleration for 0.2-second period (5% of critical damping) for Clark County (USGS, 2009)

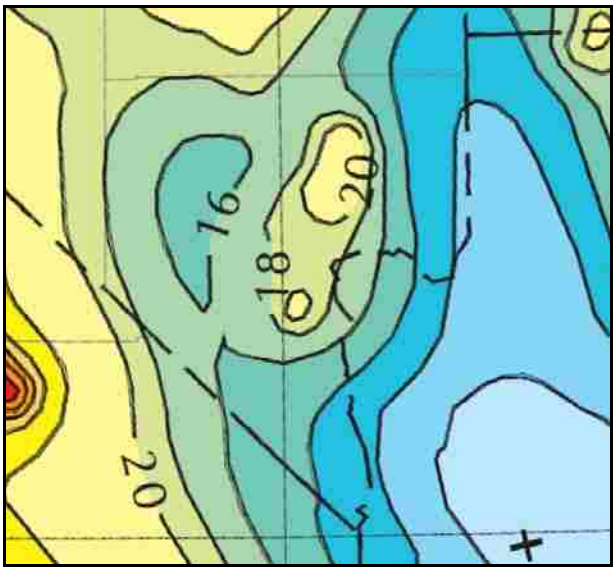

Figure 3.3 MCE's Spectral Response Acceleration for 1.0-second period (5% of critical damping) for Clark County (USGS, 2009)

The mapped spectral acceleration is then adjusted according to the bridge site classes through the following two equations:

$$S_{XS} = F_a \times S_s \qquad \text{Eq. 3.12}$$

$$S_{X1} = F_v \times S_1 \qquad \text{Eq. 3.13}$$

where S_s and S_1 are the mapped spectral accelerations extracted from the maps, S_{XS} and S_{X1} are the design short-period spectral acceleration and the design spectral acceleration response at one-second respectively, and F_a and F_v are site coefficients determined from the FEMA-356 (2000) (Tables 1-4 and 1-5) based on the site class of each bridge. The site classification input of the bridges (which is presented in the next chapter) is based on a comprehensive geotechnical study of Las Vegas valley as part of the Earthquakes in Southern Nevada (ESN) project.

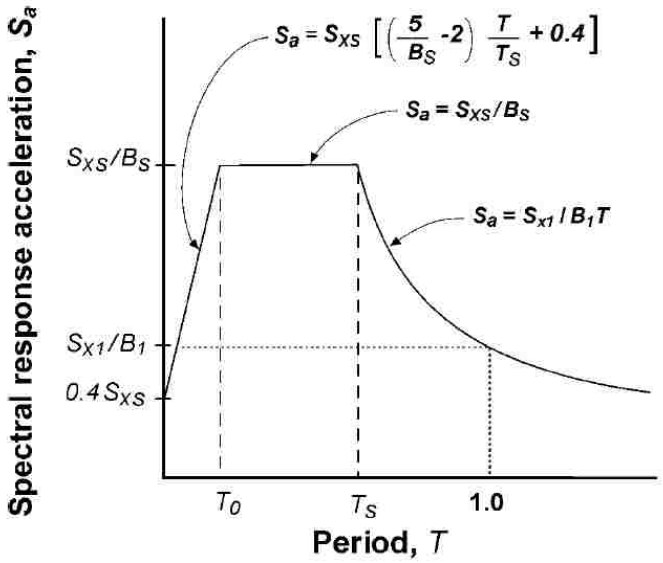

Figure 3.4 Construction of horizontal response spectrum (FEMA-356, 2000)

The horizontal response spectrum is constructed using equations shown in Figure 3.4, where the factors B_S and B_1 are the damping coefficient factors (from Table 1-6 in FEMA-356 (2000)) based on the effective viscous damping, β, chosen for the analysis.

The effective viscous damping in this work was taken as 5% as the bridges are all of concrete substructure, while 5% is a good estimation for concrete structures.

3.6. Summary of evaluation procedures

To perform the pushover analysis using the DCM method, the following step-by-step procedures are used (FEMA-356, 2000):

1. Compute the natural period of the structure for the direction under consideration using elastic dynamic analysis.
2. Define lateral load pattern from the specified load patterns mentioned before; two of them should be used in the analysis and the following steps should be repeated for each pattern.
3. The intensity of the lateral load is increased incrementally in the nonlinear analysis model and the control node displacement corresponding to each load increment is determined to plot the pushover curve (control node displacement vs. base shear force). According to the FEMA-356 (2000) specifications, the pushover curve should be established for control node displacement ranging between zero and 150% of the target displacement, δ_t.
4. The pushover curve is then idealized as a bilinear curve as shown in Figure 3.1.
5. Effective period (T_e) is calculated using Eq. 3.3.
6. Pushover curve is used to estimate the target displacement by means of Eq. 3.4. This step may require iteration if the yield strength and stiffness of the simplified bilinear relation are sensitive to the target displacement.

7. Once the target displacement is estimated, the accumulated forces and deformations at this displacement of the control node should be used to evaluate the performance of the structure components as follows:
    a. For deformation-controlled actions (e.g. flexure in beams and columns), the deformation demands are compared to the maximum permissible values for the component.
    b. For force controlled actions (e.g. shear stress and splices of reinforcement in beams and columns), the strength capacity is compared with the force demand.
8. For each action, element or component, it is considered to violate the performance criteria if either (a) the deformation demand in deformation-controlled actions, component, or elements, or (b) the force demand in the force-controlled actions, components, or elements, exceeds the permissible values.

CHAPTER 4

BRIDGES ANALYSIS AND EVALUATION

4.1. Introduction

In this chapter, a full description of the evaluation process of each bridge is presented, starting from the description of the bridge, followed by the necessary calculations for the NSP, and finally the results. Bridges are presented in the order of their importance. In section 4.2, procedures of bridges analysis and evaluation are described along with the adopted assumptions.

4.2. Modeling general assumptions

4.2.1. Spectral acceleration (S_a)

Equations for the calculations of the spectral acceleration using the FEMA-356 (2000) were discussed in the previous chapter. The inputs for the S_a calculations for the studied bridges are: (1) site classifications for the soil underneath the bridges and (2) the mapped spectral accelerations for long and short time periods for each bridge. As mentioned in the previous chapter, the mapped spectral accelerations are for the BSE-2 earthquake, with 2% probability of exceedance in 50 years. These two inputs are presented in Table 4.1.

Table 4.1 Site classifications and mapped spectral accelerations for the studied bridges

Bridge	Site Classification	Mapped Spectral Acceleration (%g)	
		S_s	S_1
G-1064	C	55.0	17.5
G-947	D	57.0	17.5
H-1211	C	55.0	17.0
G-953	D	56.5	17.5
I-2139	D	56.5	17.5

4.2.2. Bridge models

Wire frame elements (spine) were used to model the studied bridges using the SAP2000 program with the bridge module. In the transverse direction, bridges were modeled as one unit, even in the presence of expansion joints. However, in the longitudinal direction, bridges were divided into units at expansion joints (when present), and each unit is evaluated independently. In bridge engineering design, it is a common practice to divide long bridges into smaller units to alleviate the effect of thermal expansion. These units are designed to move independently in the longitudinal direction and work together in the transverse direction (AlAyed, 2002). In the analysis, each unit has its own control node and its applied inertial forces so that the pushover curve represents the base shear vs. displacement of the control node of this unit without any contribution from other units except applied loads as it may affect the columns evaluation by increasing the P-Δ effect.

In some cases of the longitudinal direction analyses of the bridge units, target displacements exceeded the values of the expansions provided between the units. In these

cases, the bridge units were still pushed to the target displacement values, because the actual behavior of the bridge deck in the vertical direction is not considered and this may increase the displaced values of the bents in the longitudinal direction.

4.2.3. Effective seismic weight

The effective seismic weight of the bridges in this work consists of the dead load and a portion of the live load. Dead load in the analyses represents the structural components with their full weights in addition to the weights of concrete barriers, pedestrian rails, wearing surfaces, etc. For the live load portion, FEMA-356 (2000) specifies a portion of the live load to be considered in the case of building evaluations, but not for bridges. For buildings, a minimum of 25% of floor live load in case of storage areas, the actual partitions load if applicable and the total operating weight of permanent equipment are required in the specifications. Live load in the current study was chosen to be 25% of the design lane load per AASHTO (2007) specifications. The design lane load is 0.64 kip/ft /10 ft wide lane. Lumped masses at the nodes of the superstructures included the additional part from the live load along with the dead load part.

4.2.4. Stiffness reduction

The stiffnesses of all elements were reduced as per the FEMA-356 (2000) specifications. Shear rigidity was reduced to 40% of its gross value for all elements. Flexural rigidity for all non-prestressed beams was reduced to 50% of its gross value. Gross flexural rigidity, with no reduction, was used for prestressed beams. For the bent columns, the effective flexural rigidity was calculated using the moment-curvature ($M-\phi$) relationship to obtain the cracked section characteristics. The proposed effective moment of inertia (I_e) by the FEMA-356 (2000) document is 0.5 to 0.7 of the gross

section moment of inertia (I_g), depending on the axial force applied on the column. The use of the $M-\phi$ relationship to evaluate the flexural rigidity of the columns is a more accurate and realistic approach compared to FEMA's approach (AlAyed, 2002).

After constructing the $M-\phi$ curve and idealizing it, the following formula for the calculation of the effective moment of inertia is used:

$$I_e = \frac{M_n}{E_c \phi_y} \qquad \text{Eq. 4.1}$$

where I_e is the effective moment of inertia for the cracked section, ϕ_y is the curvature at yield estimated using a bilinear curve to represent $M-\phi$ relationship, M_n is the nominal moment corresponding to ϕ_y and E_c is the concrete modulus of elasticity. This equation will be used for each column section to estimate its I_e.

4.2.5. Acceptance limits

4.2.5.1. Deformation-controlled actions

For deformation controlled actions, FEMA-356 (2000) expressed the acceptance criteria as deformation values for each level of performance. A generalized force-deformation relation for concrete elements and components is represented in the FEMA-356 (2000) based on the applied loads and the section properties. Table 4.2 (Table 6-8 in FEMA-356 (2000)) represents the modeling parameters and numerical acceptance criteria for columns in the nonlinear procedures. This table is used in this study to calculate the plastic hinge rotations acceptance criteria (in radians) for each of the performance levels.

The generalized load-deformation relation shown in Figure 4.1 describes the general sequence of stiffness loss of an element. A linear response from A to an effective yield at B is followed by a linear response at reduced stiffness from B to C, then a sudden

reduction in the lateral load resistance to point D, then response at reduced resistance to E, and final loss of resistance thereafter (FEMA-356, 2000). In the case of the horizontal axis of this graph taken as the plastic hinge rotation, point B should be on the vertical axis, which means that the plastic hinge rotation values of all points between A and B are equal to zero.

Table 4.2 Modeling parameters and numerical acceptance criteria for nonlinear procedures for reinforced concrete columns (FEMA-356, 2000)

Conditions			Modeling Parameters [4]			Acceptance Criteria [4]				
			Plastic Rotation Angle, radians		Residual Strength Ratio	Plastic Rotation Angle, radians				
						Performance Level				
						IO	Component Type			
							Primary		Secondary	
			A	b	C		LS	CP	LS	CP
i. Columns controlled by flexure [1]										
$\frac{P}{A_g f_c'}$	Trans. Reinf.[2]	$\frac{V}{b_w d\sqrt{f_c'}}$								
≤ 0.1	C	≤ 3	0.02	0.03	0.2	0.005	0.015	0.02	0.02	0.03
≤ 0.1	C	≥ 6	0.016	0.024	0.2	0.005	0.012	0.016	0.016	0.024
≥ 0.4	C	≤ 3	0.015	0.025	0.2	0.003	0.012	0.015	0.018	0.0025
≥ 0.4	C	≥ 6	0.012	0.02	0.2	0.003	0.01	0.012	0.013	0.02
≤ 0.1	NC	≤ 3	0.006	0.015	0.2	0.005	0.005	0.006	0.01	0.015
≤ 0.1	NC	≥ 6	0.005	0.012	0.2	0.005	0.004	0.005	0.008	0.012
≥ 0.4	NC	≤ 3	0.003	0.01	0.2	0.002	0.002	0.003	0.006	0.01
≥ 0.4	NC	≥ 6	0.002	0.008	0.2	0.002	0.002	0.002	0.005	0.008
ii. Columns controlled by shear [1, 3]										
All cases[5]			–	–	–	–	–	–	.0030	.0040
iii. Columns controlled by inadequate development or splicing along the clear height [1, 3]										
Hoop spacing ≤ d/2			0.01	0.02	0.4	0.005	0.005	0.01	0.01	0.02
Hoop spacing > d/2			0.0	0.01	0.2	0.0	0.0	0.0	0.005	0.01
iv. Columns with axial load exceeding $0.70P_o$ [1, 3]										
Conforming hoops over the entire length			0.015	0.025	0.02	0.0	0.005	0.01	0.01	0.02
All other cases			0.0	0.0	0.0	0.0	0.0	0.0	0.0	0.0

1. When more than one of the conditions i, ii, iii, and iv occurs for a given component, use the minimum appropriate numerical value from the table.
2. "C" and "NC" are abbreviations for conforming and nonconforming transverse reinforcement. A component is conforming if, within the flexural plastic hinge region, hoops are spaced at ≤ d/3, and if, for components of moderate and high ductility demand, the strength provided by the hoops (V_S) is at least three-fourths of the design shear. Otherwise, the component is considered nonconforming.
3. To qualify, columns must have transverse reinforcement consisting of hoops. Otherwise, actions shall be treated as force-controlled.
4. Linear interpolation between values listed in the table shall be permitted.
5. For column controlled shear, see section 6.5.2.4.2 for acceptance criteria.

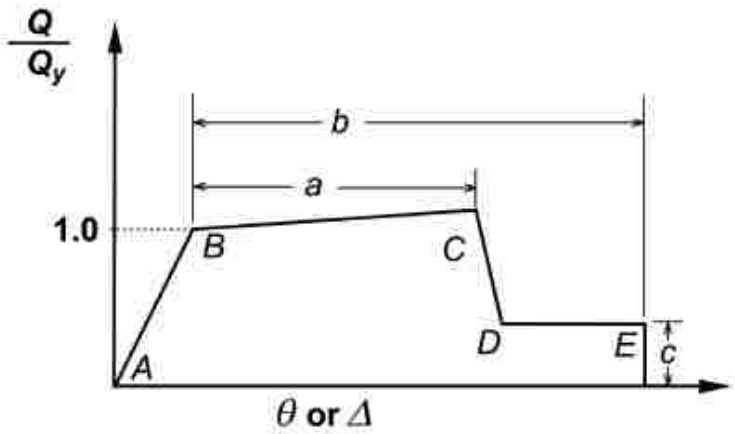

Figure 4.1 Generalized force-deformation relations for concrete elements (FEMA-356, 2000)

4.2.5.2. Force-controlled actions

Two main force controlled actions are evaluated in this study: (1) shear capacity of the columns; (2) development and splice lengths of the reinforcement. For the shear capacity calculations, FEMA-356 (2000) introduced an equation for the concrete shear strength calculation, and permitted the use of the ACI 318-08 (2008) equation. The AASHTO (2007) simplified method of calculating the shear capacity gives quite similar values to the equation used by ACI 318-08 (2008). In this study, the ACI equation for sections subjected to axial load will be used for simplicity. Shear capacity equations are as follows:

$$V_n = V_c + V_s \qquad \text{Eq. 4.2}$$

where V_n is the shear strength of the section, V_c and V_s are the the concrete contribution and the transverse reinforcement contribution to the shear strength, respectively. They are calculated using the formulas in Eq. 4.3 and Eq. 4.4.

$$V_c = 2\left(1+\frac{N_u}{2000A_g}\right)\sqrt{f_c^{'}}b_w d \qquad \text{Eq. 4.3}$$

where N_u is the axial load on the column (lbs), A_g is the gross area of the column section (in^2), $f_c^{'}$ is the concrete compressive strength (psi), b_w is the width of the concrete section (in), and d is the depth of the concrete section (in). In case of circular sections the depth of the concrete section is taken as 80% of the total depth (ACI 318-08, 2008).

$$V_s = \frac{A_v . f_{yt} . d}{s} \qquad \text{Eq. 4.4}$$

where s is the spacing of the transverse reinforcement (in), A_v is the area of the shear reinforcement within s (in^2), and f_{yt} is the yield strength of the transverse reinforcement (psi). FEMA-356 (2000) specifies that the value of V_s shall be reduced to 50% in resisting shear or torsion in case of having transverse reinforcement spacing (s) exceeding half of the member's effective depth. For the case of spacing exceeding the effective depth of the member, transverse reinforcement shall be assumed ineffective in resisting shear or torsion.

Shear force values at the target displacement for all columns are compared to the calculated values of the shear strength by Eq. 4.2. If the shear force exceeded the strength of the column, brittle failure is expected and the bent is violating the performance criteria. Concurrent multidirectional seismic effects are also considered by associating 100% of design forces and deformations of the transverse direction analysis results plus 30% of forces (not deformations) of the longitudinal direction analysis results and vice versa.

The second force controlled action evaluated in this study is the development and splice lengths of reinforcement. Two main locations within the bent are critical and subject to bond slippage under seismic loads; (1) the splice between the dowels from the foundation to the column reinforcement (if any); and (2) the beam-column (B/C) joint where the reinforcement of the column terminates. FEMA-356 (2000) refers to the ACI-318-08 (2008) development and splice length equations, which again gives quite similar values to the equations of development and splice lengths in the AASHTO (2007). The equation used in this study for the development length calculation is as follows:

$$l_d = \left(\frac{f_y \psi_t \psi_e}{20\lambda\sqrt{f_c^{'}}} \right) d_b \qquad \text{Eq. 4.5}$$

where l_d is the development length (in), f_y is the specified yield strength of reinforcement (psi), $f_c^{'}$ is the specified compressive strength of concrete (psi), ψ_t and ψ_e are factors used to modify development length based on the reinforcement location and reinforcement coating respectively, λ is a modification factor if light weight concrete is used, and d_b is the reinforcing bar diameter. The splice length in tension is taken as $1.0l_d$ for class A splice and $1.3l_d$ for class B splice, where all splice lengths are considered tension splices (FEMA-356, 2000).

For development, hook and splice lengths that do not meet the requirements of the code, FEMA-356 (2000) specifies Eq. 4.6 to calculate the capacity of the existing reinforcement at the development or splice location.

$$f_s = \left(\frac{l_b}{l_d} \right) f_y \qquad \text{Eq. 4.6}$$

where f_s is the maximum stress that can be developed in the bar for the straight development, hook, or lap splice length l_b provided, f_y and l_d are as defined before. This equation should be used for the calculations of the plastic hinge properties of the new section in case of having columns controlled by inadequate development, hook or splice lengths, and the acceptance criteria for each performance level is provided in Table 4.2.

Each of the three aspects of evaluation (which are (1) the flexural deformation; (2) the shear forces; and (3) the reinforcement development in the columns), is evaluated independently at the calculated target displacement.

4.3. Seismic evaluation of the studied bridges

4.3.1. Bridge (G-1064)

4.3.1.1. Bridge description

G-1064 is a 12-spans/11-piers bridge, located at the intersection of Sahara Avenue (overpass) and both of Industrial Road and Western Avenue (underpass). The total length of the bridge is 900.58 ft, each of the internal spans is 75.25 ft and the two external spans are 74.04 ft long. The substructure elements are skewed at an angle of 25.19 degrees from the line perpendicular to the bridge centerline. Figure 4.2 shows the plan and elevation of the bridge.

As shown in Figure 4.3, the superstructure of this bridge is a girder-type deck consisting of 12 prestressed girder members of 3.75 ft depth, spaced at 8 ft transversally, and connected by a 7 inches thick cast-in-place slab. The concrete compressive strength for this bridge is 4 ksi, and the reinforcement yield strength is 60 ksi.

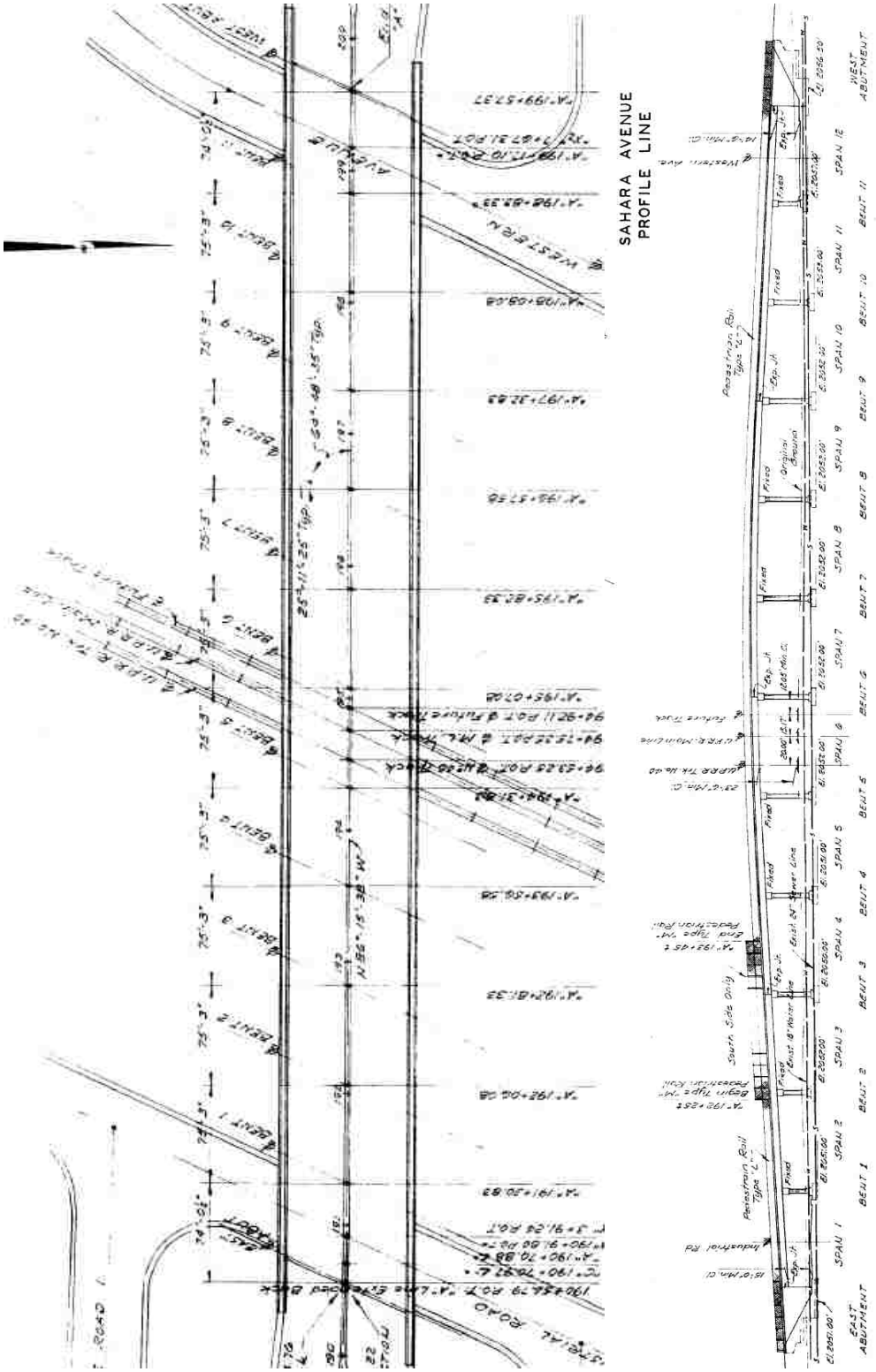

Figure 4.2 Bridge G-1064 - Plan and elevation

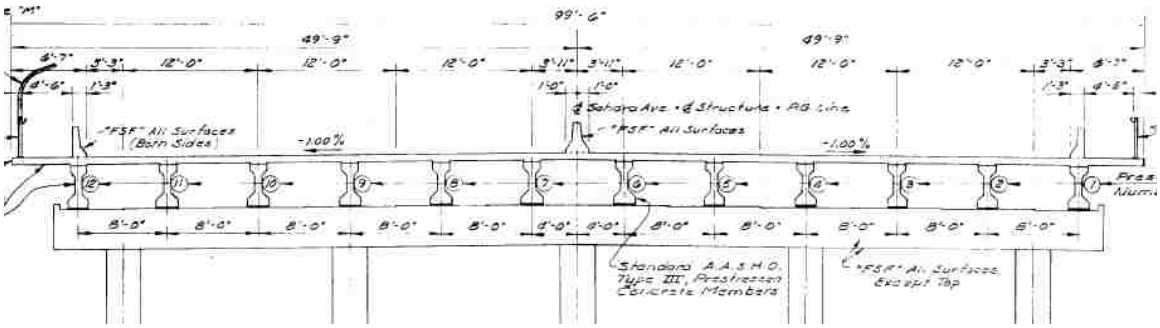

Figure 4.3 Bridge G-1064 - Superstructure

The substructure of the bridge is a five column frame bent, as shown in Figure 4.4, with a 3 ft column diameter and a cap beam dimensions of 3.5 ft depth by 4 ft width. The column length varies with the location of the bent. Figure 4.2 shows the bridge profile with the deck elevation that increases in the middle spans and decreases close to the abutments. The concrete columns are fixed to the rectangular footings, and the dowels from the footing are lap spliced with column reinforcement 8 ft away from the footing top level.

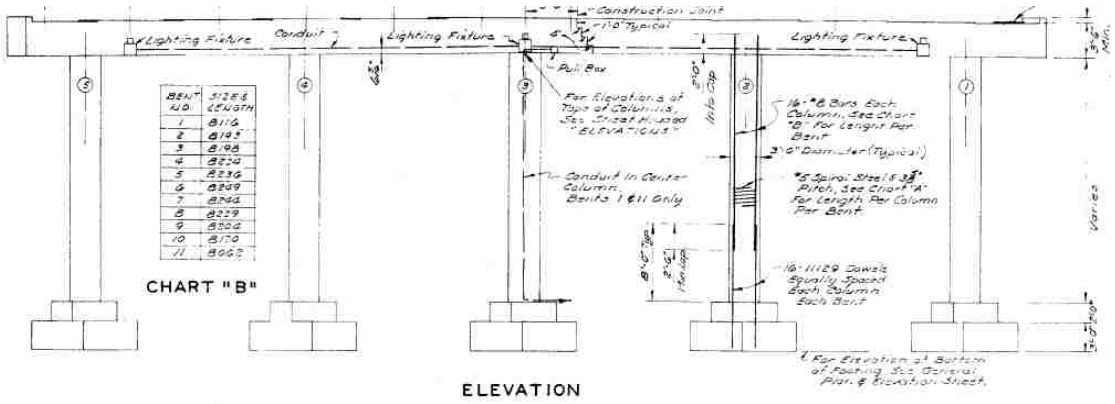

Figure 4.4 Bridge G-1064 - Elevation of a typical bent

Cross diaphragms are provided at every bent location, at the abutments and at the mid-spans between every two bents. Each three spans are separated by an expansion joint that discontinues the rotational relation between spans. At the expansion joint location, two diaphragms are provided, separated by the expansion joint filler, as shown in Figure 4.5.

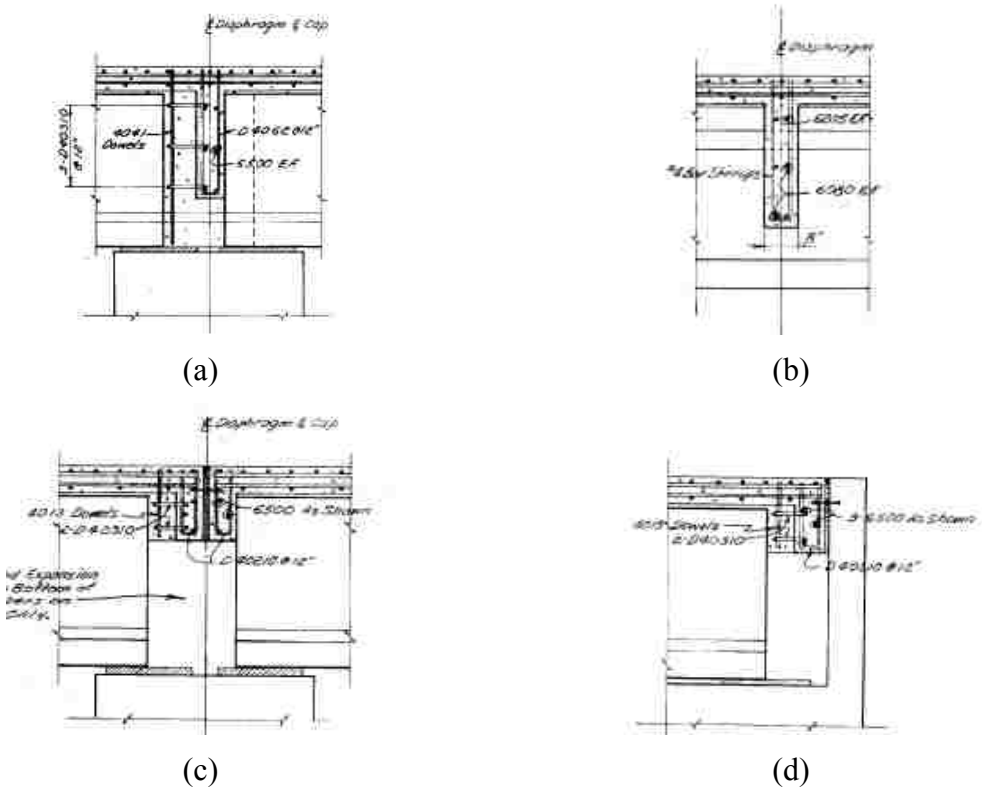

(a) (b)

(c) (d)

Figure 4.5 Bridge G-1064 - Cross diaphragms at (a) fixed bearing; (b) interior diaphragm; (c) expansion joint; and (d) abutment expansion joint

4.3.1.2. Bridge model

Figure 4.6 shows the structural model for the bridge used for the analysis and evaluation in the transverse direction, while Figure 4.7 (a) to (d) shows the structural

models used for the analyses and evaluation of the longitudinal direction. The units are separated at the locations of the expansion joints.

4.3.1.2.1. Superstructure

The superstructure was modeled with four elements per span; the frame elements are automatically located in the centroid of the superstructure. The mass of each part of the bridge deck is lumped to the nodes of the superstructure elements. The cross sectional area of the bridge deck is 106.67 ft^2 and its moment of inertia about the Y and Z axes are 234 and 84978 ft^4 respectively (the X-axis is in the longitudinal direction and the Z-axis is the vertical axis). An additional load of 4.726 kip/ft was added to represent the dead load from the concrete barriers, the pedestrian rails and the wearing surface overlay. An additional load of 3.84 kip/ft was added to account for the live load over the six lanes of the bridge.

4.3.1.2.2. Substructure

The substructure components are skewed bents at 25.19 degrees, the masses of the cap beams and half of the columns were lumped to the top node of each column. The abutments were modeled only with their stiffness (no elements), with a release in the translation in the longitudinal direction (X-axis) and the rotation about the transverse direction (Y-direction). Link elements were added to relate the superstructure to the cap beam as the centroid of the deck is higher than the level of the cap beam. These link elements translate loads but not rotations, as the deck girders are rested on bearings that isolate the rotation of the deck from the cap beam. Foundations were modeled as fixed supports.

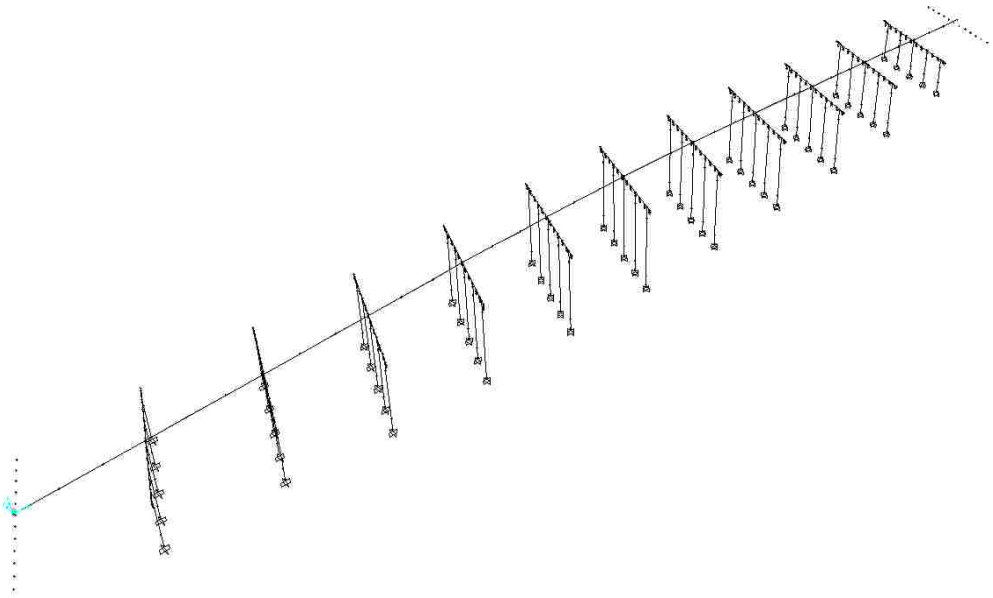

Figure 4.6 Bridge G-1064 - Structural model for transverse direction analysis

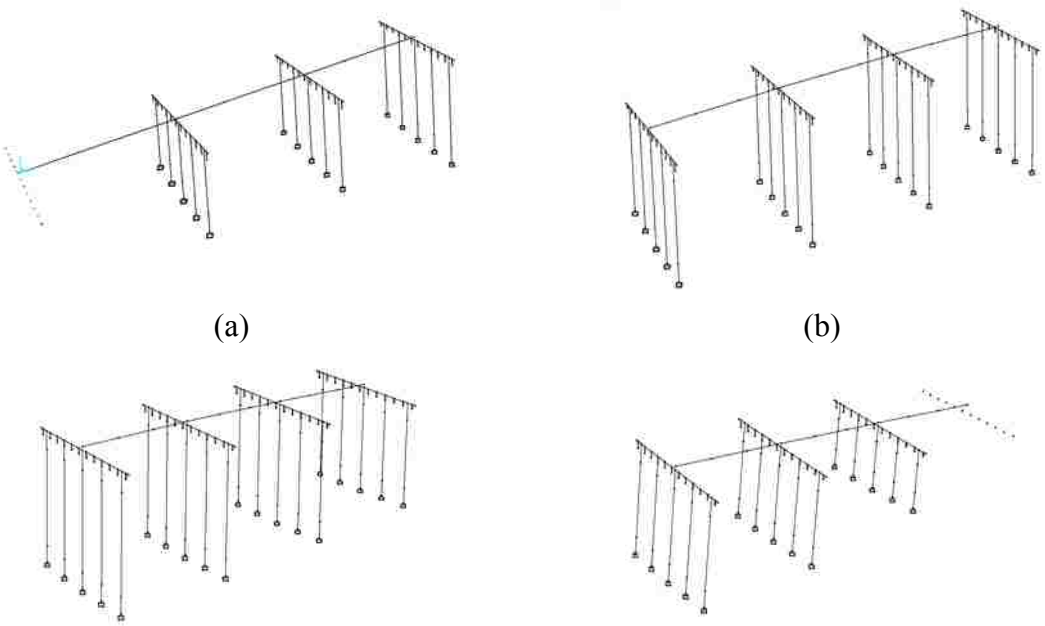

(a) (b)

(c) (d)

Figure 4.7 Bridge G-1064 - Structural models for longitudinal direction
(a) unit-1; (b) unit-2; (c) unit-3; and (d) unit-4

4.3.1.2.3. Effective moment of inertia for bent columns

All bent columns for this bridge are similar except for their height which varies from one bent to another and within each bent. The diameter of all columns is 3 ft with 16 #8 rebars attached in splice (of 2.5 ft length) to 16 #11 dowels extended from the foundations. The dowels are 8 ft long above the footings top level. Figure 4.8 shows the $M-\phi$ curves for the two sections used in the estimation of the effective moment of inertia for the bent columns. The average axial load on the columns from the preliminary analysis, which was used in constructing the $M-\phi$ curve, is 425 kips.

For a circular column with 3 ft diameter:

$I_g = 3.9761$ ft^4

From the $M-\phi$ idealized curve in Figure 4.8 (a):

$M_n = 1150$ kip-ft, $\phi_y = 0.00125$ rad/ft

using the ACI 318-08 (2008) equation "$E_c = 57{,}000\sqrt{f_c'}$"

$E_c = 519119.5$ ksf

since $I_e = \dfrac{M_n}{E_c \phi_y} \rightarrow I_e = 1.7722$ ft^4

and $\dfrac{I_e}{I_g} = \dfrac{1.7722}{3.9761} = 0.4457$

Therefore, gross flexural rigidity for columns with #8 rebars will be reduced to 45% of its value in the analysis.

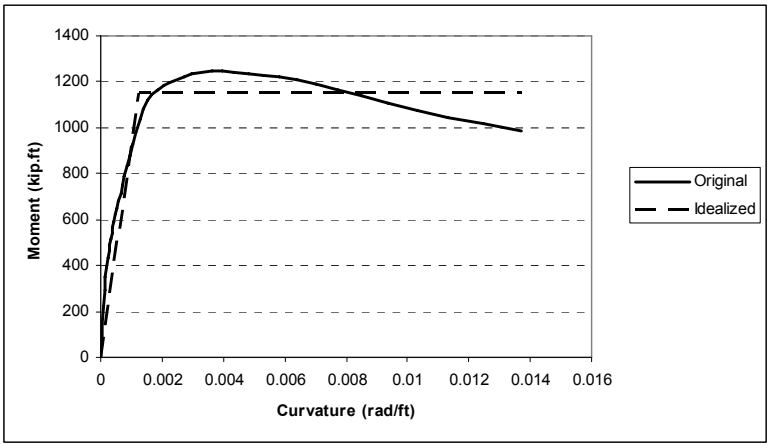

(a)

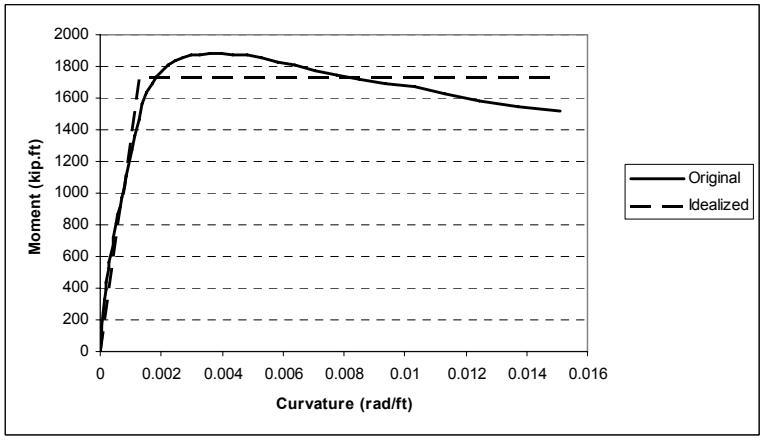

(b)

Figure 4.8 Bridge G-1064 - $M-\phi$ curves for the bent columns with (a) 16 #8 rebar and (b) 16 #11 rebar

From the $M-\phi$ idealized curve in Figure 4.8 (b):

$M_n = 1730$ kip-ft, $\phi_y = 0.00129$ rad/ft

since $I_e = \dfrac{M_n}{E_c \phi_y} \rightarrow I_e = 2.5834$ ft^4

and $\dfrac{I_e}{I_g} = \dfrac{2.5834}{3.9761} = 0.6497$

Therefore, gross flexural rigidity for columns with #11 rebars will be reduced to 65% of its value in the analysis.

4.3.1.2.4. Spectral acceleration curve

Figure 4.9 shows the response spectrum used for the estimation of (S_a) values in the target displacement calculations. From the curve $T_0 = 0.088$ sec and $T_S = 0.438$ sec.

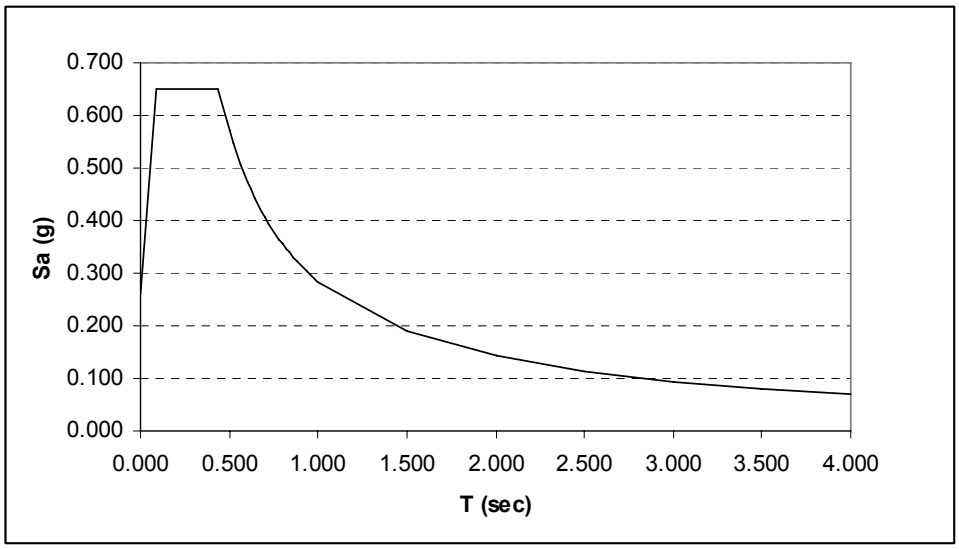

Figure 4.9 Bridge G-1064 - 5% damped response spectrum for BSE-2

4.3.1.3. Acceptance criteria

4.3.1.3.1. Load-deformation curve for plastic hinges

From the analysis, the average axial load on the columns for this bridge was 425 kips, and the maximum shear force on columns was 0.269 kips.

Therefore, $\frac{P}{A_g f_c^{'}} = 0.1044$ (which is very close to 0.1 (no need for interpolation))

and $\frac{V}{b_w d\sqrt{f_c^{'}}} = 0.0041 < 3$

The transverse reinforcement of the column is classified as conforming. Accordingly, plastic hinge rotation values used for the acceptance criteria (from Table 4.2) will be 0.005 for the Immediate Occupancy (IO), 0.015 for the Life Safety (LS) and 0.02 for the Collapse Prevention (CP) levels (Figure 4.10).

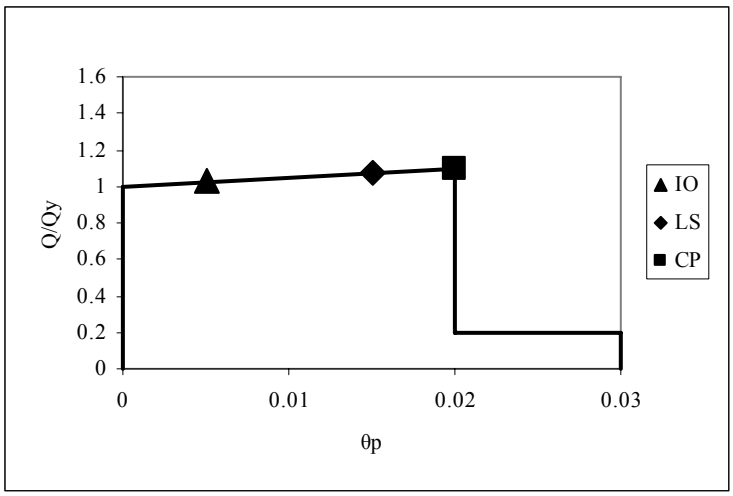

Figure 4.10 Bridge G-1064 - Generalized force-deformation relation for bridge columns

4.3.1.3.2. Force-controlled actions

a- Shear capacity:

Based on Eq. 4.2, Eq. 4.3, and Eq. 4.4;

$N_u = 425$ kips, $A_g = 1017.88$ in^2 (for 36 inches column diameter),

$s = 3.625$ in, $A_v = 0.62$ in^2 for two bars with #5 size, $b_w = 36$ in

Therefore, $V_c = 158.525$ kips and $V_s = 295.547$ kips

Shear capacity of the section is $V_n = V_c + V_s = 454.072$ kips

b- Reinforcement development:

Based on Eq. 4.5 and Eq. 4.6;

$f_y = 60000\,\text{psi},\ f_c^{'} = 4000\,\text{psi}$

As per ACI 318-08 equations, for #8 reinforcement bar;

Development length $l_d = 47.4$ in $= 3.95$ ft and the splice length is $1.3 \times l_d = 5.14$ ft.

The splice length provided at the splice location between the #11 dowels and the #8 bar of the column reinforcement is 2.5 ft and the development length provided at the beam-column (B/C) joint is 2 ft.

Therefore, maximum stress that can be developed in the rebars at the splice location is:

$$f_s = \left(\frac{2.5}{5.14}\right)60 = 29.18\,\text{ksi}$$

and the maximum stress that can be developed in the rebars at the B/C joint location is:

$$f_s = \left(\frac{2.0}{3.95}\right)60 = 30.38\,\text{ksi}$$

The load-deformation relation at these locations is shown in Figure 4.11, where the yield stress used for this curve is the new calculated stress (f_s) from the above calculations. Figure 4.11 shows the acceptance criteria for the IO and the LS performance levels coincide at 0.005 radians.

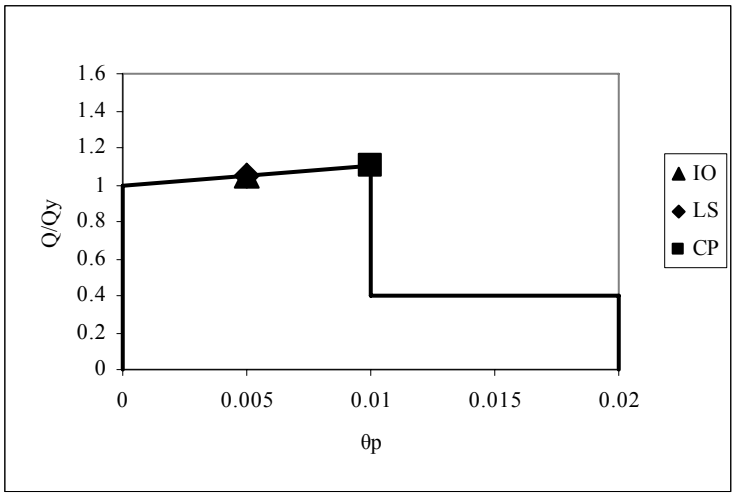

Figure 4.11 Bridge G-1064 - Generalized force-deformation with acceptance criteria for inadequate splicing in the bridge column reinforcement

4.3.1.4. Pushover curves and target displacement

4.3.1.4.1. Transverse direction

From the results of the modal analysis of the bridge, the fundamental mode in the transverse direction was mode 2, with a deformed mode shape shown in Figure 4.12. The time period for this mode was 1.213 seconds ($T_i = 1.213\,\text{sec}$). The nonlinear pushover analysis was performed using both patterns, uniform and modal, and the resulting base shear-displacement curves are displayed in Figure 4.13.

The control node in this direction was chosen to be the node of the superstructure at the location of pier number 6 (the middle pier). This node is considered the mid-point of the bridge and has the highest value of deflection using both uniform and modal patterns. The displacement of this node vs. the base shear of all columns represents the shown pushover curves.

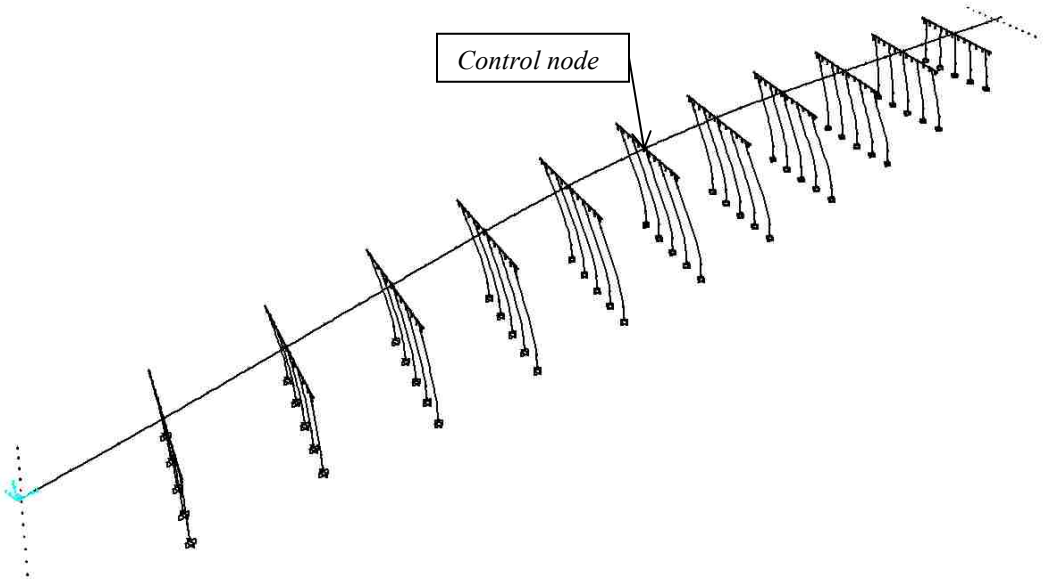

Figure 4.12 Bridge G-1064 - Mode-2, The fundamental mode in the transverse direction of the bridge

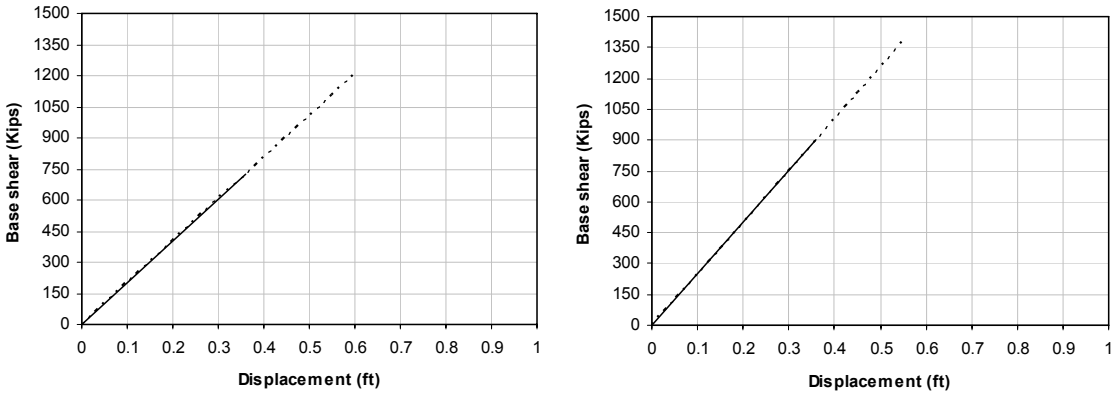

(a) (b)

Figure 4.13 Bridge G-1064 - Pushover curves for the transverse direction (a) using the uniform load pattern (b) using the modal load pattern

From the pushover curves (Figure 4.13 (a) & (b));

$K_i = K_e \rightarrow T_e = T_i = 1.213$ sec

Using the effective time period in the response spectrum curve → $S_a = 0.235g$

Using the first approach in C_0 calculations gives;

$C_0 = PF_1 \times \phi_{CN,1} = 81.33 \times 0.0161 = 1.309$

Since $T_e > T_s$ → $C_1 = 1.0$

and $C_2 = C_3 = 1.0$

Therefore, the target displacement can be calculated as

$\delta_t = 1.309 \times 1.0 \times 1.0 \times 1.0 \times 0.235 \times 32.2 \frac{1.213^2}{4\pi^2} = 0.368 ft$ (for both the uniform and modal patterns)

4.3.1.4.2. Longitudinal direction

Modal analyses results for the four units of the bridge in the longitudinal direction are shown in Table 4.3. The control node in the longitudinal direction, for each unit, was chosen to be the furthest on the superstructure to the east at the end pier. Pushover curves are presented in Figure 4.15 (a) to (h), and then the target displacements for all units are presented in Table 4.4.

Table 4.3 Bridge G-1064 - Modal analysis Output for the 4 units used in the longitudinal direction

Unit	Fundamental Mode Time period (T_i, sec)	Modal Participation Factor (PF)	Displacement of Control node (ϕ_{CN}, ft)
1	2.52	47.929	0.0209
2	5.33	56.695	0.0176
3	5.55	56.440	0.0177
4	2.57	47.996	0.0208

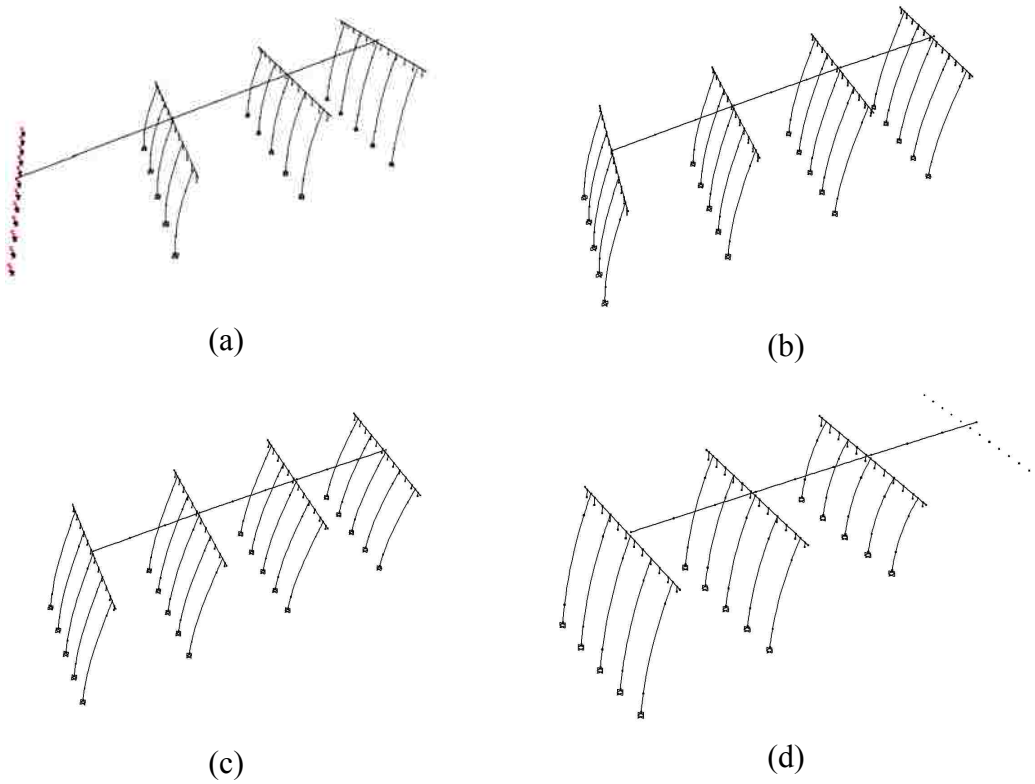

Figure 4.14 Bridge G-1064 -Fundamental mode shapes in the longitudinal direction of the bridge for (a) unit-1; (b) unit-2; (c) unit-3; and (d) unit-4

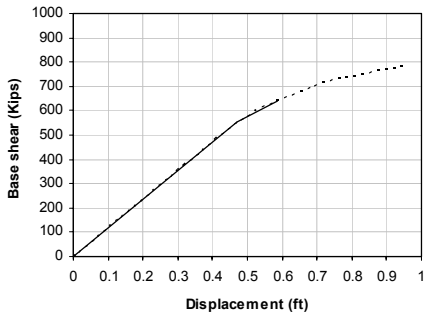

(a) Unit-1-Uniform load pattern

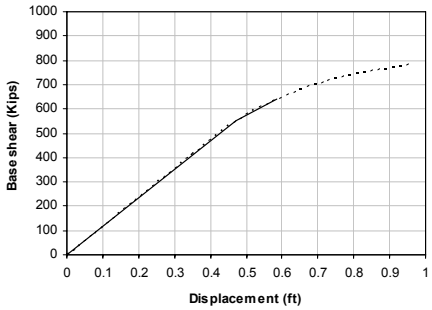

(b) Unit-1-Modal pattern

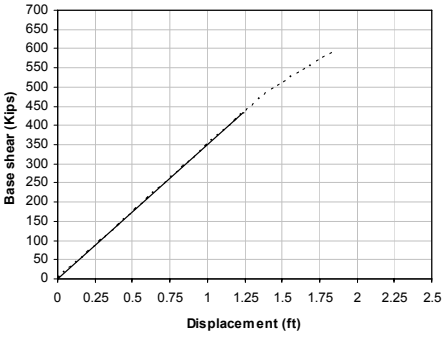

(c) Unit-2-Uniform load pattern

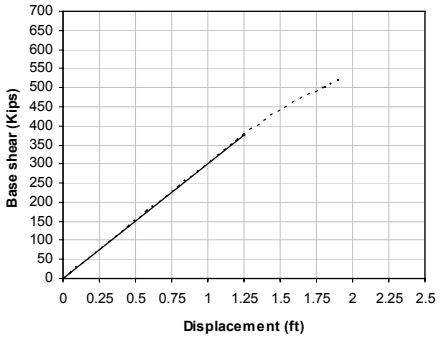

(d) Unit-2-Modal pattern

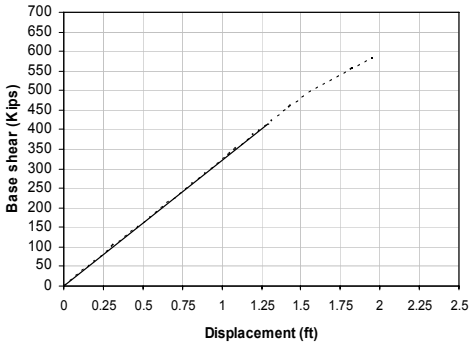

(e) Unit-3-Uniform load pattern

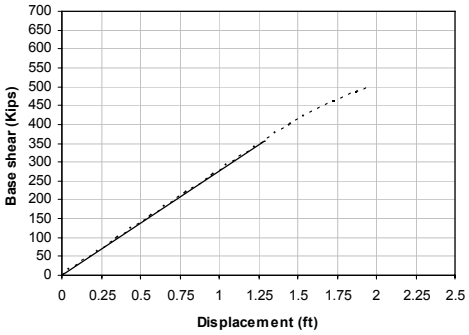

(f) Unit-3-Modal Patters

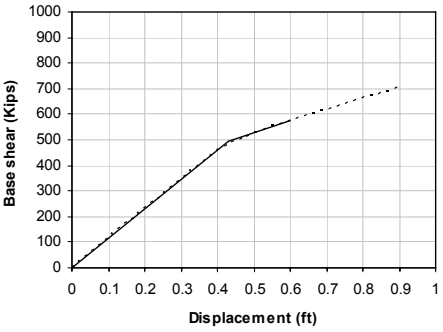

(g) Unit-4-Uniform load pattern

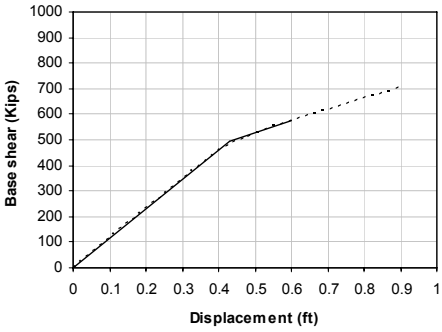

(h) Unit-4-Modal pattern

Figure 4.15 Bridge G-1064 - Pushover curves for longitudinal direction analysis

Table 4.4 Bridge G-1064 - Target displacements for different units used in the longitudinal direction

Unit	T_i (sec)	T_e (sec)	S_a (g)	C_0	C_1,C_2 and C_3	δ_t (ft)*
1	2.52	2.52	0.113	1.002	1.0	0.586
2	5.33	5.33	0.053	0.998	1.0	1.230
3	5.55	5.55	0.051	0.999	1.0	1.283
4	2.57	2.57	0.111	0.998	1.0	0.598

* Target displacement has an identical value for both uniform and modal pattern for each unit.

4.3.1.5. Results

4.3.1.5.1. Deformation-controlled actions

In the transverse direction, none of the columns experienced plastic hinge formation at the target displacement. However, in the longitudinal direction, some of the columns encountered plastic hinge formation with different rotation values depending on the location of the column. Table 4.5 presents the plastic hinge rotation values at target displacements in the longitudinal direction. All plastic hinges formed in this direction were at the bottom part of the columns. This is due to the fact that earthquake loads are applied in the out-of-plane direction of the bent frame, and the bent columns resist the lateral load as cantilevers with zero moment at the top. The bents in the bridge are labeled in a numerical sequence from east to west direction of the bridge as shown in Figure 4.2 and the column labels within the bent (from 1 to 5) is from north to south direction.

From the results presented in Table 4.5, three columns had plastic hinge rotations violated the acceptance criteria of the IO performance level in each of the two applied patterns (uniform and modal)

Table 4.5 Bridge G-1064 - Plastic hinge rotation values (radians) of bridge columns at target displacements in the longitudinal direction

Unit 1	**Bent no.**	**1**				
	Column	**1**	**2**	**3**	**4**	**5**
	Uniform	0.001633	0.001661	0.002430	0.003312	**0.005046**
	Modal	0.001632	0.001660	0.002432	0.003317	**0.005057**
	Bent no.	**2**				
	Uniform	**No Plastic Hinge Rotation Observed**				
	Modal					
Unit 2	**Bent no.**	**3**				
	Column	**1**	**2**	**3**	**4**	**5**
	Uniform	0.000000	0.000000	0.000000	0.000000	0.000000
	Modal	0.000000	0.000000	0.000000	0.000000	0.000813
	Bent no.	**4 to 6**				
	Uniform	**No Plastic Hinge Rotation Observed**				
	Modal					
Unit 3	**Bent no.**	**6 to 9**				
	Uniform	**No Plastic Hinge Rotation Observed**				
	Modal					
Unit-4	**Bent no.**	**9 and 10**				
	Uniform	**No Plastic Hinge Rotation Observed**				
	Modal					
	Bent no.	**11**				
	Column	**1**	**2**	**3**	**4**	**5**
	Uniform	**0.006938**	**0.005386**	0.004283	0.003579	0.003496
	Modal	**0.006586**	**0.005009**	0.003937	0.003221	0.003139

4.3.1.5.2. Force-controlled actions

a- Shear forces:

None of the columns at the target displacement, in both transverse and longitudinal directions, encountered a shear force exceeding the shear capacity calculated in the previous section. Shear forces at target displacements in the transverse and longitudinal directions are presented in Table 4.6 and Table 4.7, respectively.

Table 4.6 Bridge G-1064 Shear forces (kips) at target displacements in the transverse direction

Bent no.	Column	1	2	3	4	5
1	Uniform	3.48	3.56	3.81	4.35	4.95
	Modal	14.79	15.35	16.40	18.55	21.37
2	Uniform	15.22	15.71	16.57	18.33	20.68
	Modal	21.43	22.14	23.34	25.81	29.13
3	Uniform	12.46	12.77	13.22	14.26	15.61
	Modal	15.40	15.79	16.34	17.63	19.30
4	Uniform	12.58	12.79	13.11	14.01	15.17
	Modal	15.09	15.34	15.73	16.81	18.21
5	Uniform	12.74	12.67	12.67	13.23	13.93
	Modal	15.20	15.11	15.12	15.77	16.61
6	Uniform	12.34	12.03	11.79	11.98	12.37
	Modal	14.70	14.34	14.05	14.27	14.74
7	Uniform	12.67	12.10	11.64	11.66	11.76
	Modal	15.13	14.45	13.89	13.91	14.04
8	Uniform	13.68	12.82	12.17	11.92	11.75
	Modal	16.45	15.41	14.64	14.34	14.14
9	Uniform	13.60	12.67	11.93	11.68	11.56
	Modal	15.84	15.68	14.77	14.46	14.32
10	Uniform	12.71	11.19	10.50	10.21	10.08
	Modal	17.05	15.69	14.73	14.30	14.14
11	Uniform	7.54	6.50	5.81	5.55	5.38
	Modal	27.11	23.57	20.98	19.98	19.52

By combining the shear forces (100% of the longitudinal direction and 30% of the transverse direction) - for column 1 in bent number 11 (using the modal pattern outputs):

→ $100\% \times 48.65 = 148.56$ kips, and $30\% \times 27.11 = 8.13$ kips

$\sqrt{(48.65)^2 + (27.11)^2} = 49.33$ kips $<<$ 454.072 kips (from section 4.3.1.3)

Therefore, the columns are safe against shear failure.

Table 4.7 Bridge G-1064 Shear forces (kips) at target displacements in the longitudinal direction

Bent no.	Column	1	2	3	4	5
1	Uniform	34.00	37.42	36.24	41.62	43.16
	Modal	34.02	37.46	36.29	41.68	43.22
2	Uniform	23.06	24.80	26.03	30.90	37.35
	Modal	23.07	24.83	26.08	30.97	37.46
3	Uniform	24.52	25.61	26.15	29.64	33.89
	Modal	24.39	26.28	27.63	32.21	35.78
4	Uniform	17.85	18.45	18.71	21.01	23.78
	Modal	17.89	19.08	19.91	22.97	26.66
5	Uniform	15.66	15.57	15.25	16.56	17.92
	Modal	15.88	16.29	16.44	18.37	20.41
6	Uniform	14.97	14.56	13.97	14.69	15.58
	Modal	16.49	15.75	14.92	15.48	16.12
7	Uniform	16.74	15.72	14.61	14.99	15.27
	Modal	18.26	16.84	15.44	15.63	15.60
8	Uniform	21.84	19.87	18.07	17.84	17.41
	Modal	23.58	21.06	18.89	18.38	17.55
9	Uniform	30.29	27.25	24.33	23.87	23.51
	Modal	32.38	28.61	25.18	24.43	23.45
10	Uniform	21.07	18.48	16.18	15.56	15.01
	Modal	22.07	19.34	16.94	16.27	15.69
11	Uniform	48.08	43.96	39.12	39.25	37.36
	Modal	48.65	44.50	39.58	39.16	37.64

b- Reinforcement development:

For the reinforcement development and splice lengths: new sectional analyses were performed to estimate the capacity of the sections at (1) the splice locations and (2) the B/C joints. These two locations had inadequate development and splice lengths. The $M-\phi$ curves resulting from the sectional analysis at these two locations are presented in Figure 4.16. The sectional analyses of the sections at the two locations give the same results as the maximum stress in the reinforcement at the two locations is almost of the

same value ($f_s = 30$ ksi). From Figure 4.16, the yielding moment value for the sections is 820 kip-ft.

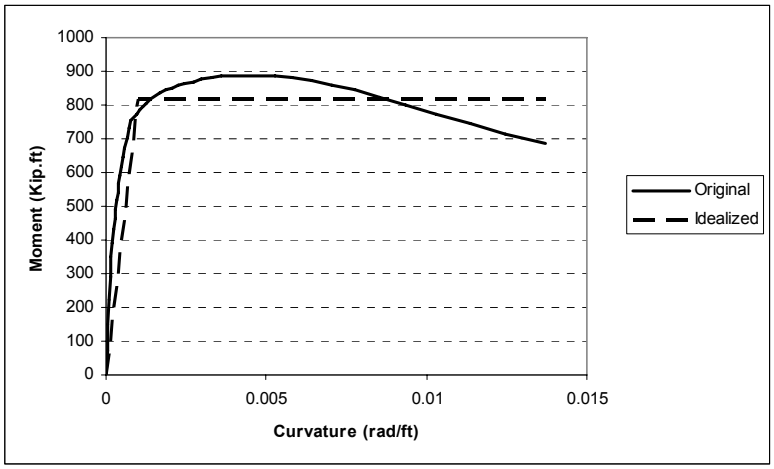

Figure 4.16 Bridge G-1064 - $M - \phi$ curve for the bent columns at locations of reinforcement splice and B/C joints

In the transverse direction (at the target displacement), all bending moment values for columns at the two locations were less than 820 kip-ft. This means that the inadequate development and splice lengths did not govern the design in this direction. Accordingly, the bridge is not at risk of reinforcement bond slippage at under the MCE, when applied in the transverse direction.

In the longitudinal direction (at the target displacement), a number of columns had moment values exceeding the capacity (820 kip-ft) at the location of the splice (not the B/C joints). The columns bending moment values at target displacements at the splice locations are presented in Table 4.8. From the values presented in the tables, a number of columns in this direction had a bending moment value exceeding the capacity (820 kip-

ft). Accordingly, new models were analyzed with the nonlinear definitions of the new plastic hinges that represent the inadequate splice lengths.

Table 4.8 Bridge G-1064 - Bending moment values (kip-ft) at splice locations of the columns at target displacement in the longitudinal direction

Bent no.	Column	1	2	3	4	5
1	Uniform	975	1016	991	1029	994
	Modal	976	1017	992	1031	996
2	Uniform	818	847	874	950	1035
	Modal	819	849	876	952	1037
3	Uniform	1168	1193	1211	1287	1371
	Modal	1198	1241	1276	1373	1428
4	Uniform	957	974	985	1042	1105
	Modal	993	1024	1049	1124	1207
5	Uniform	869	868	863	899	933
	Modal	913	924	930	981	1032
6	Uniform	851	841	827	849	873
	Modal	928	908	884	897	914
7	Uniform	908	882	854	865	873
	Modal	979	942	903	906	904
8	Uniform	1063	1017	975	969	958
	Modal	1136	1075	1020	1003	981
9	Uniform	1306	1244	1182	1173	1162
	Modal	1379	1300	1223	1202	1178
10	Uniform	739	696	656	644	634
	Modal	773	728	687	674	663
11	Uniform	982	1005	990	1015	994
	Modal	990	1015	999	1021	1003

Rotations of the plastic hinges at the target displacements in the modified models are presented in Table 4.9. Figure 4.11 shows that the acceptance criteria for the IO and the CP levels are 0.005 and 0.01 radians, respectively. The underlined values displayed in Table 4.9 represent the plastic hinges that violated the acceptance criteria.

Table 4.9 Bridge G-1064 - Plastic hinge rotation (radians) at splice locations at target displacement in the longitudinal direction

Bent no.	Column	1	2	3	4	5
1	Uniform	**0.00893**	**0.00739**	**0.00932**	**0.00893**	**0.01197**
	Modal	**0.00969**	**0.00819**	**0.01011**	**0.00981**	**0.01288**
2	Uniform	0.00380	0.00251	0.00429	0.00355	0.00617
	Modal	0.00445	0.00316	0.00497	0.00426	0.00693
3	Uniform	**0.00927**	**0.00811**	**0.00980**	**0.00951**	**0.01247**
	Modal	**0.00933**	**0.00854**	**0.01090**	**0.01084**	**0.01421**
4	Uniform	0.00301	0.00182	0.00354	0.00318	**0.00564**
	Modal	0.00304	0.00214	0.00395	0.00413	**0.00700**
5	Uniform	0.00096	0.00000	0.00056	0.00000	0.00197
	Modal	0.00134	0.00000	0.00137	0.00107	0.00342
6	Uniform	0.00275	0.00116	0.00217	0.00116	0.00279
	Modal	0.00374	0.00168	0.00258	0.00166	0.00343
7	Uniform	0.00215	0.00000	0.00054	0.00000	0.00109
	Modal	0.00257	0.00061	0.00115	0.00000	0.00114
8	Uniform	**0.00549**	0.00311	0.00344	0.00187	0.00299
	Modal	**0.00612**	0.00340	0.00364	0.00212	0.00320
9	Uniform	**0.01210**	**0.00957**	**0.00965**	**0.00790**	**0.00922**
	Modal	**0.01268**	**0.00976**	**0.00985**	**0.00803**	**0.00922**
10	Uniform	0.00173	0.00000	0.00000	0.00000	0.00000
	Modal	0.00095	0.00000	0.00000	0.00000	0.00000
11	Uniform	**0.01383**	**0.01051**	**0.01057**	**0.00829**	**0.00966**
	Modal	**0.01255**	**0.00932**	**0.00942**	**0.00712**	**0.00838**

4.3.2. Bridge (G-947)

4.3.2.1. Bridge description

G-947 is a 23-piers bridge located at the intersection of the U.S. 95-highway (overpass) and North Casino Boulevard (underpass). In this study, a part of this bridge is evaluated. Figure 4.17 shows the layout of the whole bridge in addition to the part that was chosen to be studied. This part of the bridge was chosen for three reasons: (1) it has an underpass street (North Casino Boulevard) which increases its importance than other parts of the bridge; (2) it is a straightforward part of the bridge that contains no curvatures in its horizontal or vertical profile; and (3) its location is far from the abutments' locations and their stiffnesses would not affect the analysis.

The studied part, which is named as "Deck 6W" by the NDOT, consists of 3-spans with 2-bents. It is separated from the previous and the next bridge decks with expansion joints. The total length of this part of the bridge is 255.906 ft, divided into three spans of 79.953 ft, 95.953 ft, and 80 ft long. The concrete compressive strength for this bridge is 3 ksi, and the reinforcement yield strength is 60 ksi.

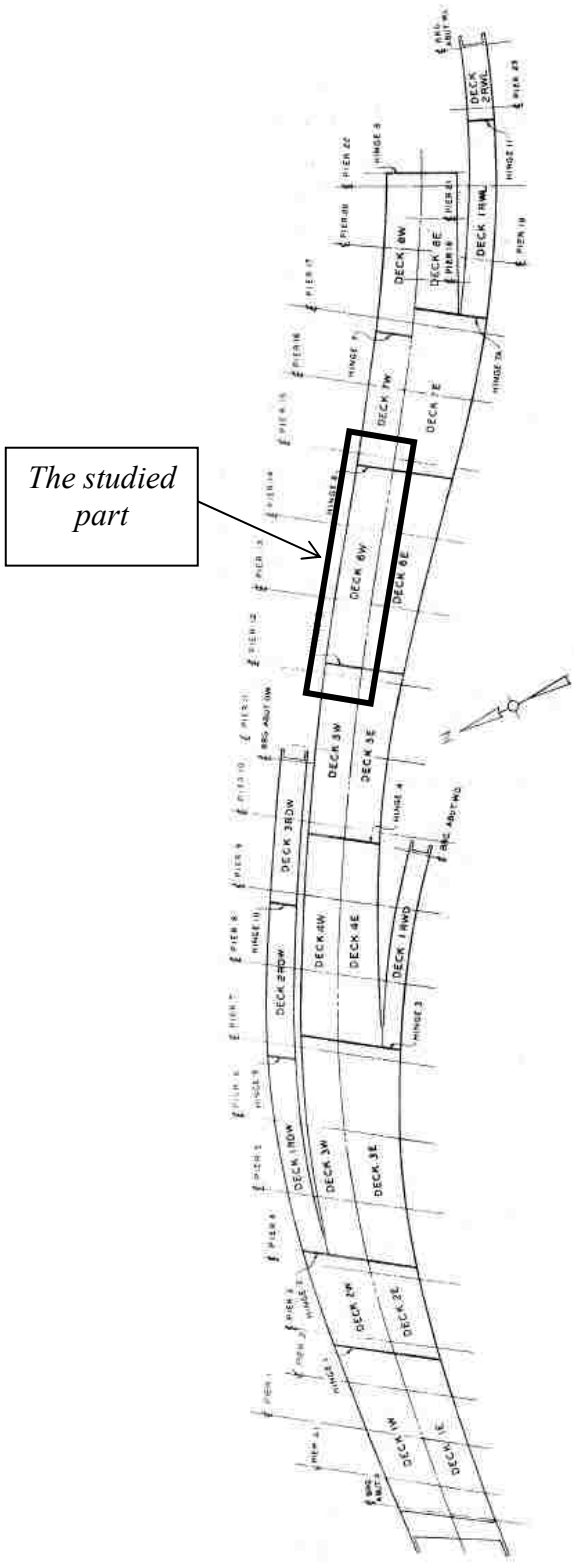

Figure 4.17 Bridge G-947 - Layout and the location of the studied part

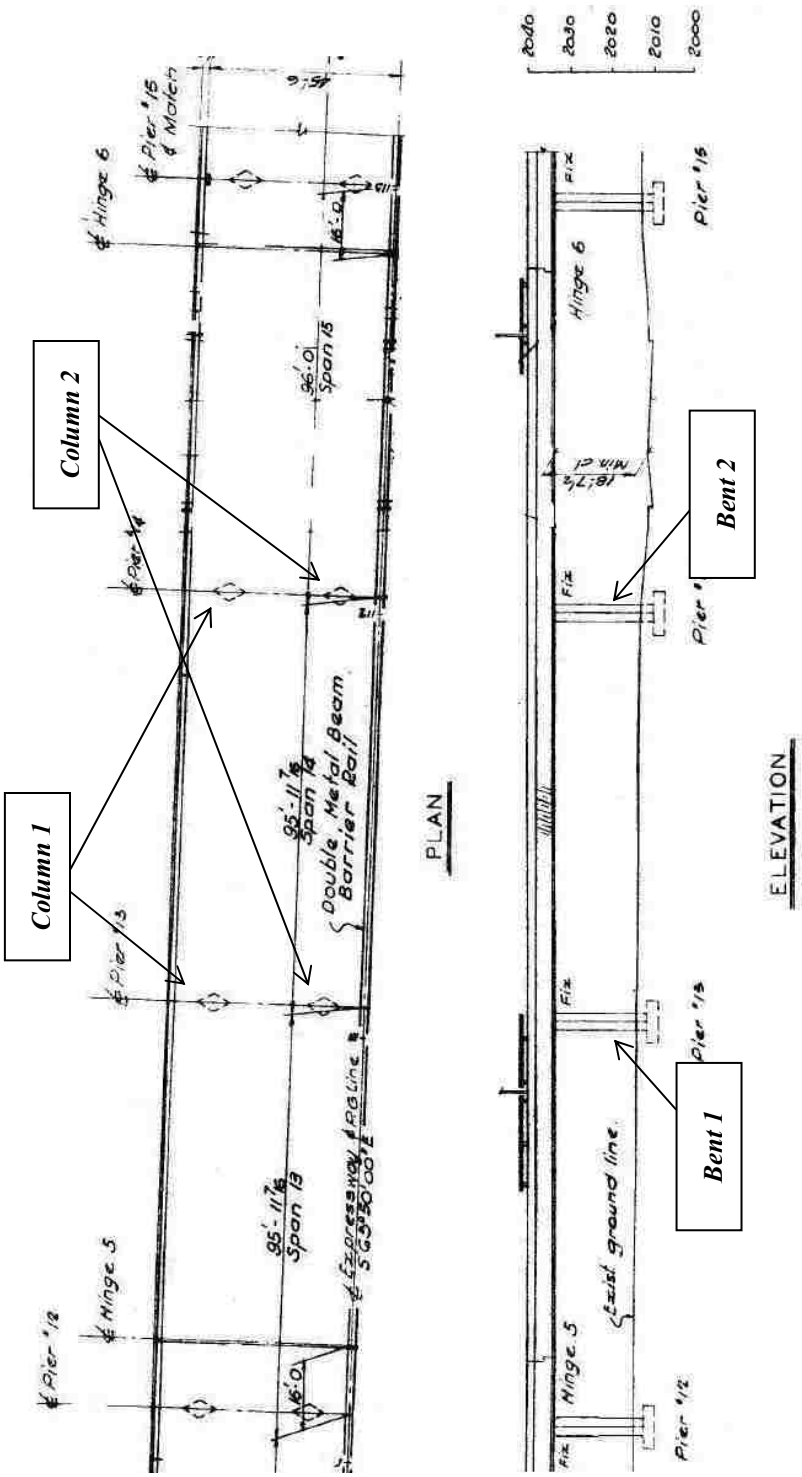

Figure 4.18 Bridge G-947 - Deck 6W, Plan and elevation

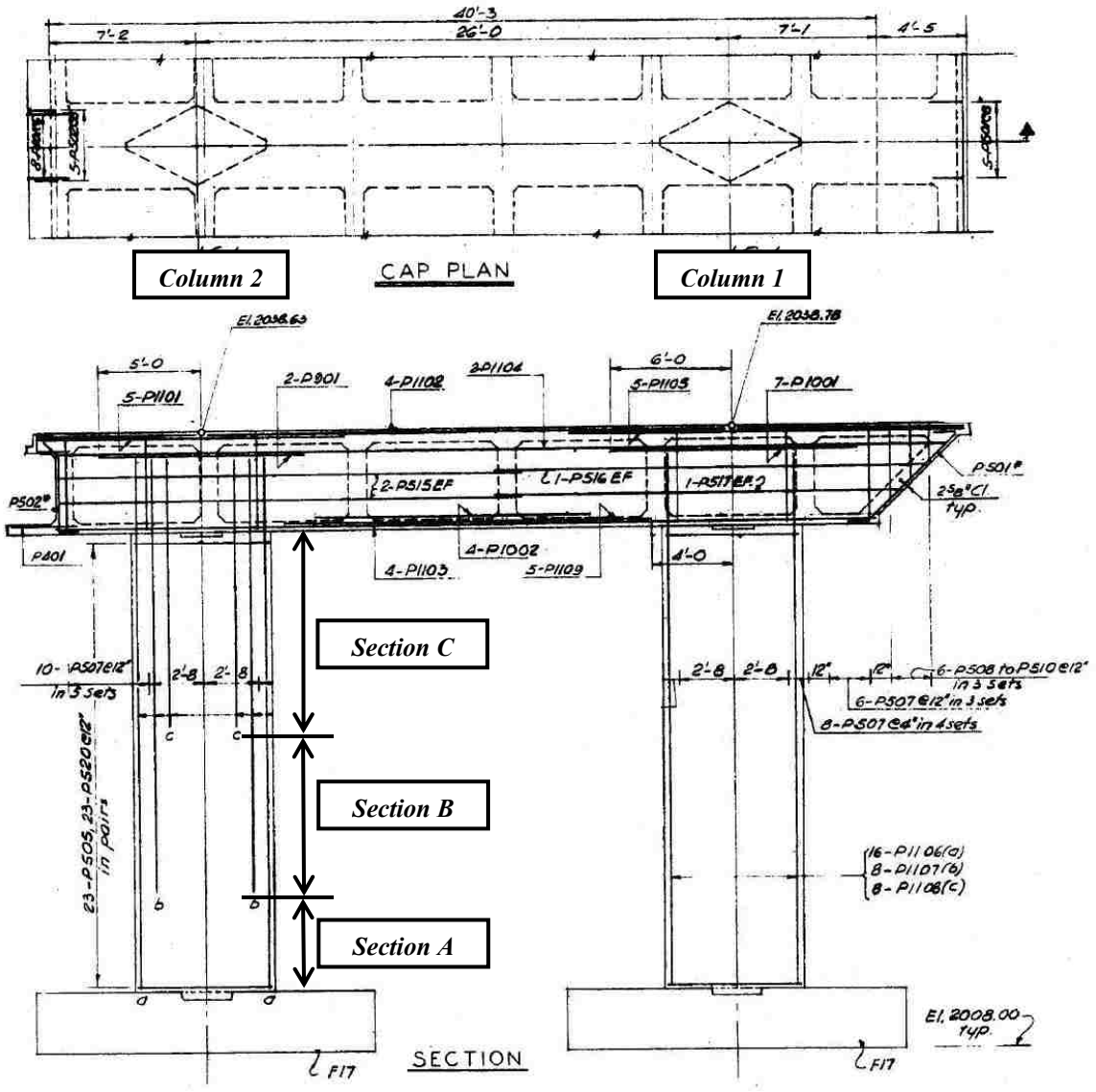

Figure 4.19 Bridge G-947 - Bent 1 and 2 typical elevation and cap beam plan

The superstructure of the bridge is a cast-in-place box girder concrete deck, with five intermediate webs. The total width of the bridge deck is 44.67 ft and its depth is 5 ft. Figure 4.19 illustrates the typical elevation of the two bents in the studied part. It shows that each of the columns consists of three sections. Sections A, B, and C (as named in Figure 4.19) have the same dimensions. The only difference between the three sections is in the longitudinal reinforcement values that curtails from each section to the next one.

Figure 4.20 shows the column sections for the two bents, where the only difference between the two bent columns is the reinforcement bars used. In the two columns of bent 1, #11 rebars are used, while in the two columns of bent 2, #14 rebars are used.

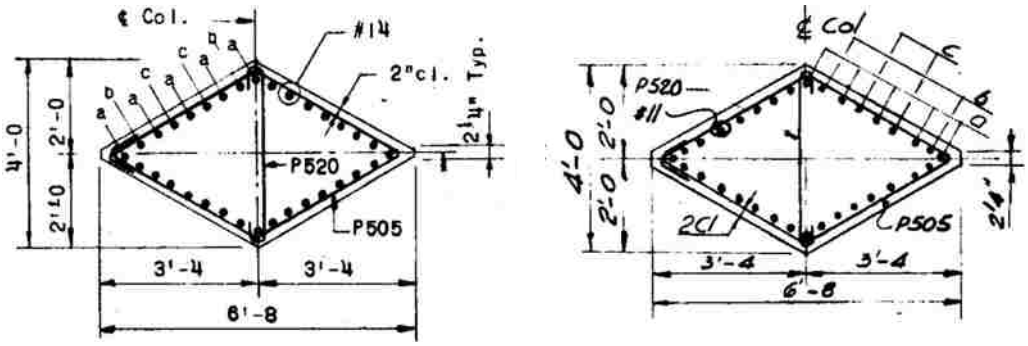

(a) (b)

Figure 4.20 Bridge G-947 - Column section for (a) bent 1 and (b) bent 2

4.3.2.2. Bridge model

Figure 4.21 shows the structural model used in the bridge analysis for both transverse and longitudinal directions

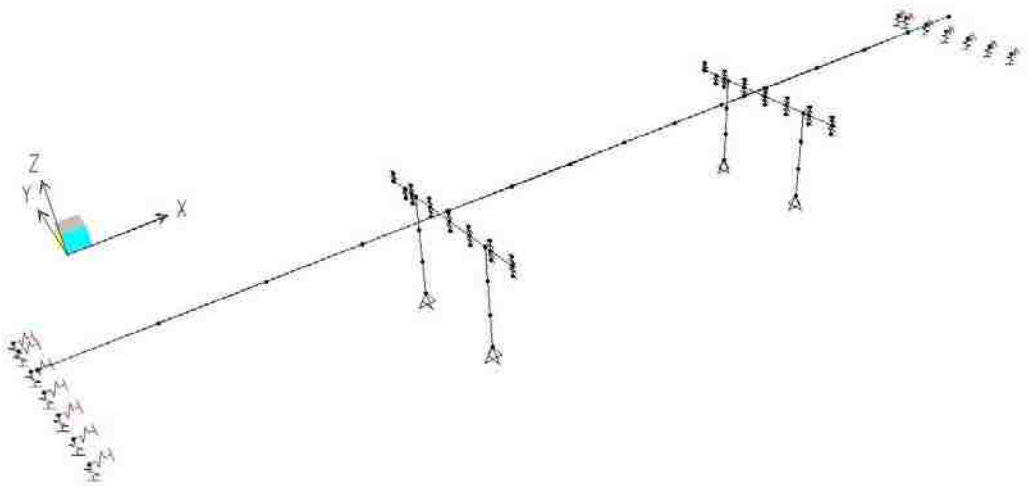

Figure 4.21 Bridge G-947 - Bridge structural model

4.3.2.2.1. Superstructure

The superstructure was modeled with four elements in each of the first and the third spans, and five elements in the second span. The masses of the superstructure elements are lumped to the nodes. The cross sectional area of the superstructure is 66.73 ft^2, and the moment of inertia about the Y and Z axes are 259.77 and 11489.19 ft^4, respectively. An additional load of 2.067 kip/ft was added to represent the dead load from the concrete barrier, the pedestrian rails and the wearing surface overlay. An additional load of 2.56 kip/ft was added to represent the live load over the four lanes of the bridge.

4.3.2.2.2. Substructure

The masses of the cap beams and half of the column masses were lumped to the top nodes of each column. The abutments were modeled only with their stiffnesses (no elements), with a release in the longitudinal direction (X-axis) translation and the rotation about the transverse direction (Y-axis). Link elements were added to relate the superstructure to the cap beam as the centroid of the deck is higher than the level of the cap beam. These link elements translate loads and rotations, as the cap beams of the bridge bents are integrated in the deck box girder. Foundations were modeled as hinged supports.

4.3.2.2.3. Effective moment of inertia for bent columns

Each of the bent columns was modeled with three column sections (A, B, and C as in Figure 4.19).Sectional analyses were performed to the six sections in both directions to estimate the effective moment of inertia to be used in the model. $M-\phi$ curves for the six sections in their strong and week axes for bent 1 and 2 are presented in Figure 4.22

and Figure 4.23, respectively. Parameters obtained from these figures are used in the calculations of I_e for each column section.

Table 4.26 and Table 4.27 present these parameters in addition to the final percentage used in the analysis for the strong and weak axes of column sections for bent 1 and 2, respectively. Calculations in the two tables are following Eq. 4.1, and the concrete modulus of elasticity used for this bridge (E_c) is 449570 ksf.

Table 4.10 Bridge G-947-Calculation of effective moment of inertia for column sections in bent 1

Axis	Column section	I_g (ft^4)	M_n (kip-ft)	Φ_y (rad/ft)	I_e (ft^4)	I_e / I_g
Strong axis	A	24.13	4000	0.00060	14.83	0.60
	B	24.13	5100	0.00067	16.93	0.70
	C	24.13	6100	0.00070	19.38	0.80
Weak axis	A	8.82	2500	0.00105	5.30	0.60
	B	8.82	3200	0.00115	6.19	0.70
	C	8.82	3880	0.00123	7.02	0.80

Table 4.11 Bridge G-947-Calculation of effective moment of inertia for column sections in bent 2

Axis	Column section	I_g (ft^4)	M_n (kip-ft)	Φ_y (rad/ft)	I_e (ft^4)	I_e / I_g
Strong axis	A	24.13	5100	0.00072	15.76	0.65
	B	24.13	6500	0.00080	18.07	0.75
	C	24.13	7850	0.00085	20.54	0.85
Weak axis	A	8.82	3100	0.00120	5.75	0.65
	B	8.82	4100	0.00138	6.61	0.75
	C	8.82	5050	0.00150	7.49	0.85

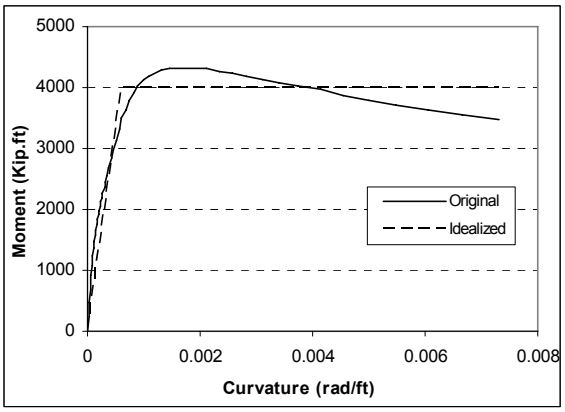

Section-A (Strong axis)

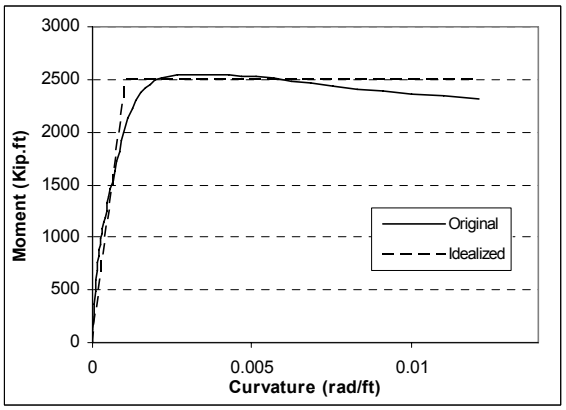

Section-A (Weak axis)

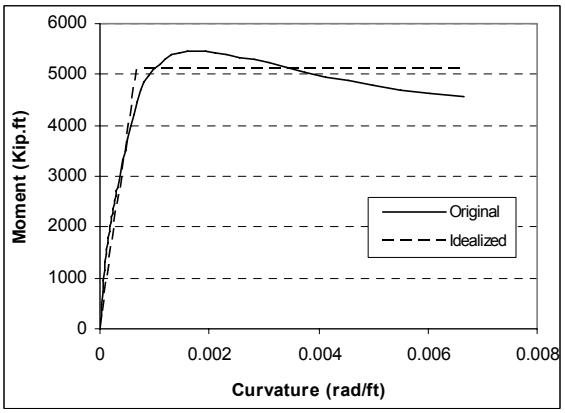

Section-B (Strong axis)

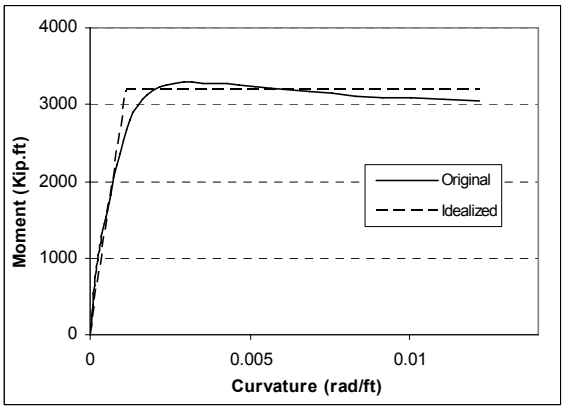

Section-B (Weak axis)

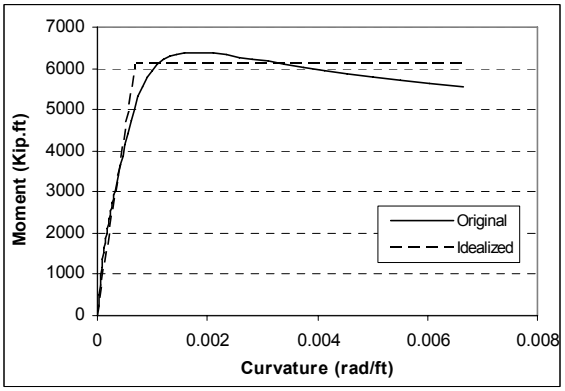

Section-C (Strong axis)

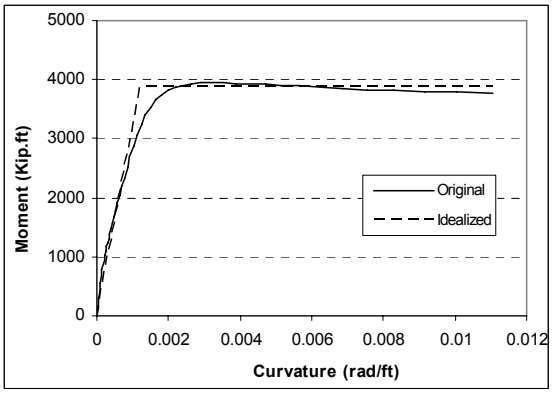

Section-C (Weak axis)

Figure 4.22 Bridge G-947 - $M-\phi$ curves for the three column sections along the columns height of bent-1

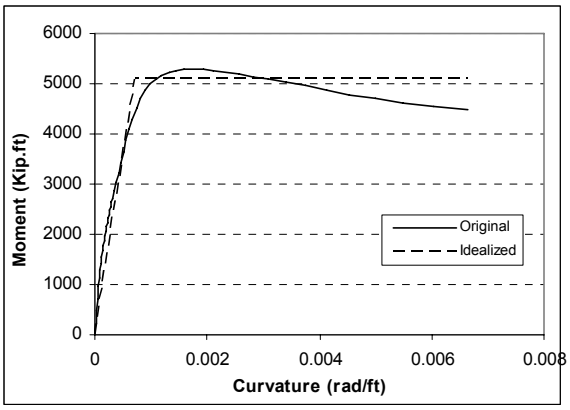

Section-A (Strong axis)

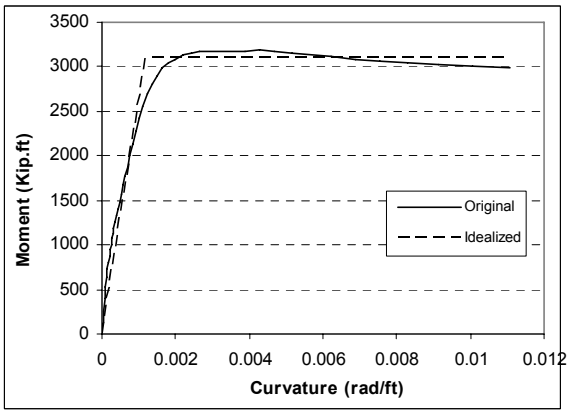

Section-A (Weak axis)

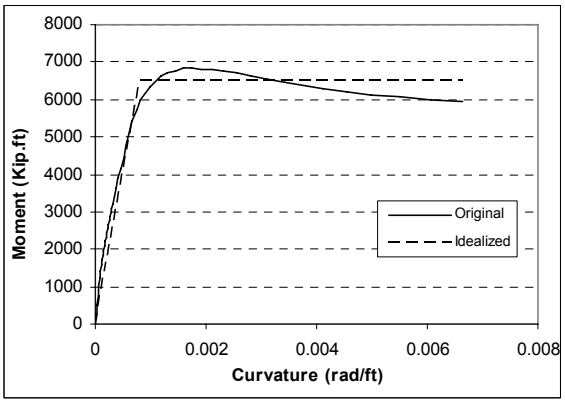

Section-B (Strong axis)

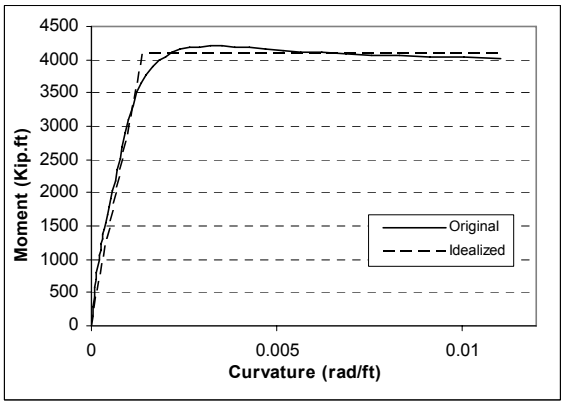

Section-B (Weak axis)

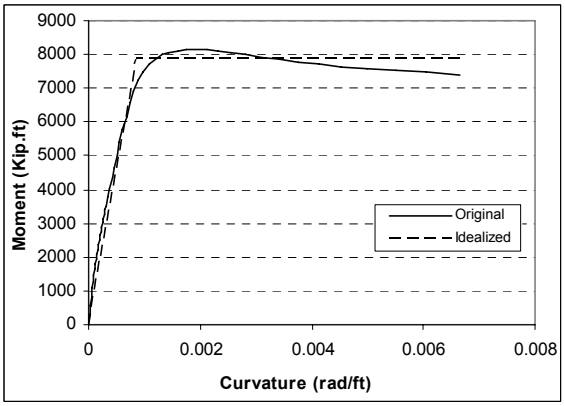

Section-C (Strong axis)

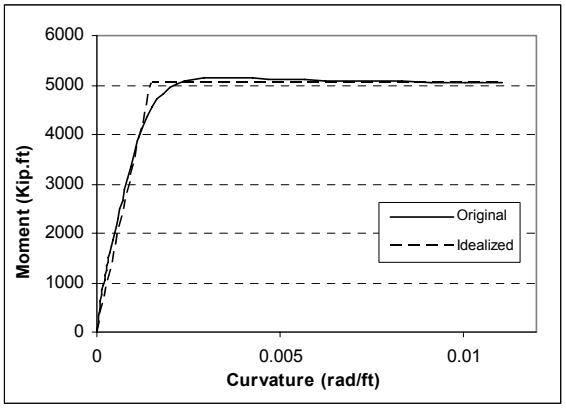

Section-C (Weak axis)

Figure 4.23 Bridge G-947 - $M-\phi$ curves for the three column sections along the columns height of bent-2

4.3.2.2.4. Spectral acceleration curve

Figure 4.24 shows the response spectrum used for the estimation of (S_a) values in the target displacement calculations. From the curve $T_0 = 0.096$ sec and $T_S = 0.480$ sec.

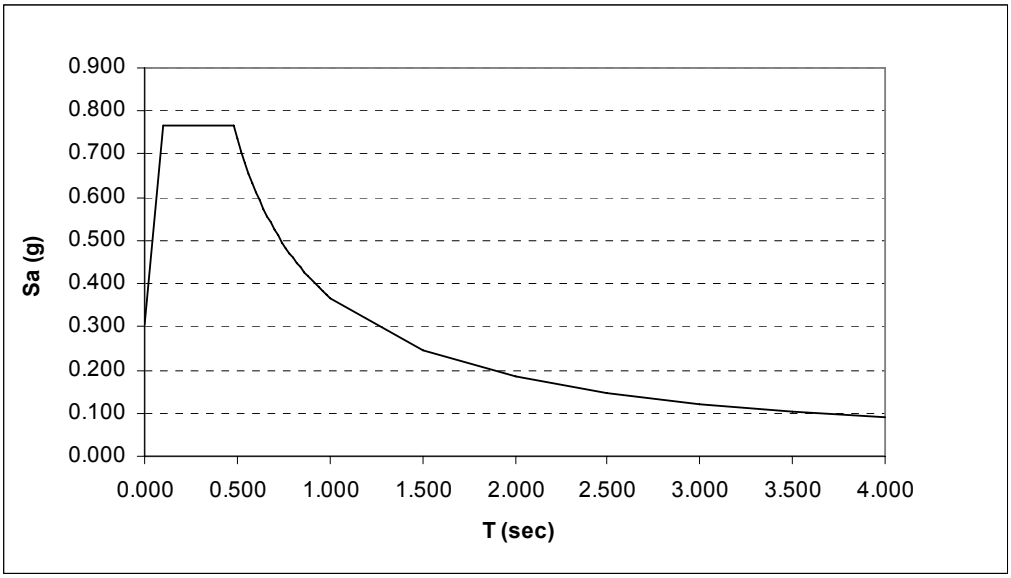

Figure 4.24 Bridge G-947- 5% damped response spectrum for BSE-2

4.3.2.3. Acceptance criteria

4.3.2.3.1. Load-deformation curve for plastic hinges

Table 4.12 presents the applied loads on the bridge columns, from which the acceptance criteria are calculated. The shear force values are negligible, which makes the values of $\left(V / b_w d\sqrt{f_c^{'}}\right)$ for all columns less than 3. From the results of Table 4.12, the acceptance criteria are presented in Table 4.13.

Table 4.12 Bridge G-947 - Applied loads on bridge columns for load-deformation calculations

	Bent 1		Bent 2	
	Column 1	**Column 2**	**Column 1**	**Column 2**
P **(lbs)**	695720	801750	693010	799360
$A_g f_c^{'}$	6030000	6030000	6030000	6030000
$\frac{P}{A_g f_c^{'}}$	0.1154	0.1330	0.1149	0.1326

Table 4.13 Bridge G-947 - Acceptance criteria of the bridge column at each performance level

	Bent 1		Bent 2	
	Column 1	**Column 2**	**Column 1**	**Column 2**
IO	0.0049	0.0048	0.0049	0.0048
LS	0.0148	0.0147	0.0149	0.0147
CP	0.0197	0.0195	0.0198	0.0195

4.3.2.3.2. Force-controlled actions

a- Shear capacity:

Based on Eq. 4.2, Eq. 4.3, and Eq. 4.4, shear capacities for each of the bridge columns were calculated. Table 4.14 presents the shear capacity calculations for each column section. Shear capacity calculations for the bridge columns were done in the direction illustrated in Figure 4.25. The indicated direction was chosen to have more defined column dimensions, which is not easy in the principle axes of the bridge.

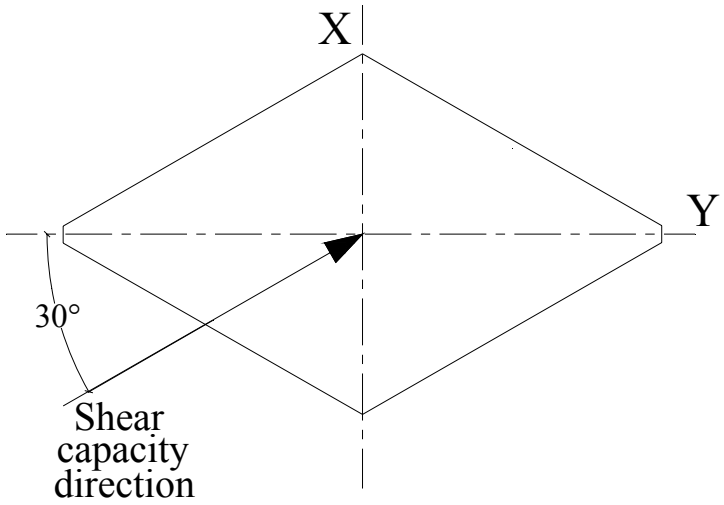

Figure 4.25 Bridge G-947- Direction used for columns shear capacity calculations

Table 4.14 Bridge G-947 - Shear capacity calculations for bridge columns

	Bent 1		**Bent 2**	
	Column 1	**Column 2**	**Column 1**	**Column 2**
Applied axial load - N_u (kips)	695.720	801.750	693.010	799.360
Column width - b (in)	42	42	42	42
Column depth - d (in)	46	46	46	46
Gross sectional area - A_g (in^2)	2010.00	2010.00	2010.00	2010.00
V_c (kips)	**248.267**	**253.850**	**248.125**	**253.724**
Area of trans. reinf. - A_v (in^2)	0.31x2.5 = 0.775	0.31x2.5 = 0.775	0.31x2.5 = 0.775	0.31x2.5 = 0.775
Spacing of trans. reinf. - s (in)	12	12	12	12
V_s (kips)	**178.250**	**178.250**	**178.250**	**178.250**
Total shear capacity - V_n (kips)	**426.517**	**432.100**	**426.375**	**431.974**

b- Reinforcement development:

As the columns in this part of the bridge contained hinged bases, there were no splices within the column heights. Reinforcement development was only identified at B/C joint locations. The development length of the reinforcement had a typical value of 3.5 ft. Based on Eq. 4.6, Table 4.15 presents the maximum stresses that can be developed in the reinforcement bars at the B/C joints of the bent columns. Accordingly, the sectional analyses for these sections were performed using the new values of the maximum stresses. The resulting $M-\phi$ curves from the sectional analyses are presented in Figure 4.26.

Table 4.15 Bridge G-947 - Calculation of maximum stress that can be developed in the reinforcement bars at B/C joint

	Bent 1		**Bent 2**	
	Column 1	**Column 2**	**Column 1**	**Column 2**
Actual length - l_b (ft)	3.5	3.5	3.5	3.5
Required length - l_d (ft)	6.44	6.44	7.71	7.71
f_s (ksi)	**32.609**	**32.609**	**27.237**	**27.237**

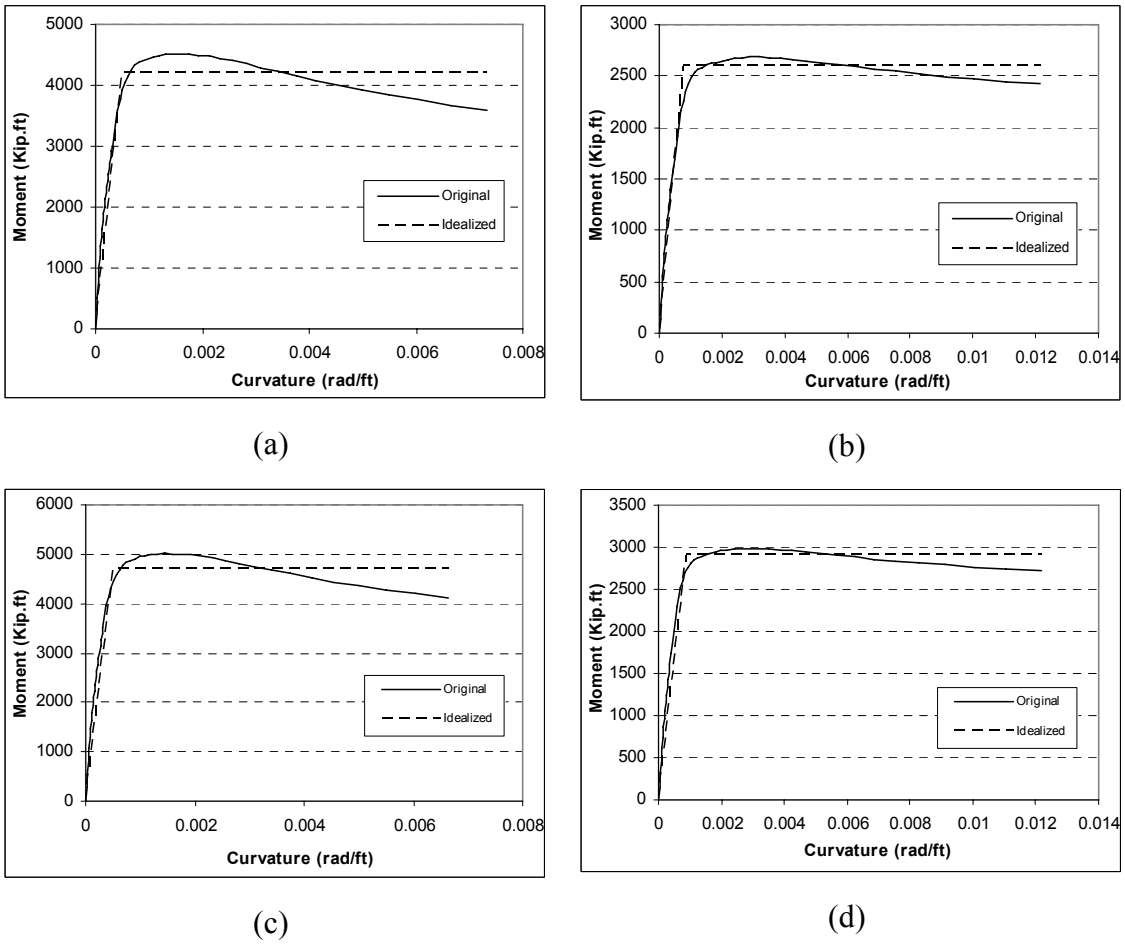

Figure 4.26 Bridge G-947 - $M-\phi$ curves for sections with inadequate reinforcement development at B/C joints (a) at bent 1 columns - strong axis; (b) at bent 1 columns - weak axis; (c) at bents 2 columns - strong axis; and (d) at bent 2 columns - weak axis

The maximum bending moment values that can be developed corresponding to the maximum stresses calculated for each section are presented in Table 4.16.

Table 4.16 Bridge G-947 - Maximum moment that can be developed in column sections at B/C joints

Column	Bent 1 - Column 1 and 2		Bent 2 - Column 1 and 2	
Axis	**Strong**	**Weak**	**Strong**	**Weak**
M_n (kip-ft)	4210	2600	4700	2900

4.3.2.4. Pushover curves and target displacements

The fundamental modes in the transverse and longitudinal directions were mode-3 and mode-1, respectively. Figure 4.27 and Figure 4.28 illustrate the fundamental modes in the two directions. The time period for mode-3 was 0.831 sec, and that for mode-1 was 1.319 sec. Pushover curves for the transverse and longitudinal directions using both load patterns are shown in Figure 4.29 and Figure 4.30, respectively.

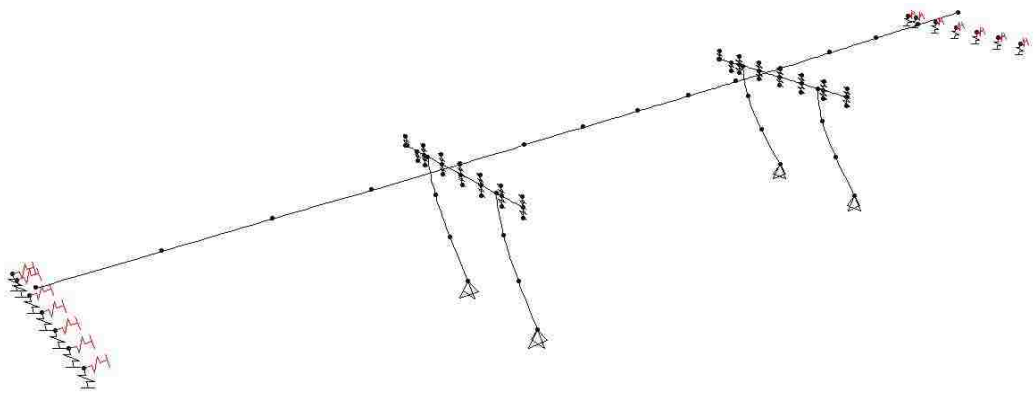

Figure 4.27 Bridge G-947 - Mode-3, the fundamental mode in the transverse direction

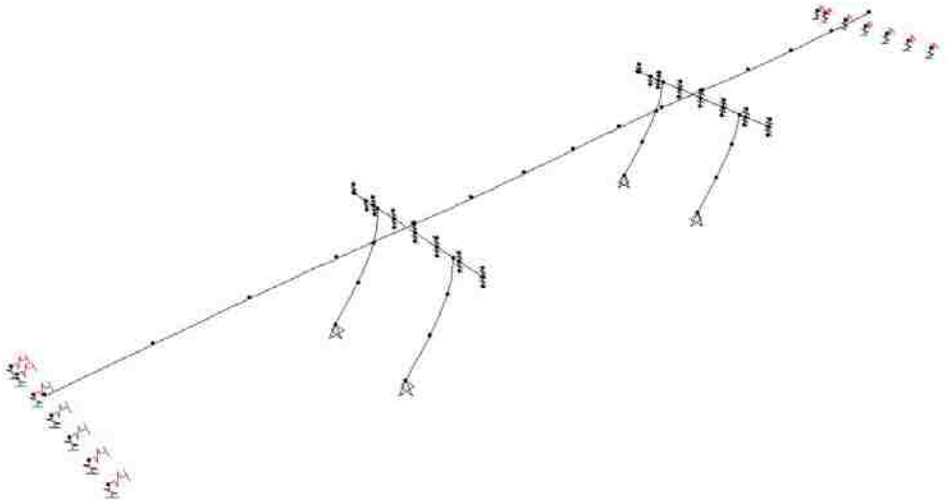

Figure 4.28 Bridge G-947 - Mode-1, the fundamental mode
in the longitudinal direction

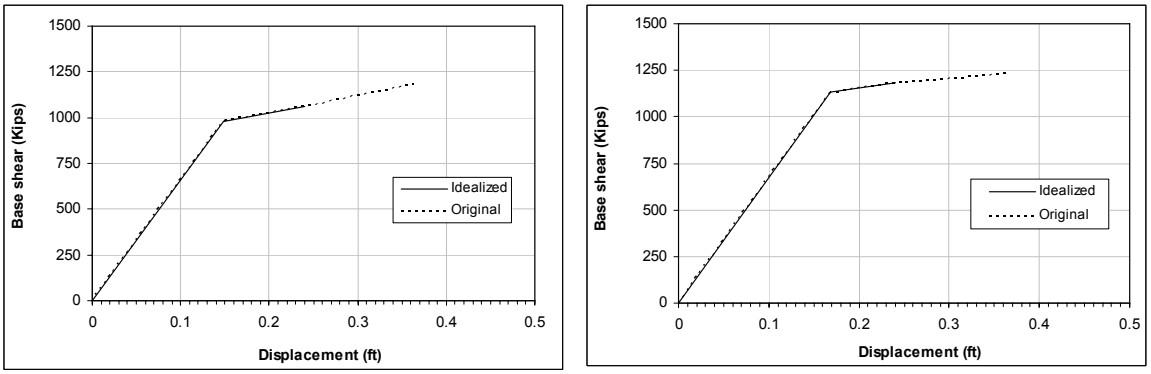

(a) (b)

Figure 4.29 Bridge G-947 - Pushover curves in the transverse direction
(a)using uniform load pattern (b)using modal pattern

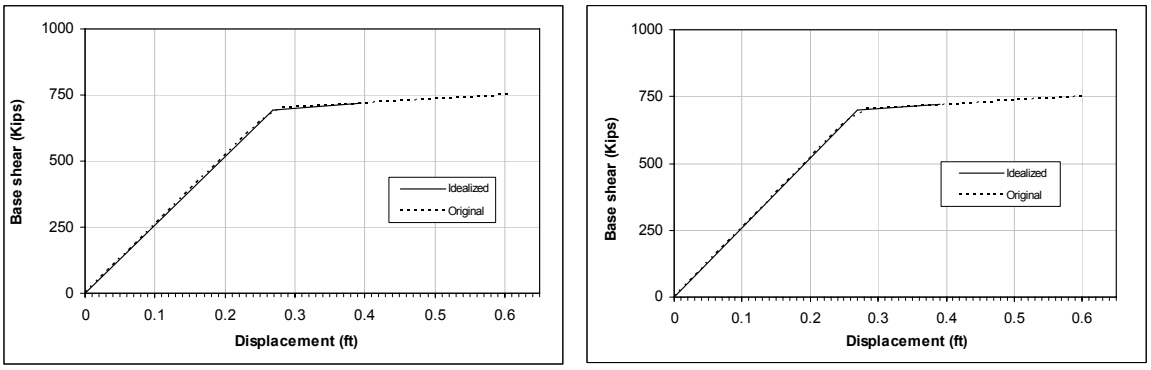

(a) (b)

Figure 4.30 Bridge G-947 - Pushover curves in the longitudinal direction
(a)using uniform load pattern (b)using modal pattern

Using the modal analysis outputs and the parameters obtained from the pushover curves, the target displacements are calculated in Table 4.17 and Table 4.18 for the transverse and the longitudinal directions, respectively.

Table 4.17 Bridge G-947 - Target displacement calculations for the transverse direction

Load Pattern	T_i (sec)	K_i	K_e	T_e (sec)	S_a (g)	PF	ϕ_{CN} (ft)	C_0*	δ_t (ft)
Uniform	0.831	6550	6550	0.831	0.442	10.586	0.0903	0.955	0.238
Modal	0.831	6700	6700	0.831	0.442	10.586	0.0903	0.955	0.238

*Values of C_1, C_2 and C_3 are equal to 1.0

Table 4.18 Bridge G-947 - Target displacement calculations for the longitudinal direction

Load Pattern	T_i (sec)	K_i	K_e	T_e (sec)	S_a (g)	PF	ϕ_{CN} (ft)	C_0*	δ_t (ft)
Uniform	1.319	2600	2600	1.319	0.279	10.665	0.0934	0.996	0.394
Modal	1.319	2580	2580	1.319	0.279	10.665	0.0934	0.996	0.394

*Values of C_1, C_2 and C_3 are equal to 1.0

4.3.2.5. Results

4.3.2.5.1. Deformation-controlled actions

At target displacement, plastic hinges at the top of the columns occurred in the two directions. Plastic hinge rotation values are presented in Table 4.19 and Table 4.20 for the transverse and longitudinal directions, respectively. In the two directions, a number of plastic hinge rotation values violated the acceptance criteria of the IO performance level. The underlined values in the tables represent the violating plastic hinges.

Table 4.19 Bridge G-947 - Plastic hinge rotations (radians) at target displacements in the transverse direction

	Bent 1		**Bent 2**	
	Column 1	**Column 2**	**Column 1**	**Column 2**
Uniform	**0.00668**	**0.00696**	0.00000	0.00000
Modal	**0.00553**	0.00097	**0.00533**	**0.00566**

Table 4.20 Bridge G-947 - Plastic hinge rotations (radians) at target displacements in the longitudinal direction

	Bent 1		**Bent 2**	
	Column 1	**Column 2**	**Column 1**	**Column 2**
Uniform	**0.00595**	**0.00591**	0.00490	**0.00496**
Modal	**0.00578**	**0.00576**	0.00473	0.00470

4.3.2.5.2. Force-controlled actions

a- Shear forces:

Shear forces in the columns at the target displacements are presented in Table 4.45 and Table 4.47 for the transverse and longitudinal directions, respectively.

Table 4.21 Bridge G-947 - Shear forces (kips) at target displacement (transverse direction)

	Bent 1		**Bent 2**	
	Column 1	**Column 2**	**Column 1**	**Column 2**
Uniform	262.99	261.65	267.09	267.97
Modal	249.05	236.75	348.93	344.76

Table 4.22 Bridge G-947 - Shear forces (kips) at target displacement (longitudinal direction)

	Bent 1		**Bent 2**	
	Column 1	**Column 2**	**Column 1**	**Column 2**
Uniform	152.51	154.38	205.73	205.94
Modal	152.21	154.14	204.87	207.63

The presented shear force values are in the principle axes of the columns (axes X and Y in Figure 4.25). To be able to compare these values to the shear capacity, components of the shear force values were obtained after combining the forces in the directions. Only the maximum value was selected for this check.

For column 1 in bent 2, by combining the shear forces (100% of the transverse direction and 30% of the longitudinal direction)

→ $100\% \times (348.93) = 348.93$ kips in the Y-axis direction

and $30\% \times 204.87 = 61.46$ kips in the X-axis direction

$348.93 \times Cos\,(30^\circ) + 61.46 \times Sin\,(30^\circ) = 332.92$ kips < 426.37 kips (from Table 4.14)

Therefore, all bridge columns are safe against brittle shear failure at the MCE level.

b- Reinforcement development:

The bending moment values at the column sections that had inadequate reinforcement development or splice lengths were observed at the target displacement. These values are presented in Table 4.23.

Table 4.23 Bridge G-947 - Bending moment values (kip-ft) at target displacement at the B/C joint locations of the columns

	Bent 1		**Bent 2**	
	Column 1	**Column 2**	**Column 1**	**Column 2**
Transverse - (Uniform)	6088.53	5823.72	5766.30	5713.67
Transverse - (Modal)	5687.23	5314.21	7599.87	7247.68
Longitudinal - (Uniform)	3451.71	3496.43	4423.77	4425.77
Longitudinal - (Modal)	3443.49	3491.73	4406.13	4461.61

From the results presented in Table 4.23, the bending moment values at the B/C joint locations in all columns at the target displacement exceeded the values obtained from the sectional analysis (in Table 4.16). Accordingly, new models were developed with the nonlinear definitions of the new plastic hinges that represent the inadequate development lengths. These hinges replaced the other hinges as they are in the same location. The

bridge was pushed to the same values of the target displacement in both directions and the resulting plastic hinge rotation values are presented in Table 4.24 and Table 4.25.

Table 4.24 Bridge G-947 - Plastic hinge rotations (radians) at target displacements in the transverse direction

	Bent 1		Bent 2	
	Column 1	**Column 2**	**Column 1**	**Column 2**
Uniform	**0.00773**	**0.00832**	0.00125	0.00164
Modal	0.00175	0.00233	**0.00752**	**0.00772**

Table 4.25 Bridge G-947 - Plastic hinge rotations (radians) at target displacements in the longitudinal direction

	Bent 1		Bent 2	
	Column 1	**Column 2**	**Column 1**	**Column 2**
Uniform	**0.00848**	**0.00865**	**0.00908**	**0.00932**
Modal	**0.00847**	**0.00865**	**0.00905**	**0.00932**

The underlined values of the plastic hinge rotations violated the acceptance criteria of the IO level. Some of the values are very near to the CP level. Accordingly, the design of this bridge is governed by the inadequate development lengths of columns longitudinal reinforcement into the cap beams, and the bridge is at risk of bond slippage at this location under the MCE level.

4.3.3. Bridge (H-1211)

4.3.3.1. Bridge description

H-1211 is a 2-spans/1-pier bridge located at the intersection of Washington Avenue (overpass) and the U.S. 95-highway (underpass). The total length of the bridge is 250 ft, divided into two unequal spans of 130 ft and 120 ft as a west side span and an east side span, respectively. The plan and elevation of the bridge are shown in Figure 4.31.

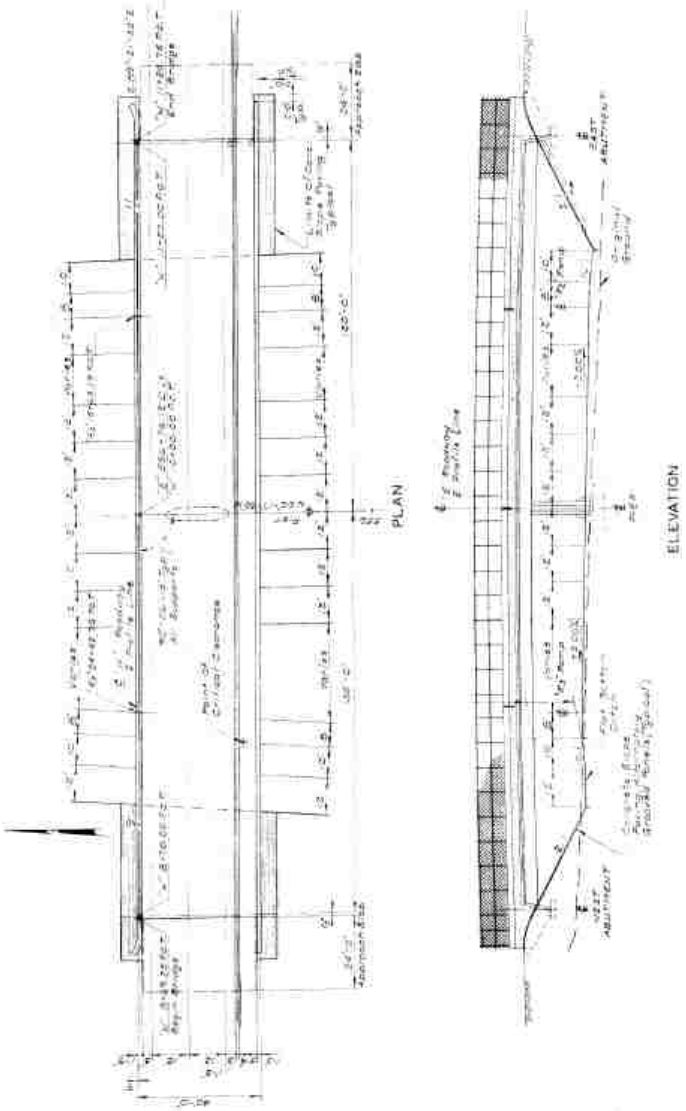

Figure 4.31 Bridge H-1211 - Plan and elevation

The superstructure of the bridge is a cast-in-place box girder concrete deck, with three intermediate webs. Figure 4.32 shows the bridge deck section along with the pier column. The total width of the deck is 40 ft and its total depth is 5 ft. These dimensions are constant over the bridge length.

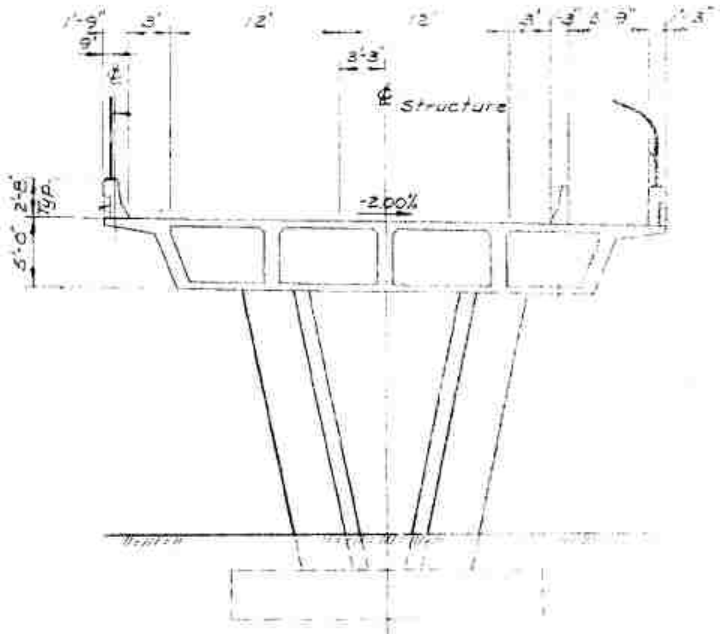

Figure 4.32 Bridge H-1211 - Bridge section

The substructure of the bridge consists of a single column pier. The column section is variable along its height from 12 ft width at the foundation level to 20 ft at the deck soffit. The two sections of the column (the upper and the lower parts of the column) are shown in Figure 4.33 (a) and (b). All the longitudinal reinforcement bars in the column are #11, and all the transverse reinforcement bars are #4. At the end spans (at both abutments), the bridge deck ends with an end diaphragm. Each of the two diaphragms rests on a foundation along its length, with a neoprene pad in between to allow for the expansion of the bridge deck in the longitudinal direction. Figure 4.34 (a) and (b) shows

the details of the end diaphragm and its footing. The concrete compressive strength for this bridge is 3.5 ksi and the reinforcement yield strength is 60 ksi.

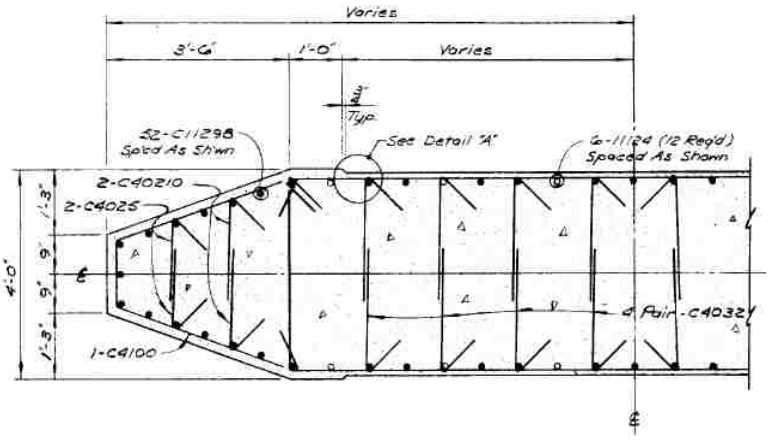

(a)

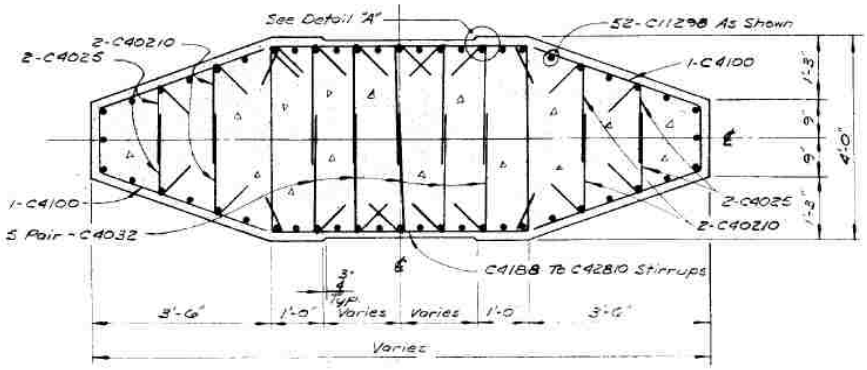

(b)

Figure 4.33 Bridge H-1211 - Column sections at (a) top section and (b) bottom section of the column

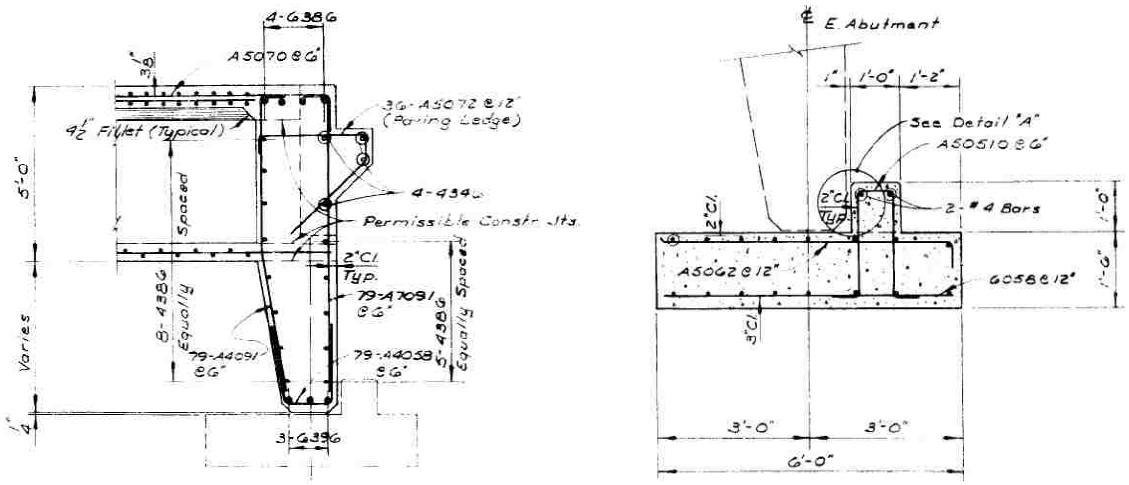

(a) (b)

Figure 4.34 Bridge H-1211 - (a) End diaphragm section and (b) abutment footing section

4.3.3.2. Bridge model

Figure 4.35 shows the structural model used for the evaluation of the bridge in both transverse and longitudinal directions. The control node in the analysis was chosen to be the deck node at the location of the pier.

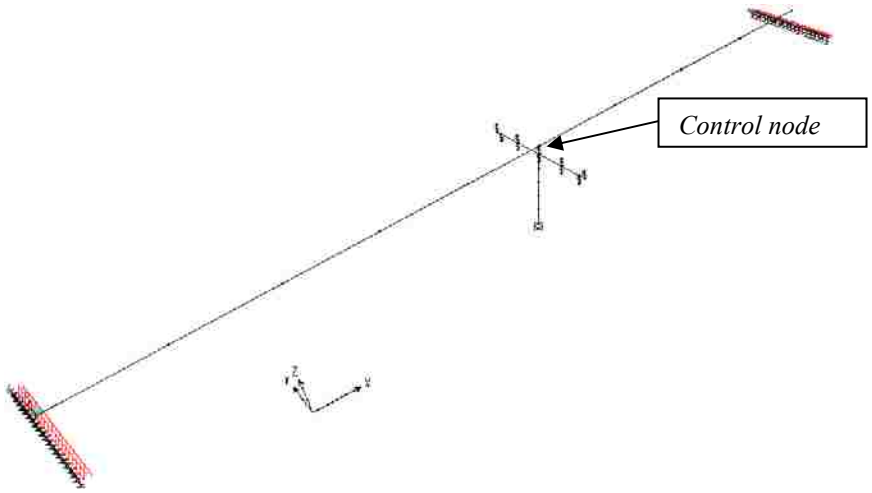

Figure 4.35 Bridge H-1211 - Structural model for both transverse and longitudinal direction

4.3.3.2.1. Superstructure

The superstructure of the bridge was modeled with five (equal in length) elements in the west span (the longer span) and four elements in the east span of the bridge. The cross sectional area of the bridge deck is 61.13 ft^2, the moment of inertia about the Y-axis is 217.13 ft^4 and about the Z-axis is 7192.73 ft^4. An additional dead load with a value of 2.864 kip/ft was added to account for the wearing surfaces, the concrete barriers, and the pedestrian rails. An additional load of 1.25 kip/ft was added to account for the live load from two traffic lanes.

4.3.3.2.2. Substructure

The variable pier column was modeled as five different sections gradually varying with its length from 12 ft at the bottom section to 20 ft at the top one. Figure 4.36 shows the variable sections used in the model.

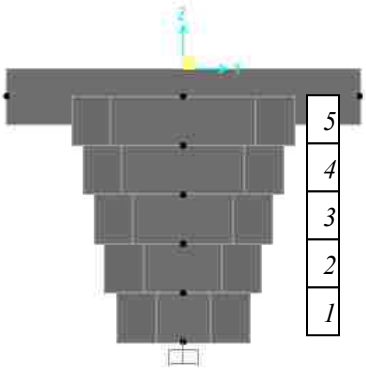

Figure 4.36 Bridge H-1211 - Column sections as modeled in SAP2000 and their labels

4.3.3.2.3. Effective moment of inertia for pier column

In order to estimate the stiffness reduction in the column, each section (out of the five sections used in the model) was analyzed to calculate its effective moment of inertia in both directions. $M-\phi$ curves for the five sections in their strong and week axes are presented in Figure 4.37 and Figure 4.38, respectively. Parameters obtained from these figures are used in the calculations of I_e for each column section.

Table 4.26 and Table 4.27 present these parameters in addition to the final percentage used in the analysis for the strong and weak axis of the column sections, respectively. Calculations in the two tables are following Eq. 4.1, and the concrete modulus of elasticity used for this bridge (E_c) is 485592 ksf.

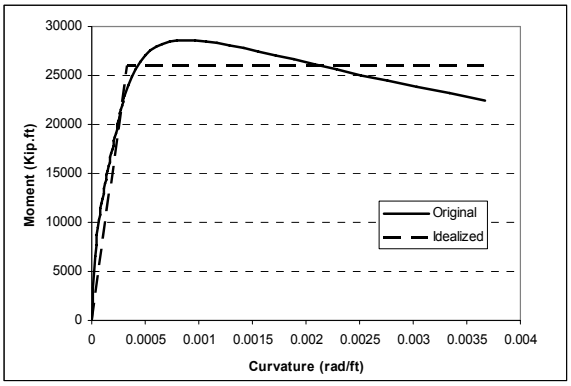

column section-1

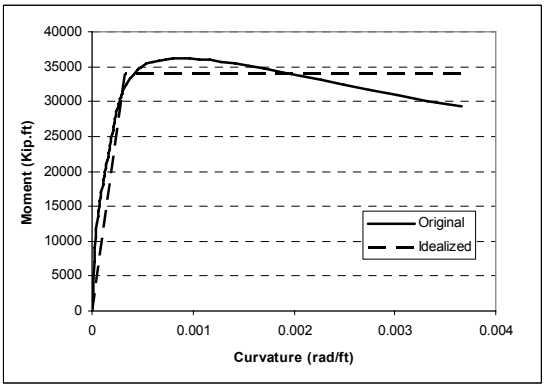

column section-2

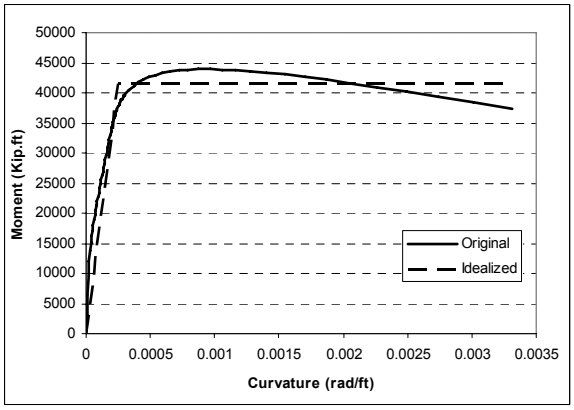

column section-3

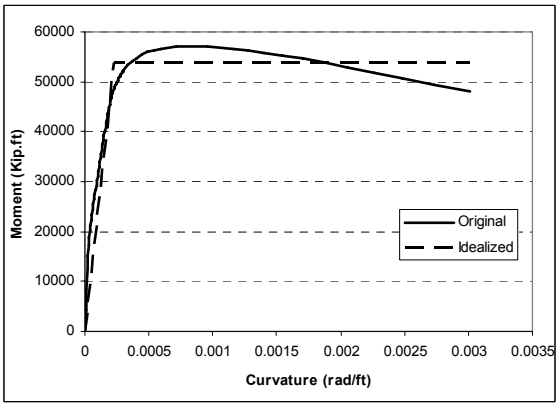

column section-4

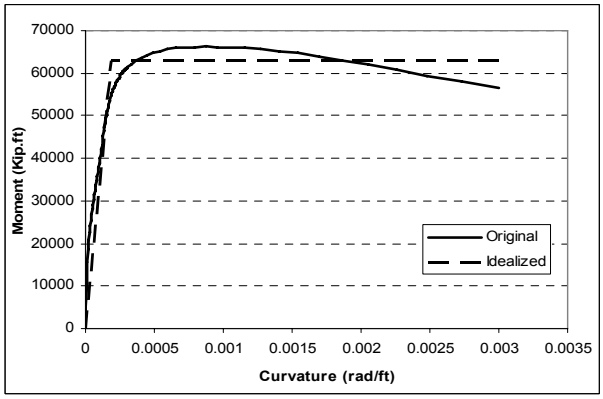

column section-5

Figure 4.37 Bridge H-1211 - $M-\phi$ curves in the strong axis for the five column sections along the pier height

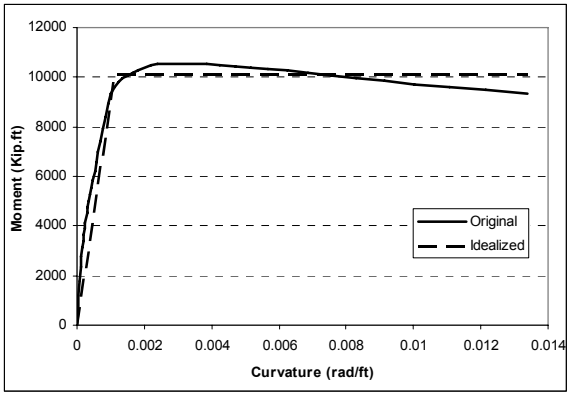

column section-1

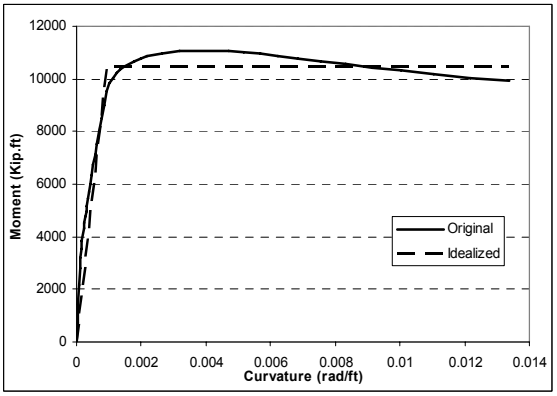

column section-2

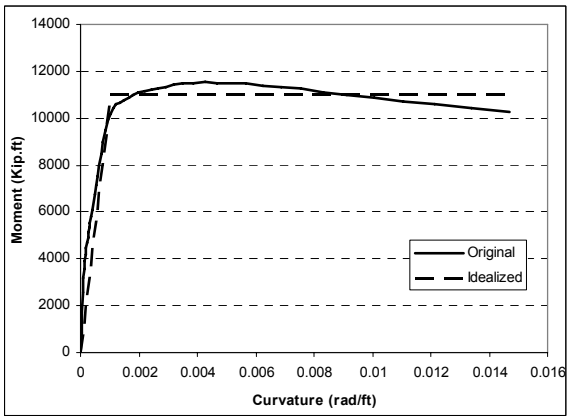

column section-3

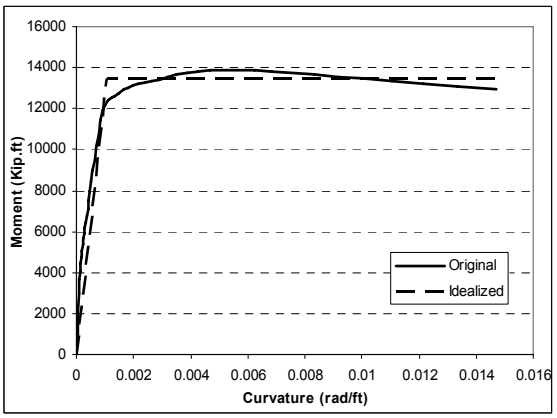

column section-4

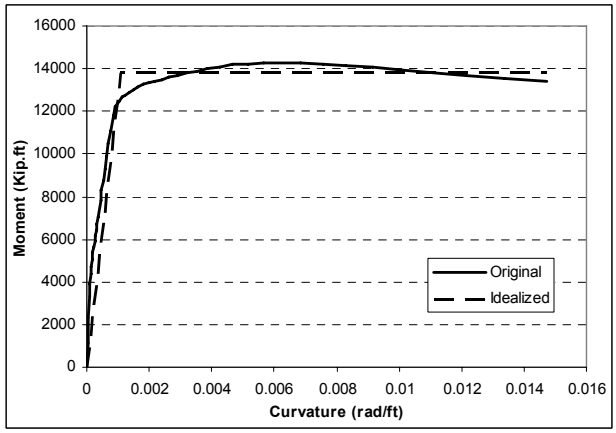

column section-5

Figure 4.38 Bridge H-1211 - $M-\phi$ curves in the weak axis
for the five column sections along the pier height

Table 4.26 Bridge H-1211- Calculation of effective moment of inertia for column sections in the strong axis

Column section	I_g (ft^4)	M_n (kip-ft)	Φ_y (rad/ft)	I_e (ft^4)	I_e / I_g
1	365.64	26000	0.000325	164.75	0.45
2	623.14	34000	0.000325	215.43	0.35
3	967.26	41500	0.000250	341.85	0.35
4	1422.55	54000	0.000227	489.89	0.35
5	2004.99	63000	0.000185	701.29	0.35

Table 4.27 Bridge H-1211- Calculation of effective moment of inertia for column sections in the weak axis

Column section	I_g (ft^4)	M_n (kip-ft)	Φ_y (rad/ft)	I_e (ft^4)	I_e / I_g
1	41.30	10100	0.00110	18.91	0.45
2	52.42	10500	0.00092	23.63	0.45
3	63.08	11000	0.00102	22.20	0.35
4	73.75	13450	0.00108	25.65	0.35
5	84.42	13800	0.00109	26.07	0.30

4.3.3.2.4. Spectral acceleration curve

Figure 4.39 shows the response spectrum used for the estimation of (S_a) values in the target displacement calculations. From the curve $T_0 = 0.085$ sec and $T_S = 0.427$ sec.

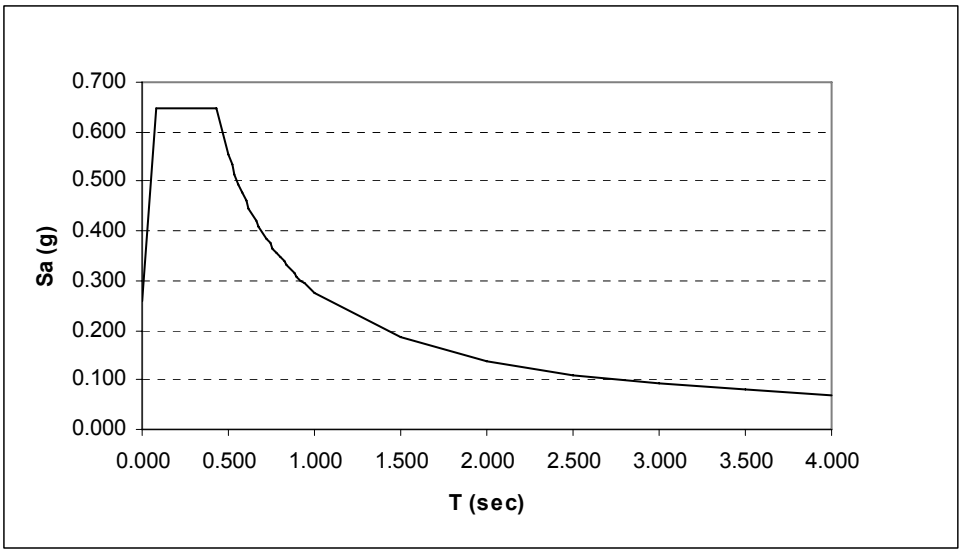

Figure 4.39 Bridge H-1211- 5% damped response spectrum for BSE-2

4.3.3.3. Acceptance criteria

4.3.3.3.1. Load-deformation curve for plastic hinges

The applied loads on the column, from which the acceptance criteria are calculated, are presented in Table 4.28. Calculations in this table are done for the lower section (section 1) as the potential plastic hinge location is at the lower part of the column.

Table 4.28 Bridge H-1211 - Applied loads on bridge column for load-deformation calculations

Axial Load (*P*)	2235 kips
Shear Force (*V*)	0.00 kips
$\frac{P}{A_g f_c^{'}}$	0.113
$\frac{V}{b_w d \sqrt{f_c^{'}}}$	0.00

The generalized load-deformation relation for each bridge is estimated based on the values calculated in Table 4.28, and the acceptance criteria are presented in Table 4.29.

Table 4.29 Bridge H-1211 - Acceptance criteria for the lower column section of the bridge

Performance level	Column section 1
IO	0.00491
LS	0.01487
CP	0.01978

4.3.3.3.2. Force-controlled actions

a- Shear capacity:

Shear capacity of the column was calculated at its lower section. This section is the smallest section in its dimensions, which makes it the most critical along the column's height. Based on Eq. 4.2, Eq. 4.3, and Eq. 4.4, calculations of the column's shear capacity in the two directions are presented in Table 4.30.

Table 4.30 Bridge H-1211 - Shear capacity calculations for bridge columns

	Transverse direction	**Longitudinal direction**
Applied axial load - N_u (kips)	2235	2235
Column depth - d (in)	141	36.25
Column width - b (in)	39.25	144
Gross sectional area - A_g (in^2)	5652	5652
V_c (kips)	**784.291**	**739.756**
Area of trans. reinf. - A_v (in^2)	0.2 x 2 = 0.4	0.2 x 7 = 1.4
Spacing of trans. reinf. - s (in)	4	4
V_s (kips)	**846.000**	**761.250**
Total shear capacity - V_n (kips)	**1630.291**	**1501.006**

b- Reinforcement development:

The bridge column has no splices along its height, and is properly hooked to the foundation. However, at the location of the beam-column joint, the development length provided for the longitudinal reinforcement bars is 5 ft.

Based on Eq. 4.5 and Eq. 4.6;

For #11 rebars,

Development length $l_d = 5.96$ ft, which means that the provided development length is insufficient and Eq. 4.6 should be used to estimate the maximum stress that can be developed in the rebar as follows:

$$f_s = \left(\frac{l_b}{l_d}\right) f_y = \left(\frac{5.0}{5.96}\right) 60 = 50.336 \text{ ksi}$$

Sectional analysis for the top section of the column was performed using the new value (f_s) instead of f_y for the reinforcement and the resulting $M - \phi$ relationships are presented in Figure 4.40 for both the strong and the weak axes of the column. The strong

axis is used for the transverse direction and the weak axis is used for the longitudinal direction.

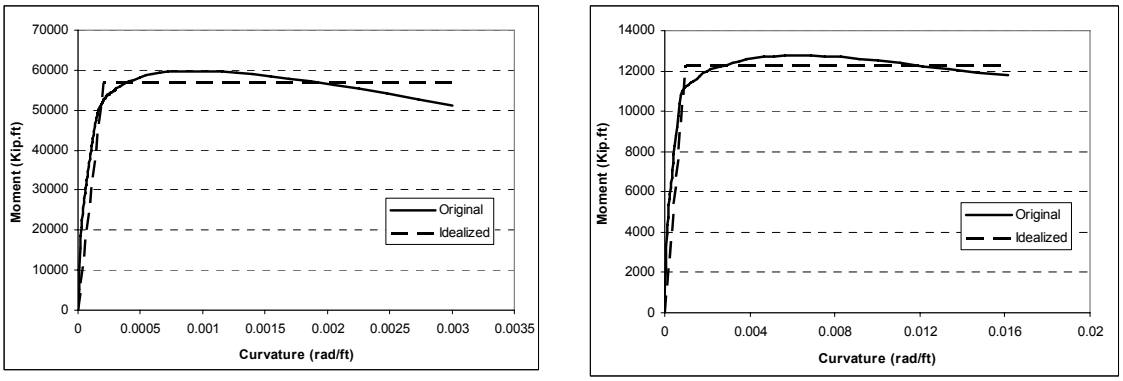

(a) (b)

Figure 4.40 Bridge H-1211- $M-\phi$ curves at the location of the B/C joint for (a)the strong axis and (b)the weak axis of the column top section

Figure 4.40 shows that the maximum moment that can be reached at the top column section is 57,000 kip-ft in the transverse direction and 12,300 kip-ft in the longitudinal direction.

4.3.3.4. Pushover curves and target displacement

Evaluation of this bridge was performed using only the uniform load pattern. The reason for choosing only one pattern is having only one column is the bridge, and the control node is above this column. In this case using different patterns will be of insignificant value.

The fundamental modes in the transverse and longitudinal directions were mode-4 and mode-1, respectively. The two modes are illustrated in Figure 4.41 (a) and (b). The time period for mode-4 was 0.276 sec, while the time period for mode-1 was 0.692 sec. Figure 4.42 shows the pushover curves for both the transverse and the longitudinal

directions. From the pushover curves, parameters used in calculating the target displacement are presented in Table 4.31 along with its final values.

Table 4.31 Bridge H-1211 - Target displacement calculations for both directions

Direction	T_e (sec)	S_a (g)	PF	ϕ_{CN} (ft)	C_0	C_1^*	δ_t (ft)
Transverse	0.276	0.649	9.723	0.120	1.165	0.901	0.0423
Longitudinal	0.692	0.409	12.821	0.084	1.076	1.0	0.1718

*Values of C_2 and C_3 are equal to 1.0

The pushover curves in the two directions show that $K_e = K_i$. Accordingly, the effective time period equals the fundamental time period for the analysis in both directions ($T_e = T_i$). In addition to that, the value of C_1 in the transverse direction is calculated based on Eq. 3.8 as $T_e < T_s$. However, in the longitudinal direction, $C_1 = 1.0$ as $T_e > T_s$.

From the pushover curves, in the transverse direction:

$V_y = 1470$ kips and the effective weight of the bridge $W = 2235$ kips

$$R = \frac{0.649}{1470/2235} \times \frac{1}{1.165} = 0.847$$

$$C_1 = \left[1.0 + (R-1)T_s / T_e\right] / R = \left[1.0 + (0.847-1)0.427/0.276\right] / 0.847 = 0.901$$

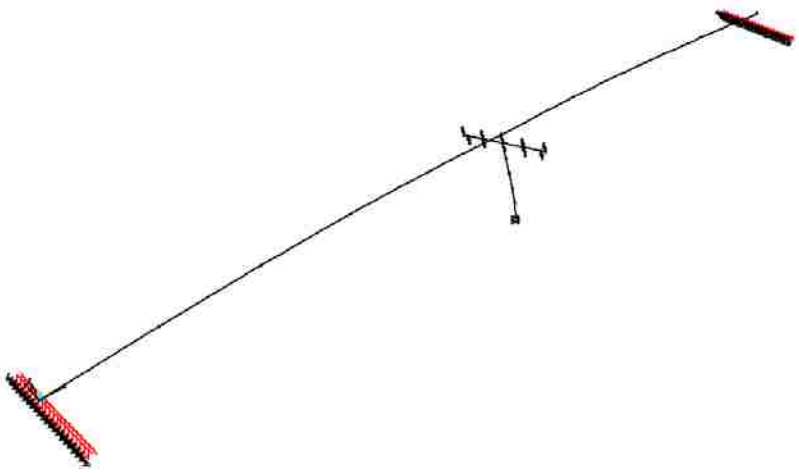

(a)

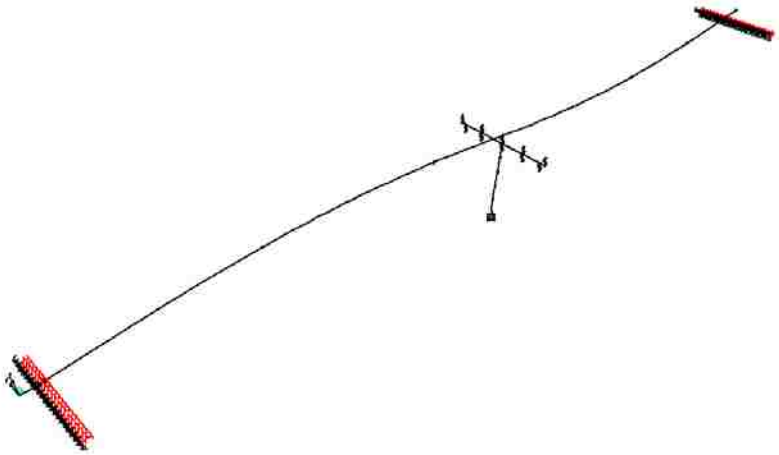

(b)

Figure 4.41 Bridge H-1211 - (a) Mode-4, the fundamental mode in the transverse direction and (b) Mode-1, the fundamental mode in the longitudinal direction

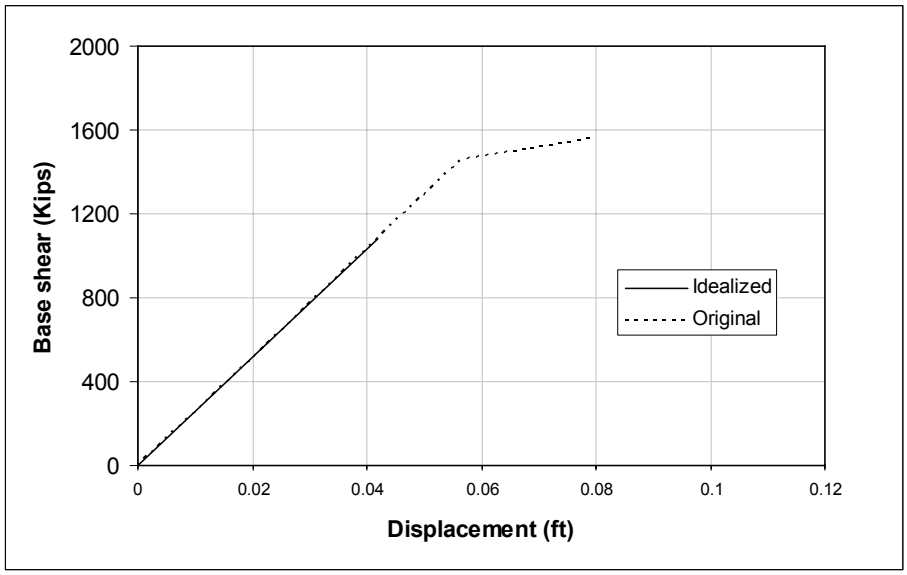

(a)

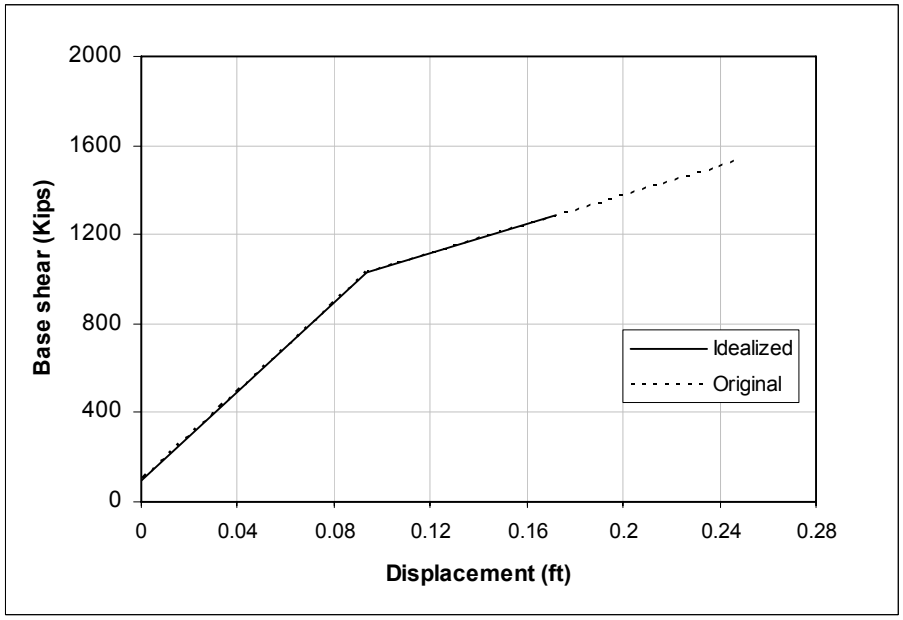

(b)

Figure 4.42 Bridge H-1211 - Pushover curves in (a) the transverse direction and (b) the longitudinal direction

4.3.3.5. Results

4.3.3.5.1. Deformation-controlled actions

Plastic hinge rotations formed at the target displacements in both directions are presented in Table 4.32. It shows that the column did not encounter any plastic hinge

rotation in the transverse direction. However, in the longitudinal direction, a plastic hinge was formed with rotation value 0.00417 radians. When compared to the value presented in Table 4.29, the plastic hinge rotation did not violate the acceptance criteria of the IO performance level.

Table 4.32 Bridge H-1211 - Plastic hinge rotation values (radians) at target displacement in both directions

	Transverse	**Longitudinal**
Plastic hinge rotation	0.00000	0.00417

4.3.3.5.2. Force-controlled actions

a- Shear forces:

Shear forces in the bridge column at the target displacement for both transverse and longitudinal directions are presented in Table 4.33.

Table 4.33 Bridge H-1211 - Shear force values (kips) in the bridge column at target displacement

Direction	**Transverse**	**Longitudinal**
Shear Force (kips)	1146.23	1280.83

The two values of the shear forces are lower than the shear capacity of the column section presented in Table 4.30. Thus, the bridge column is safe against shear failure under the MCE level.

b- Reinforcement development:

At the target displacement in the transverse direction the bending moment value at the column's top section is near zero (i.e. did not reach 57,000 kip-ft). However, in the longitudinal direction, the moment at the column's top section was 14,872.89 kip-ft (which exceeded 12,300 kip-ft). Accordingly, another model was analyzed; including the definition of the plastic hinge at the column's top section with its reinforcement maximum stress equals $f_s = 50.336\,\text{ksi}$. The bridge was pushed to the same target displacement and the top hinge rotation value was 0.00229 radians. From Table 4.2, the acceptance value is 0.005 radians. Accordingly, the plastic hinge rotation in this direction did not violate the acceptance criteria and the bridge is not at risk of reinforcement bond slippage under the MCE level.

4.3.4. Bridge (G-953)

4.3.4.1. Bridge description

G-953 is a 6-spans/5-bents bridge located at the intersection of Carey Avenue (overpass) and I-15 highway (underpass). The total length of the bridge is 492.1 ft, measured along the centerline of Carey Avenue. The profile of this bridge is curved in the horizontal and the vertical directions. This profile makes the evaluation of the bridge in the transverse direction different than the other bridges in this study as it should be pushed in the two opposite directions transversely. As shown in the Figure 4.43, the bridge includes 4 expansion joints. The substructure elements of the bridge are skewed bents at angles ranging from 38.47 degrees with the line perpendicular to Carey Avenue's centerline at the west side to 30.73 degrees at the east side of the bridge. The superstructure of the bridge is a cast-in-place box girder concrete deck, with 8 intermediate webs. Figure 4.44 (a) to (c) shows the bridge deck sections along with the different bents of the bridge. The total width of the bridge deck is 75.17 ft. The total depth of the bridge deck is 4 ft in the first three spans, 5 ft in the last two spans and varies linearly from 4 ft to 5 ft in span 4. The substructure of the bridge consists of five bents with variations in their structural systems. Bent 1 contains fixed base columns to the foundations and fixed to the cap beam. Bents 2 to 5 are frames with hinged base columns to the foundations and fixed to the cap beams. Each of the bridge bents is symmetric around its vertical centerline. Accordingly, all bents have two typical external columns and two typical internal columns. The concrete compressive strength for this bridge is 5 ksi and 3 ksi for the substructure and the superstructure components, respectively. And the reinforcement yield strength is 60 ksi.

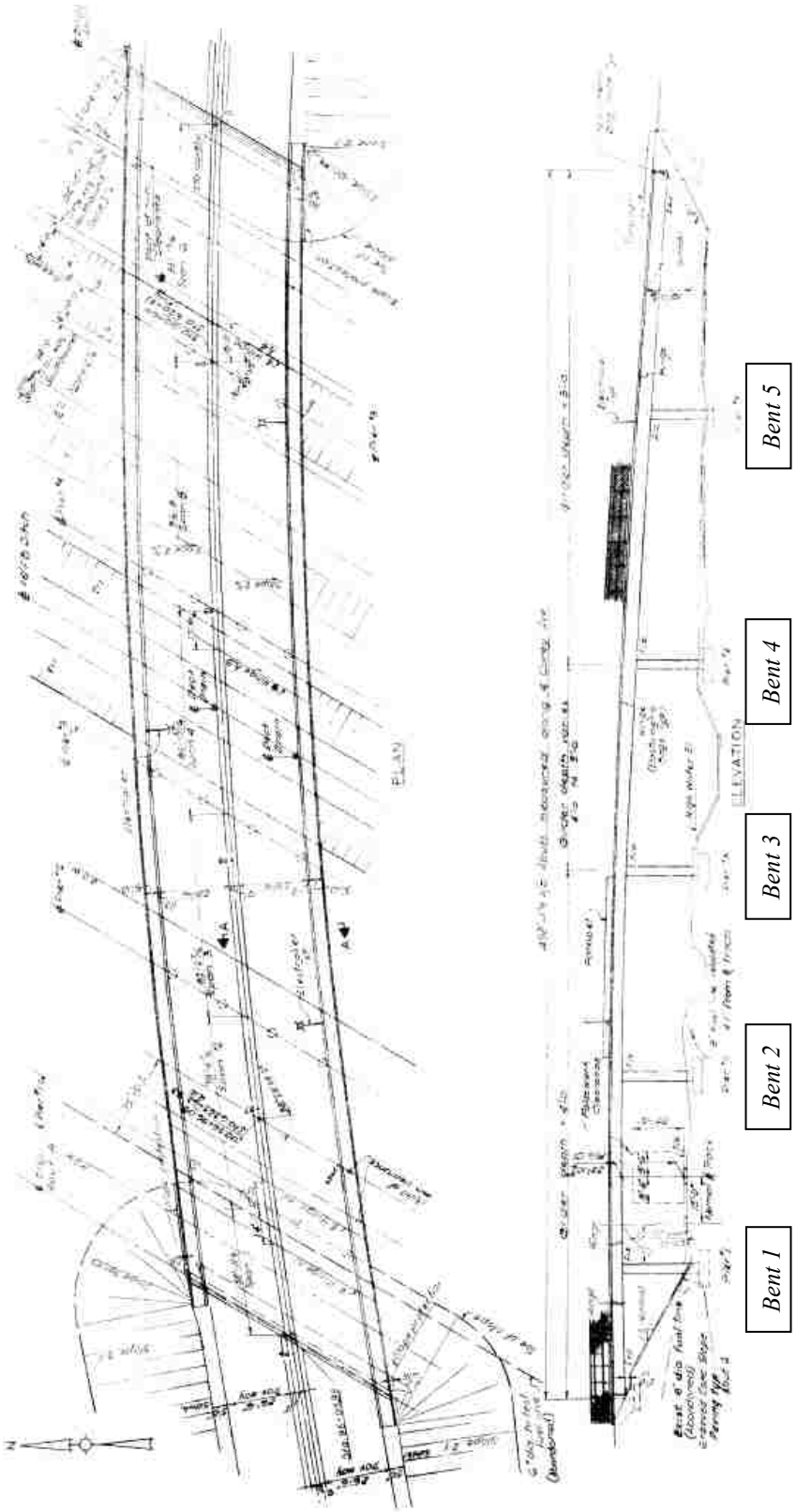

Figure 4.43 Bridge G-953 - Plan and elevation

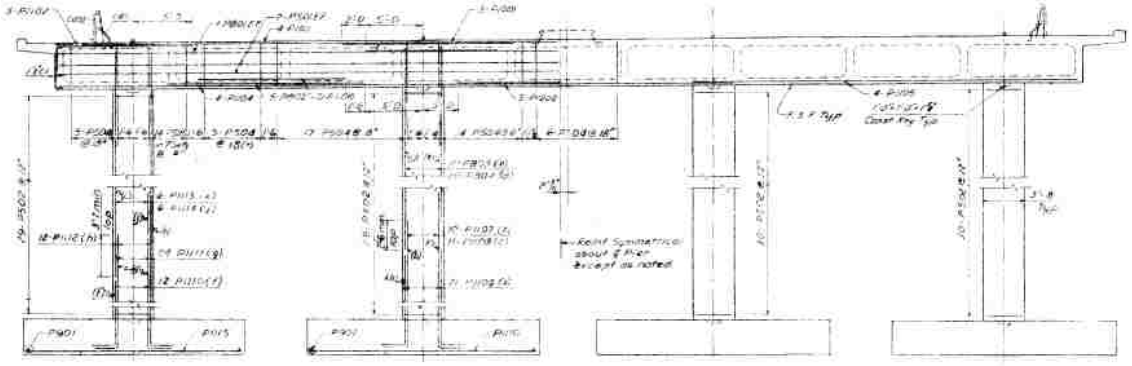

(a)

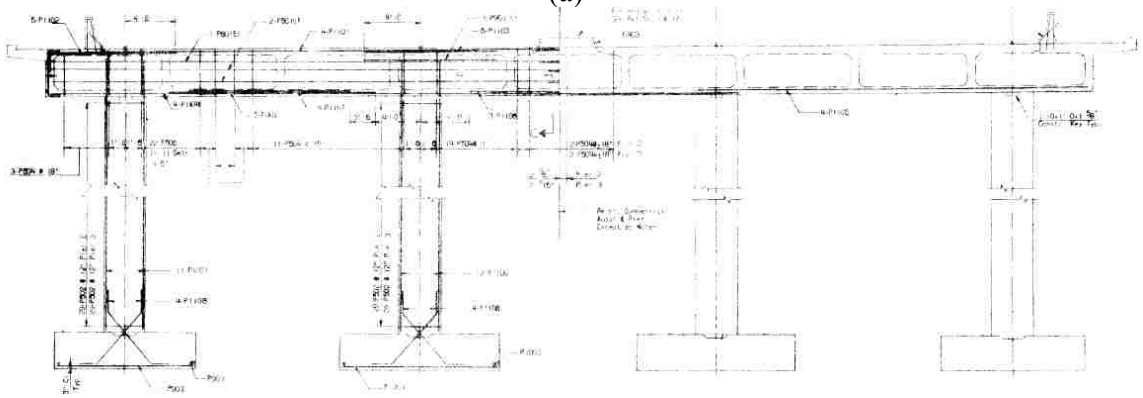

(b)

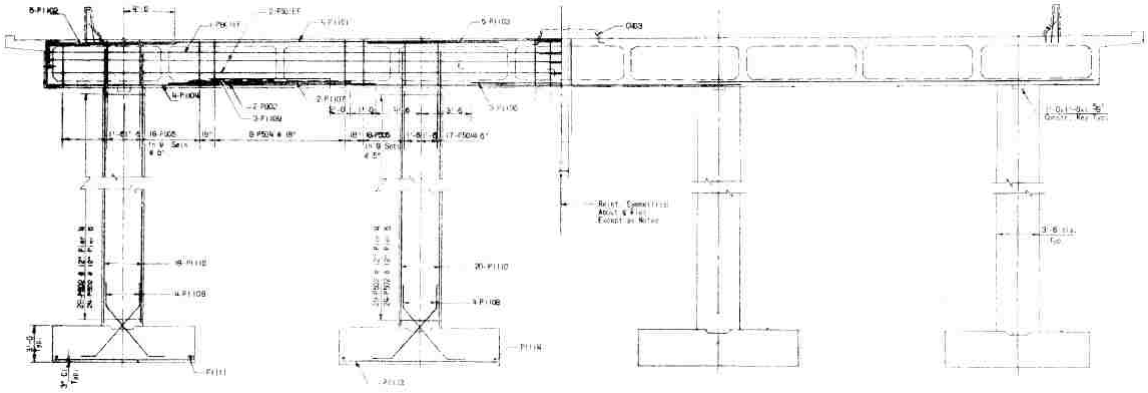

(c)

Figure 4.44 Bridge G-953 - Deck section at (a) bent 1; (b) bents 2 and 3; and (c) bents 4 and 5

4.3.4.2. Bridge model

Figure 4.45 shows the structural model used for the analysis of the bridge in the transverse direction, and Figure 4.46 (a) to (c) shows the structural models used for the

analyses of the bridge in the longitudinal direction. The units are separated at the locations of the expansion joints.

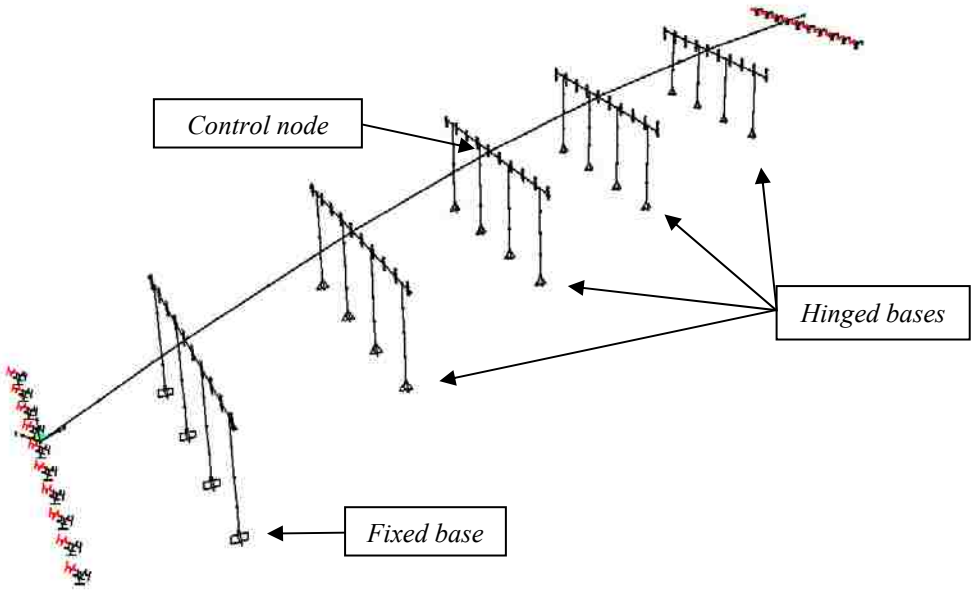

Figure 4.45 Bridge G-953 - Structural model for transverse direction analysis

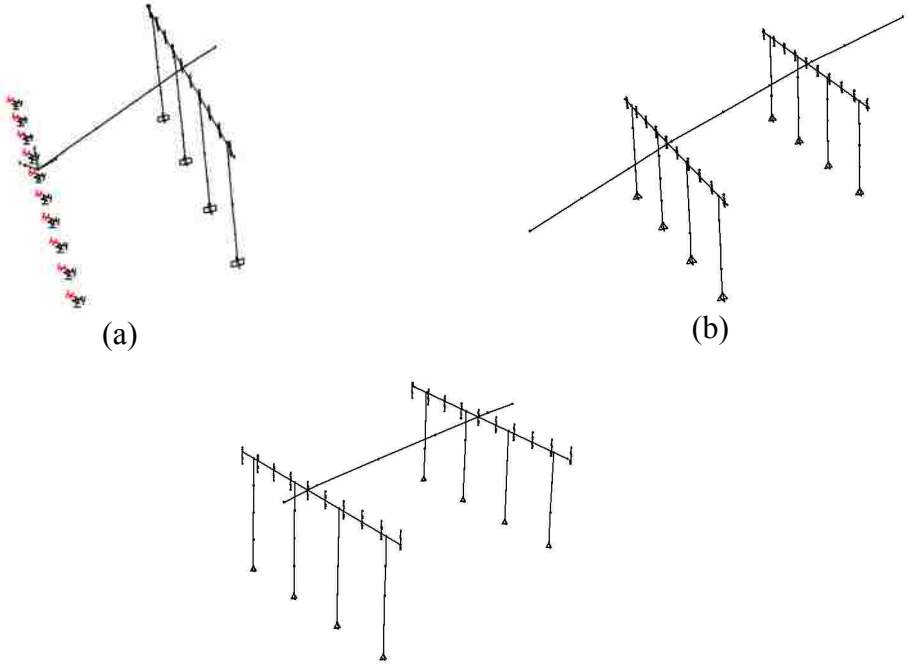

Figure 4.46 Bridge G-953 - Structural models for longitudinal direction
(a) unit-1; (b) unit-2; and (c) unit-3.

4.3.4.2.1. Superstructure

The superstructure was modeled as 3 or 4 frame elements at each span located at the centerline of the bridge deck. The masses of the bridge deck were lumped at the nodes of the superstructure elements. The bridge deck section properties are presented in Table 4.34, where the properties at span 4 vary from span 3 to 5 as mentioned in the previous section.

Table 4.34 Bridge G-953 - Sectional properties of the bridge deck

	Spans 1, 2, and 3	**Spans 5 and 6**
Cross sectional area (ft^2)	101.04	107.71
Moment of inertia about Y-axis (ft^4)	253.63	432.07
Moment of inertia about Z-axis (ft^4)	46141	49374.19

4.3.4.2.2. Substructure

In modeling the five bents of the substructure, the masses of the cap beams and half of the columns were lumped to the top node of the column. Bent 1 was modeled with fixed supports at its column bases. Bents 2 to 5 were modeled with their column bases as hinged supports. Accordingly, in the plastic hinges definitions, each column in bent 1 had two plastic hinges defined (bottom and top), while columns in bents 2 to 5 had only one plastic hinge defined at the top part of the column. Abutments were modeled only with their stiffness, with a release in the longitudinal direction (X-axis) translation and the rotation about the transverse direction (Y-axis). Link elements were used to relate the

superstructure to the cap beams. These link elements translate all degrees of freedom as the cap beam is integrated in the deck at all bents.

4.3.4.2.3. Effective moment of inertia for bent columns

Each of the bridge bents had different column sections defined. Bent 1 had four column sections, two for the external columns and two for the internal columns. Bents 2 and 3 had the same column section definitions (one for the external and one for the internal column of the bent), and bents 4 and 5 had the same column section definitions (also one for the external and one for the internal column of the bent). All columns in the bridge are circular columns with equally distributed reinforcement within the sections. Table 4.35 presents the columns diameter and reinforcement (longitudinal and transverse) for each bent.

Table 4.35 Bridge G-953 - Column sections definition in the bridge bents

	Bent 1				**Bent 2 and 3**		**Bent 4 and 5**	
	External column		**Internal column**		**External column**	**Internal column**	**External column**	**Internal column**
	Lower	**Upper**	**Lower**	**Upper**				
Column diameter (ft)	3.67	3.67	3.67	3.67	3.50	3.50	3.50	3.50
Longitudinal Reinforcement*	24 x 2 #11	12 #11	21 x 2 #11	21 #8	11 #10	12 #11	18 #11	20 #11
Transverse Reinforcement	#5 @12 inches							

* The 2 #11 are bundled bars, used in the lower part of the external and internal column of bent 1.

$M-\phi$ curves for the column sections are presented in Figure 4.47 and Figure 4.48. And the parameters used in the calculations of the effective moment of inertia of the columns with its final values are presented in Table 4.36.

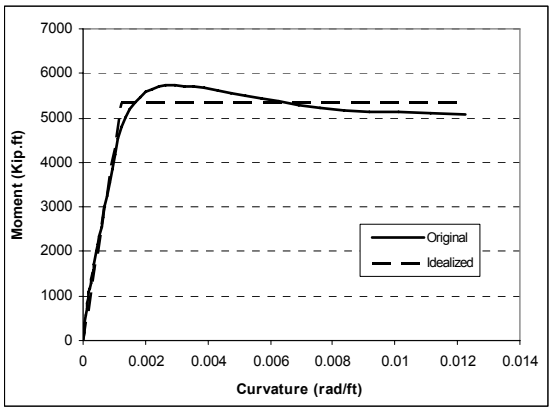

(a)

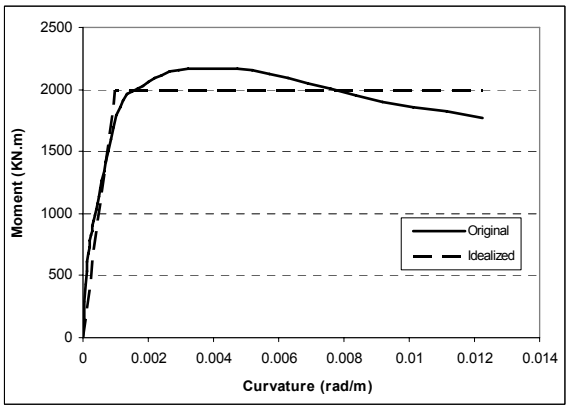

(b)

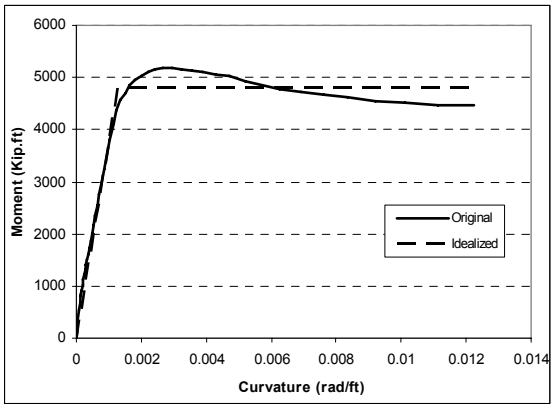

(c)

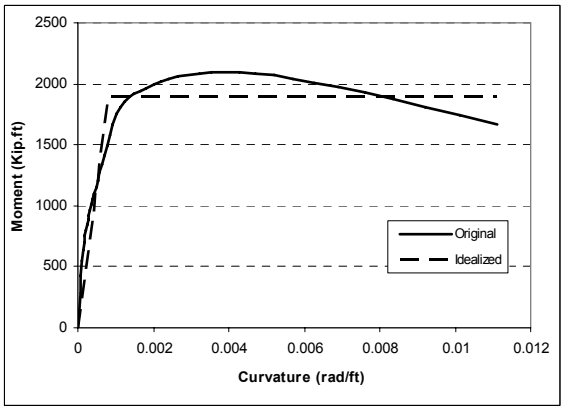

(d)

Figure 4.47 Bridge G-953 - $M-\phi$ curves for bent 1 column sections at (a) external lower column; (b) external upper column; (c) internal lower column; and (d) internal upper column

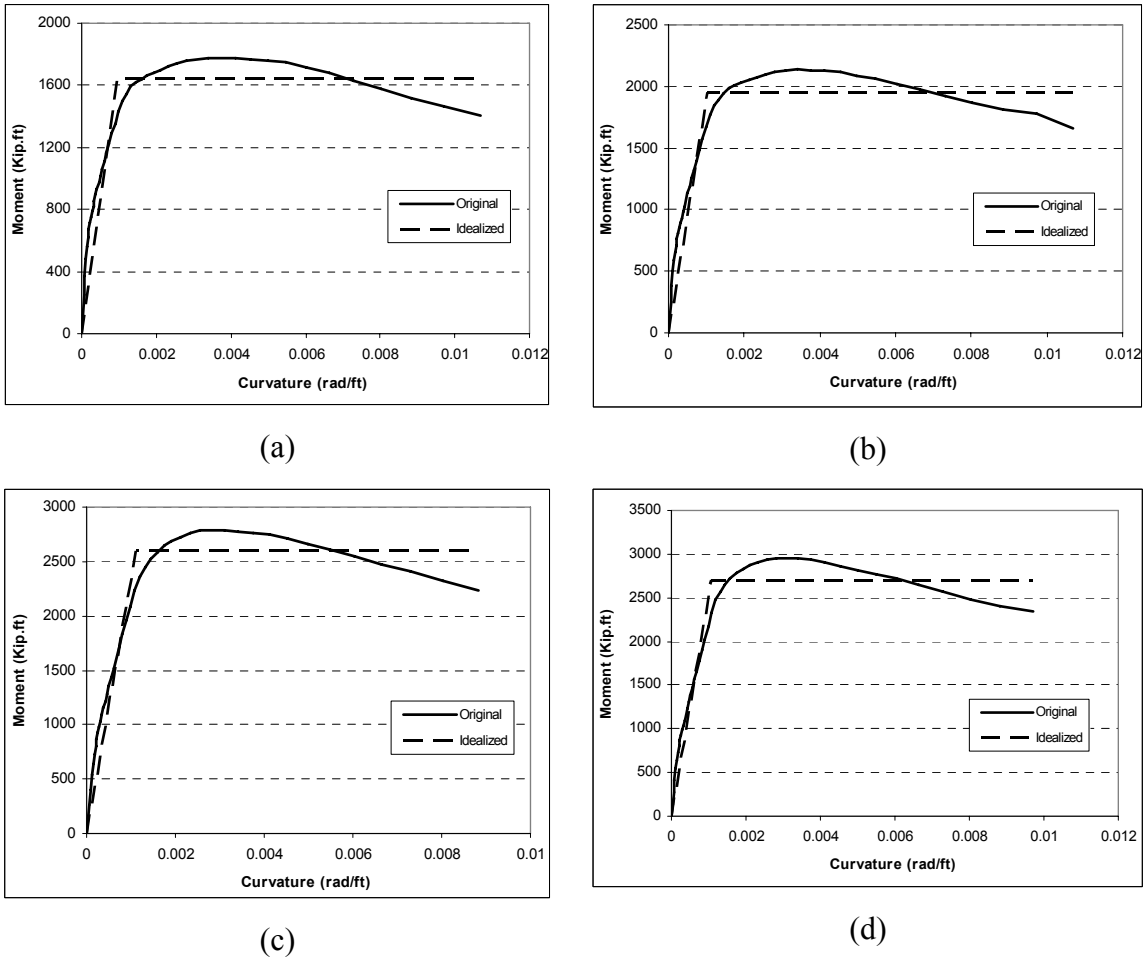

Figure 4.48 Bridge G-953 - $M-\phi$ curves for column sections at (a) bents 2 and 3 external column; (b) bents 2 and 3 internal column; (c) bents 4 and 5 external column; and (d) bents 4 and 5 internal column

Table 4.36 Bridge G-953 - Calculations of the effective moment of inertia for column sections

Column section	Bent 1				Bent 2 and 3		Bent 4 and 5	
	External column		Internal column		External column	Internal column	External column	Internal column
	Lower	Upper	Lower	Upper				
I_g (ft^4)	8.88	8.88	8.88	8.88	7.37	7.37	7.37	7.37
M_n (kip-ft)	5350	2000	4800	1900	1650	1950	2600	2700
Φ_y (rad/ft)	0.00123	0.00096	0.00125	0.00083	0.00095	0.00102	0.00110	0.00108
I_e (ft^4)	7.49	3.60	6.62	3.94	2.99	3.29	4.07	4.3
I_e / I_g	0.85	0.40	0.75	0.45	0.40	0.45	0.55	0.58

4.3.4.2.4. Spectral acceleration curve

Figure 4.49 shows the response spectrum used for the estimation of (S_a) values in the target displacement calculations. From the curve $T_0 = 0.097$ sec and $T_S = 0.485$ sec.

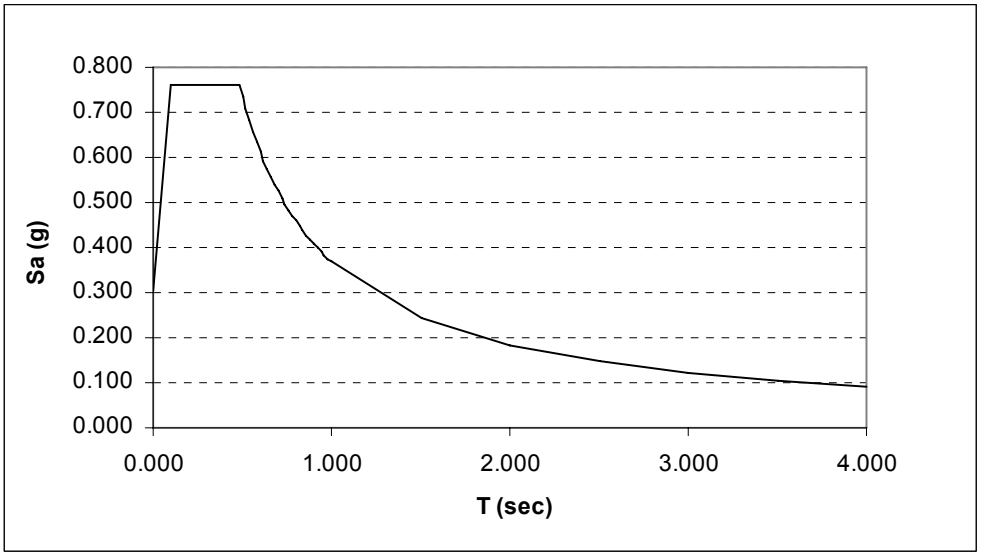

Figure 4.49 Bridge G-953 - 5% damped response spectrum for BSE-2

4.3.4.3. Acceptance criteria

4.3.4.3.1. Load-deformation curve for plastic hinges

The axial loads applied on each of the bridge columns are presented in Table 4.37. The shear forces values are negligible, which makes the values of $\left(V / b_w d \sqrt{f_c^{'}}\right)$ for all columns less than 3. From the results in Table 4.37, all values of $\left(P / A_g f_c^{'}\right)$ for different column sections are less than 0.1. Accordingly, plastic hinge rotation values used for the acceptance criteria will be 0.005 radians for the IO, 0.015 radians for the LS, and 0.02 radians for the CP level (same as the values in Figure 4.10).

Table 4.37 Bridge G-953 - Applied loads on bridge columns for load-deformation calculations

	Bent 1		**Bent 2 and 3**		**Bent 4 and 5**	
	External column	**Internal column**	**External column**	**Internal column**	**External column**	**Internal column**
P **(lbs)**	400000	480000	485410	566883	637026	595451
$A_g f_c^{'}$	7602654	7602654	6927212	6927212	6927212	6927212
$\frac{P}{A_g f_c^{'}}$	0.0526	0.0631	0.0701	0.0818	0.0920	0.0860

4.3.4.3.2. Force-controlled actions

a- Shear capacity:

Based on Eq. 4.2, Eq. 4.3, and Eq. 4.4, shear capacities for each of the bridge columns were calculated. Table 4.38 presents the shear capacity calculations for each column section.

Table 4.38 Bridge G-953 - Shear capacity calculations for bridge columns

	Bent 1		**Bent 2 and 3**		**Bent 4 and 5**	
	External column	**Internal column**	**External column**	**Internal column**	**External column**	**Internal column**
Applied axial load - N_u (kips)	400000	480000	485410	566883	637026	595451
Column diameter - d (in)	44	44	42	42	42	42
Gross sectional area - A_g (in^2)	1520.53	1520.53	1385.44	1385.44	1385.44	1385.44
V_c (kips)	**247.844**	**253.606**	**234.536**	**240.404**	**245.456**	**242.461**
Area of trans. reinf. - A_v (in^2)	0.31x2 =0.62	0.62	0.62	0.62	0.62	0.62
Spacing of trans. reinf. - s (in)	12	12	12	12	12	12
V_s (kips)	**109.120**	**109.120**	**104.160**	**104.160**	**104.160**	**104.160**
Total shear capacity - V_n (kips)	**356.964**	**362.726**	**338.696**	**344.564**	**349.616**	**346.621**

b- Reinforcement development:

Two locations of reinforcement development were identified in the bridge. The first location is at the B/C joints of all bridge columns, and the second location is at the splices in bent 1 columns. These splices connect the dowels from the foundations to the upper column longitudinal reinforcement.

Table 4.39 Bridge G-953 - Calculation of maximum stresses that can be developed in the reinforcement bars (B/C joint)

Column	Bent 1		Bent 2 and 3		Bent 4 and 5	
	External column	Internal column	External column	Internal column	External column	Internal column
Actual length - l_b (ft)	4.0	4.0	4.0	4.0	5.0	5.0
Required length - l_d (ft)	4.98	3.53	4.49	4.98	4.98	4.98
f_s (ksi)	**48.198**	60.00	**53.452**	**48.193**	60.00	60.00

Table 4.40 Bridge G-953 - Calculation of maximum stresses that can be developed in the reinforcement bars at bent 1 (splices location)

Column	Bent 1	
	External column	Internal column
Actual length - l_b (ft)	3.58	2.5
Required length - l_d (ft)	4.98	3.53
f_s (ksi)	**43.169**	**42.493**

From Table 4.39, three columns had inadequate development lengths of longitudinal reinforcement at the B/C joint location. On the other hand, from Table 4.40, two locations (in bent 1 columns) had inadequate splice length. Accordingly, the maximum stresses that can be developed in the rebars for the two cases were calculated (in the same tables) and sectional analyses were performed using the new values of f_s. The $M-\phi$ curves resulting from the sectional analyses are presented in Figure 4.50 and Figure 4.51.

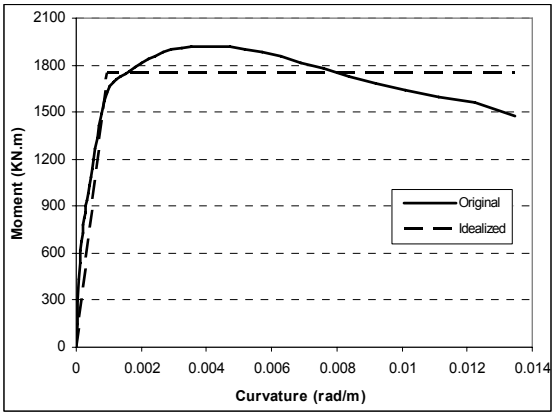

(a)

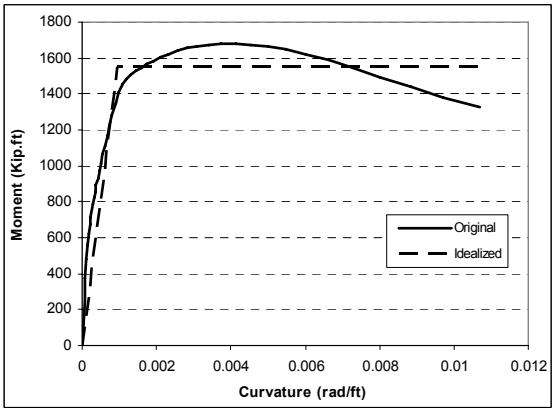

(b)

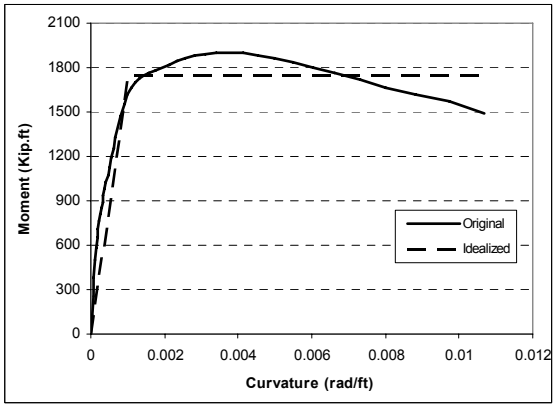

(c)

Figure 4.50 Bridge G-953 - $M-\phi$ curves for sections with inadequate reinforcement development at B/C joints (a) at bent 1-external columns; (b) at bents 2 and 3 - external columns; and (c) at bents 2 and 3 - internal columns

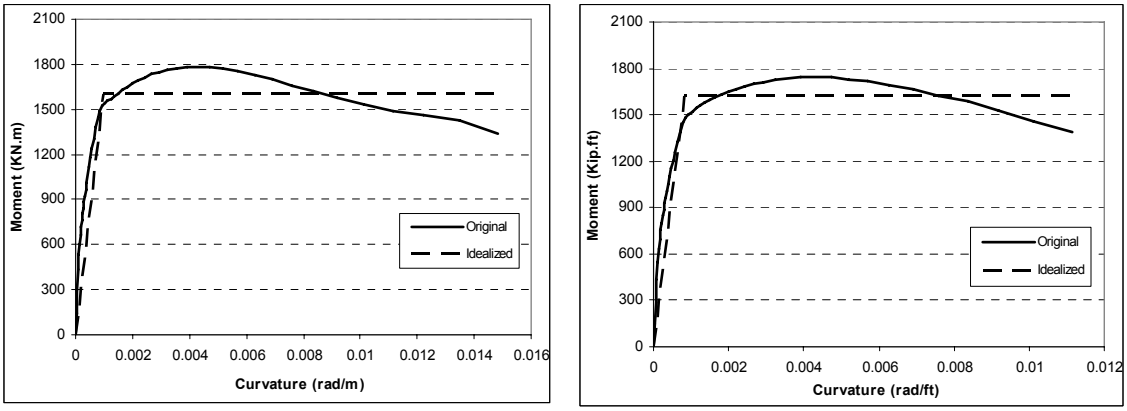

(a) (b)

Figure 4.51 Bridge G-953 - $M-\phi$ curves for sections with inadequate reinforcement splices in bent 1 (a) at the external columns and (b) at the internal columns

The maximum bending moment values that can be developed corresponding to the maximum stresses calculated for each section are presented in Table 4.41.

Table 4.41 Bridge G-953 - Maximum moment that can be developed in column sections at B/C joint and splices location without plastic hinge formation

Section location	**B/C joint**			**Splices**	
Column	**Bent 1**	**Bent 2 and 3**		**Bent 1**	
	External column	**External column**	**Internal column**	**External column**	**Internal column**
M_n (kip-ft)	1750	1550	1750	1600	1620

4.3.4.4. Pushover curves and target displacement

4.3.4.4.1. Transverse direction

Due to the asymmetry profile of the bridge (being curved in the horizontal direction), the evaluation of the bridge transversely was done in the two directions, the north and the south direction of the bridge. The fundamental mode in the transverse direction is shown

in Figure 4.52. Its fundamental time period was 0.630 sec. The pushover curves for the transverse direction in the north and south directions are shown in Figure 4.53 (a) to (d).

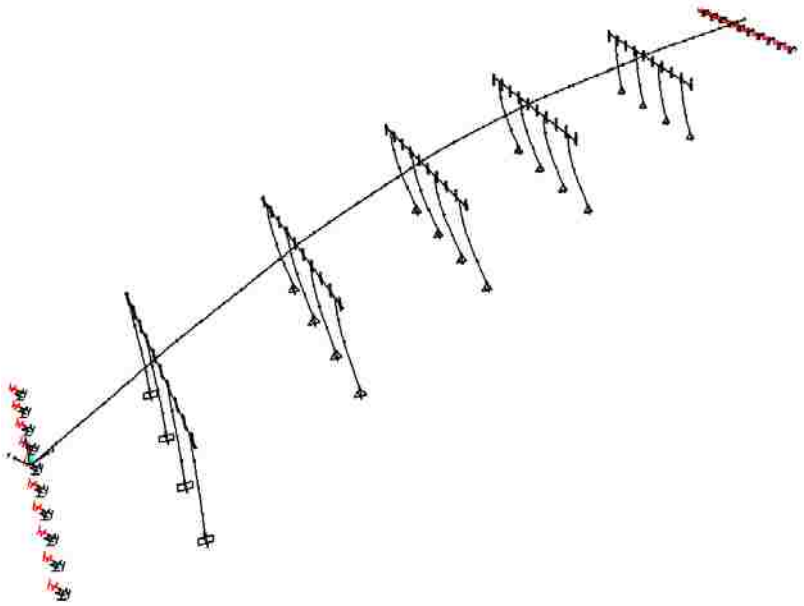

Figure 4.52 Bridge G-953 - Mode-2, the fundamental mode
in the transverse direction

Based on the values obtained from the modal analysis and the pushover curves, the target displacement was calculated, and is presented in Table 4.42 along with the parameters used in its calculations. The values of all parameters obtained from the north and south direction analyses are quite similar. This is due to the fact that the curvature of the bridge in the horizontal direction is not of a significant value. Accordingly, the values of the target displacements in both directions are exactly the same.

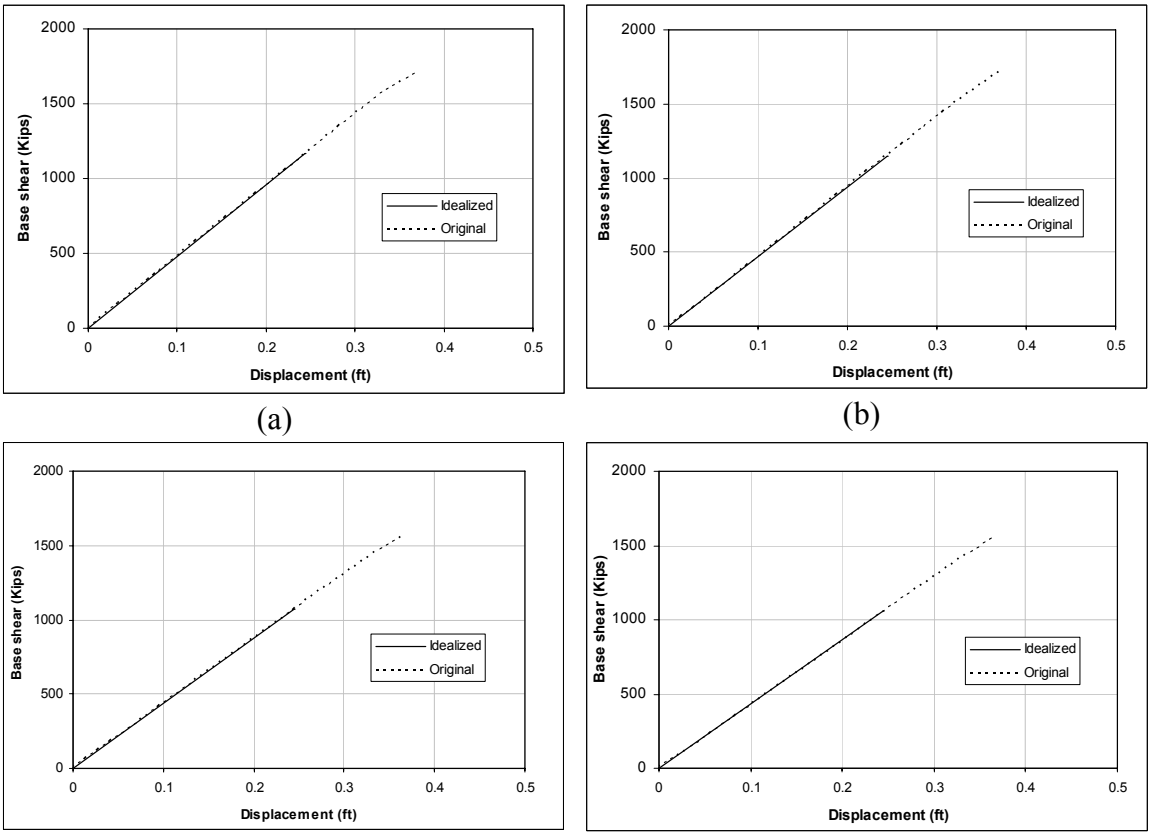

Figure 4.53 Bridge G-953 - Pushover curves in the transverse direction using (a) uniform load pattern pushed in the north direction; (b) uniform load pattern pushed in the south direction; (c) modal pattern pushed in the north direction; and (d) modal pattern pushed in the south direction,

Table 4.42 Bridge G-953 - Target displacement calculations in the transverse direction

Load Pattern	T_i (sec)	K_i	K_e	T_e (sec)	S_a (g)	PF	ϕ_{CN} (ft)	C_0*	δ_t (ft)
Uniform (North)	0.630	4790	4790	0.630	0.583	16.88	0.0768	1.295	0.244
Uniform (South)	0.630	4700	4700	0.630	0.583	16.88	0.0768	1.295	0.244
Modal (North)	0.630	4380	4380	0.630	0.583	16.88	0.0768	1.295	0.244
Modal (South)	0.630	4300	4300	0.630	0.583	16.88	0.0768	1.295	0.244

*Values of C_1, C_2 and C_3 are equal to 1.0

4.3.4.4.2. Longitudinal direction

Figure 4.54 (a) to (c) illustrate the fundamental mode shapes of the three units in the longitudinal direction. The fundamental time periods for unit 1, unit 2 and unit3 are 0.775, 2.094, and 1.262 sec, respectively. The pushover curves for this direction using the two patterns are illustrated in Figure 4.55 (a) to (f). Parameters used in calculating the target displacement for each of the three units along with its final values, for both patterns, are presented in Table 4.43.

Table 4.43 Bridge G-953 - Target displacement calculations in the longitudinal direction

Unit # - Load Pattern	T_i (sec)	K_i	K_e	T_e (sec)	S_a (g)	PF	ϕ_{CN} (ft)	C_0*	δ_t (ft)
Unit 1 - Uniform	0.775	3866	3866	0.775	0.474	7.695	0.132	1.019	0.237
Unit 1 - Modal	0.775	3753	3753	0.775	0.474	7.695	0.132	1.019	0.237
Unit 2 - Uniform	2.094	1520	1520	2.094	0.176	12.96	0.0774	1.003	0.631
Unit 2 - Modal	2.094	1520	1520	2.094	0.176	12.96	0.0774	1.003	0.631
Unit 3 - Uniform	1.262	3288	2889	1.346	0.273	11.12	0.0903	1.004	0.405
Unit 3 - Modal	1.262	3322	2978	1.333	0.276	11.12	0.0903	1.004	0.402

**Values of C_1, C2 and C_3 are equal to 1.0 for all cases*

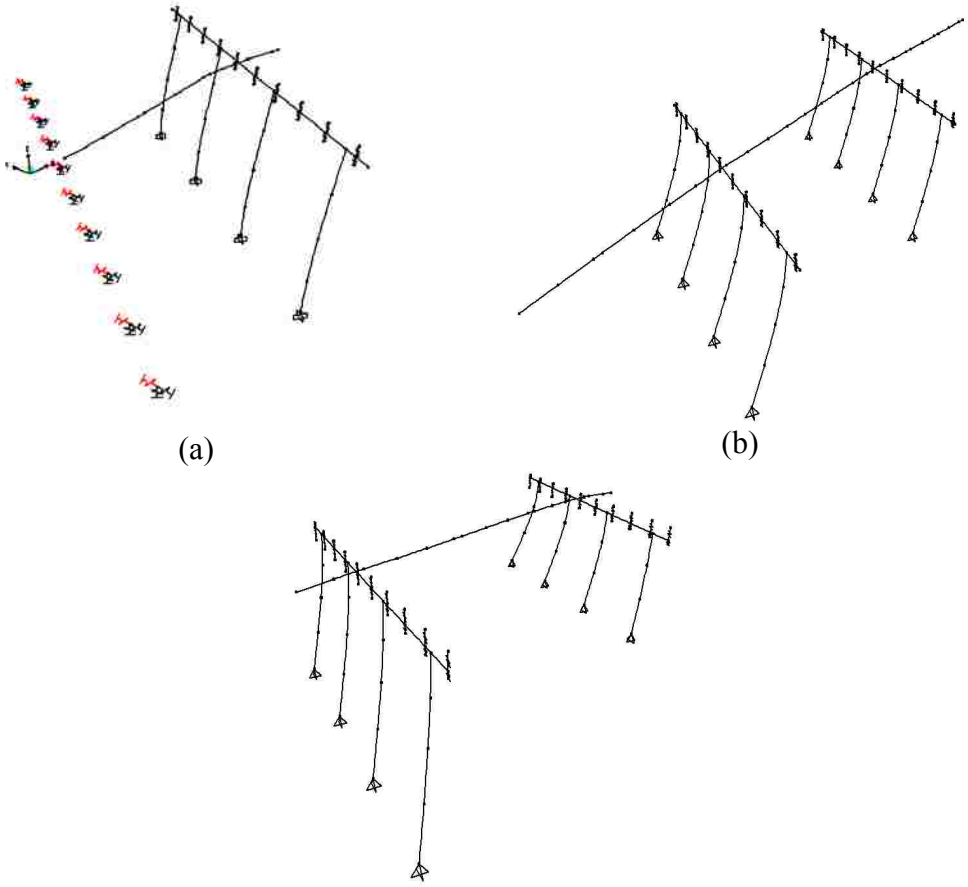

(a) (b)

(c)

Figure 4.54 Bridge G-953 -Fundamental mode shapes in the longitudinal direction of the bridge for (a) unit-1; (b) unit-2; and (c) unit-3

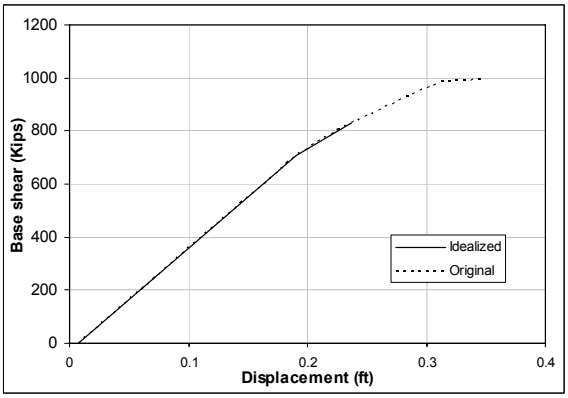

(a) Unit-1-Uniform load pattern

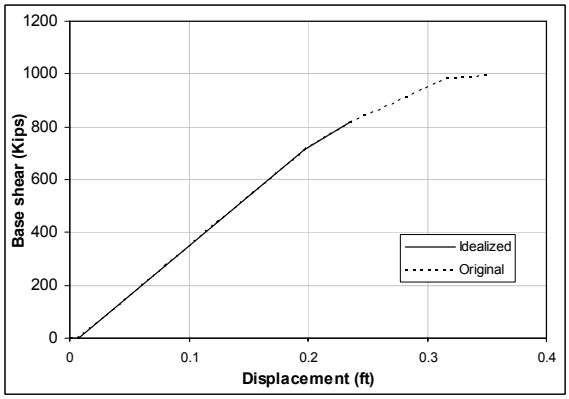

(b) Unit-1-Modal pattern

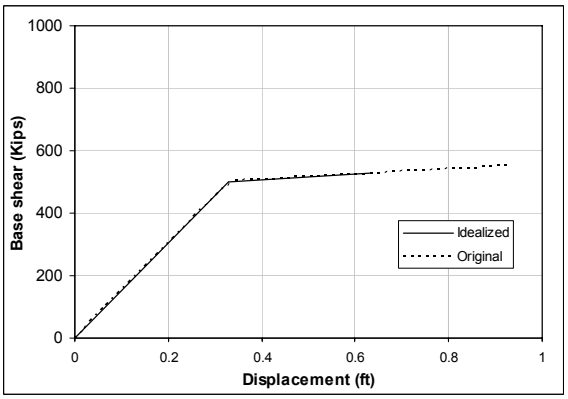

(c) Unit-2-Uniform load pattern

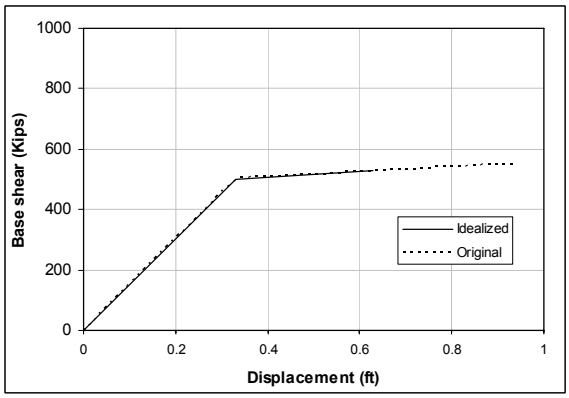

(d) Unit-2-Modal pattern

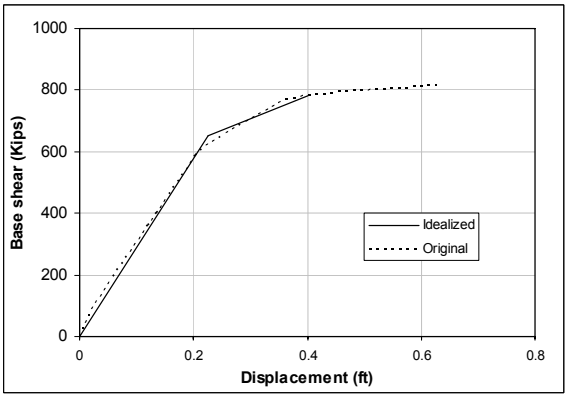

(e) Unit-3-Uniform load pattern

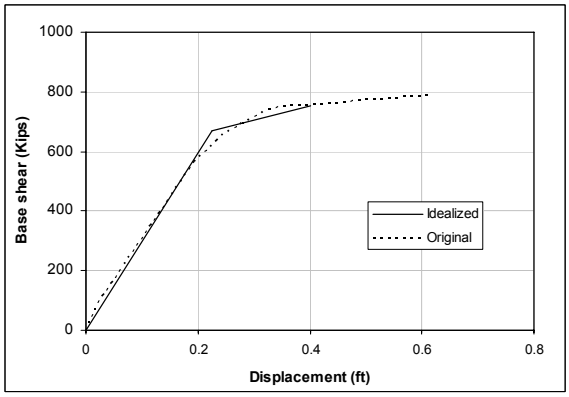

(f) Unit-3-Modal Patters

Figure 4.55 Bridge G-953 - Pushover curves for longitudinal direction analysis

4.3.4.5. Results

4.3.4.5.1. Deformation-controlled actions

In the transverse direction, none of the plastic hinges were formed at the target displacement in any of the considered directions (north and south) under any of the load patterns. However, in the longitudinal direction some plastic hinges were formed at the target displacement. The plastic hinge rotation values of the columns for the three units at the target displacement are presented in Table 4.44.

Table 4.44 Bridge G-953 - Plastic hinge rotation values (radians) of bridge bents at target displacement in longitudinal direction

Unit 1	**Bent no.**	**1 (Column top hinges)**			
	Column*	**1**	**2**	**3**	**4**
	Uniform	0.00063	0.00080	0.00061	0.00000
	Modal	0.00070	0.00084	0.00059	0.00000
	Bent no.	**1 (Column bottom hinges)**			
	Column*	**1**	**2**	**3**	**4**
	Uniform	**No Plastic Hinge Rotation Observed**			
	Modal				
Unit 2	**Bent no.**	**2**			
	Column*	**1**	**2**	**3**	**4**
	Uniform	**0.00875**	**0.00817**	**0.00817**	**0.00878**
	Modal	**0.00875**	**0.00817**	**0.00817**	**0.00878**
	Bent no.	**3**			
	Column*	**1**	**2**	**3**	**4**
	Uniform	**0.00819**	**0.00768**	**0.00770**	**0.00819**
	Modal	**0.00819**	**0.00768**	**0.00770**	**0.00819**
Unit 3	**Bent no.**	**4**			
	Column*	**1**	**2**	**3**	**4**
	Uniform	0.00169	0.00101	0.00054	0.00000
	Modal	0.00257	0.00209	0.00178	0.00139
	Bent no.	**5**			
	Column*	**1**	**2**	**3**	**4**
	Uniform	**0.00668**	**0.00643**	**0.00614**	**0.00577**
	Modal	**0.00527**	**0.00626**	**0.00719**	**0.00805**

**Columns are named sequentially from south to north direction*

Some of the plastic hinges, formed in the bent columns, violated the acceptance criteria for the IO level. These plastic hinges are in bents 2, 3 and 5 and their values are underlined in Table 4.44.

4.3.4.5.2. Force-controlled actions

a- Shear forces:

Shear forces in the columns at the target displacements are presented in Table 4.45, Table 4.46, and Table 4.47 for the transverse (north), the transverse (south), and the longitudinal directions, respectively.

Table 4.45 Bridge G-953 - Shear forces (kips) in the columns at target displacement in the transverse direction (north)

Bent no.	**1**			
Column*	**1**	**2**	**3**	**4**
Uniform	81.00	80.67	80.00	80.06
Modal	83.94	83.59	82.89	82.94
Bent no.	**2**			
Column*	**1**	**2**	**3**	**4**
Uniform	31.58	35.62	35.08	30.88
Modal	33.07	37.24	36.61	32.17
Bent no.	**3**			
Column*	**1**	**2**	**3**	**4**
Uniform	39.12	43.85	43.09	38.16
Modal	40.94	45.71	44.80	39.55
Bent no.	**4**			
Column*	**1**	**2**	**3**	**4**
Uniform	56.56	61.32	60.86	56.02
Modal	56.04	60.62	60.08	55.23
Bent no.	**5**			
Column*	**1**	**2**	**3**	**4**
Uniform	47.91	51.31	50.80	47.54
Modal	41.44	44.41	43.90	41.11

**Columns are named sequentially from south to north direction*

Table 4.46 Bridge G-953 - Shear forces (kips) in the columns at target displacement in the transverse direction (south)

Bent no.	**1**			
Column*	**1**	**2**	**3**	**4**
Uniform	79.02	79.14	79.40	79.87
Modal	81.93	82.07	82.32	82.81
Bent no.	**2**			
Column*	**1**	**2**	**3**	**4**
Uniform	30.71	34.86	35.46	31.41
Modal	32.04	36.45	37.12	32.94
Bent no.	**3**			
Column*	**1**	**2**	**3**	**4**
Uniform	37.79	42.68	43.40	38.74
Modal	39.14	44.35	45.22	40.53
Bent no.	**4**			
Column*	**1**	**2**	**3**	**4**
Uniform	55.14	59.93	60.47	55.60
Modal	54.26	59.05	59.68	54.97
Bent no.	**5**			
Column*	**1**	**2**	**3**	**4**
Uniform	46.52	49.66	50.18	46.83
Modal	40.10	42.78	43.29	40.38

**Columns are named sequentially from south to north direction*

Table 4.47 Bridge G-953 - Shear forces (kips) in the columns at target displacement in the longitudinal direction

Unit 1	**Bent no.**	**1**			
	Column*	**1**	**2**	**3**	**4**
	Uniform	149.67	141.99	144.08	156.48
	Modal	149.66	141.63	144.53	157.42
Unit 2	**Bent no.**	**2**			
	Column*	**1**	**2**	**3**	**4**
	Uniform	48.25	58.84	59.11	48.04
	Modal	48.26	58.84	59.11	48.06
	Bent no.	**3**			
	Column*	**1**	**2**	**3**	**4**
	Uniform	48.12	57.33	57.59	47.82
	Modal	48.14	57.35	57.61	47.85
Unit 3	**Bent no.**	**4**			
	Column*	**1**	**2**	**3**	**4**
	Uniform	59.62	67.92	69.76	66.32
	Modal	39.26	44.25	44.83	42.23
	Bent no.	**5**			
	Column*	**1**	**2**	**3**	**4**
	Uniform	98.86	99.73	95.27	85.91
	Modal	95.68	103.11	105.56	101.85

**Columns are named sequentially from south to north direction*

For column 4 in bent 1, by combining the shear forces (100% of the longitudinal direction and 30% of the transverse direction)

→ $100\% \times 156.48 = 156.48$ kips, and $30\% \times 80.06 = 24.02$ kips

$\sqrt{(156.48)^2 + (24.02)^2} = 158.31$ kips $<<$ 349.616 kips (from Table 4.38)

Therefore, the bridge columns are safe against shear failure under the MCE level.

b- Reinforcement development:

In the transverse direction, bending moment values at the column sections that had inadequate reinforcement development or splice lengths were observed at the target displacement. These values are presented in Table 4.48.

Table 4.48 Bridge G-953 - Maximum bending moment values (kip-ft) at target displacement at locations with inadequate reinforcement development lengths

Section location	**B/C joint**			**Splices**	
Column	**Bent 1**	**Bent 2 and 3**		**Bent 1**	
	External column	**External column**	**External column**	**External column**	**Internal column**
Transverse - (Uniform-north)	895.90	1121.89	1121.89	432.01	187.31
Transverse - (Uniform-south)	884.13	1112.33	1112.33	425.21	183.12
Transverse - (Modal-north)	927.83	1167.34	1167.34	447.90	194.28
Transverse - (Modal-south)	916.03	1157.78	1157.78	441.15	190.07

By comparing the bending moment values in Table 4.48 to the bending moment values presented in Table 4.41, none of the sections have exceeded the maximum value. Accordingly, the design of the columns in this bridge, in the transverse direction is not governed by the inadequate development lengths of the longitudinal reinforcement.

In the longitudinal direction, plastic hinge rotations were formed in unit 2 (bents 2 and 3) in the top part of the column. This indicates that the reduction in the maximum stress, which will reduce the capacity of the plastic, will give higher values of plastic hinge rotations. Accordingly, new models for unit 2 were developed with the values of f_s

as presented in Table 4.39 for the bents' external and internal columns. The new models were pushed to the same target displacements using the uniform load and the modal patterns. The resultant plastic hinge rotations are presented in Table 4.49.

Table 4.49 Bridge G-953 – Plastic hinge rotation values (radians) in the longitudinal direction at target displacement at B/C joints for unit 2

Bent no.	**2**			
Column	**1**	**2**	**3**	**4**
Uniform	**0.00930**	**0.00919**	**0.00928**	**0.00928**
Modal	**0.00930**	**0.00919**	**0.00913**	**0.00913**
Bent no.	**3**			
Column	**1**	**2**	**3**	**4**
Uniform	**0.00871**	**0.00877**	**0.00879**	**0.00871**
Modal	**0.00871**	**0.00877**	**0.00879**	**0.00871**

All plastic hinge rotation values presented in In the longitudinal direction, plastic hinge rotations were formed in unit 2 (bents 2 and 3) in the top part of the column. This indicates that the reduction in the maximum stress, which will reduce the capacity of the plastic, will give higher values of plastic hinge rotations. Accordingly, new models for unit 2 were developed with the values of f_s as presented in Table 4.39 for the bents' external and internal columns. The new models were pushed to the same target displacements using the uniform load and the modal patterns. The resultant plastic hinge rotations are presented in Table 4.49.

Table 4.49 for the columns of bents 2 and 3 violated the acceptance criteria of IO (which is 0.005 radians). Following the same steps, a new model for unit 1 was developed with (1) an additional definition of plastic hinges at the reinforcement splice locations and (2) a change in the plastic hinge definition of the external column at the B/C joints. These plastic hinges are defined based on the f_s values presented in Table 4.40

for the splice locations and Table 4.39 for B/C joints locations. Unit 1 was pushed in the new model to the target displacement and the resultant plastic rotations at different locations are presented in Table 4.50.

Table 4.50 Bridge G-953 – Plastic hinge rotation values (radians) in the longitudinal direction at target displacement for unit 1 (bent 1)

	Splice locations			
Column	**1**	**2**	**3**	**4**
Uniform	**No Plastic hinge rotation formed**			
Modal				
	B/C joint locations			
Column	**1**	**2**	**3**	**4**
Uniform	0.00146	0.00111	0.00089	0.00083
Modal	0.00220	0.00172	0.00234	0.00271

From the results presented in Table 4.50, at the target displacement, none of the columns in bent 1 experienced any plastic hinges rotations at their splice locations. However, at the B/C joint locations, which had new plastic hinges defined (columns 1 and 4), plastic hinges were formed. As shown in the table, plastic hinge rotation values at the target displacement did not violate the acceptance criteria, which is 0.005 radians.

4.3.5. Bridge (I-2139)

4.3.5.1. Bridge description

I-2139 is a 3-spans bridge (or part of a bridge) that connects two highways (95 to I-15) at the “Spaghetti Bowl”. The total length of this part of the bridge is 101.75 meters (m), divided into three spans of 32, 34.75, and 35 m from east to west direction respectively. Figure 4.56 shows the plan and elevation of the bridge.

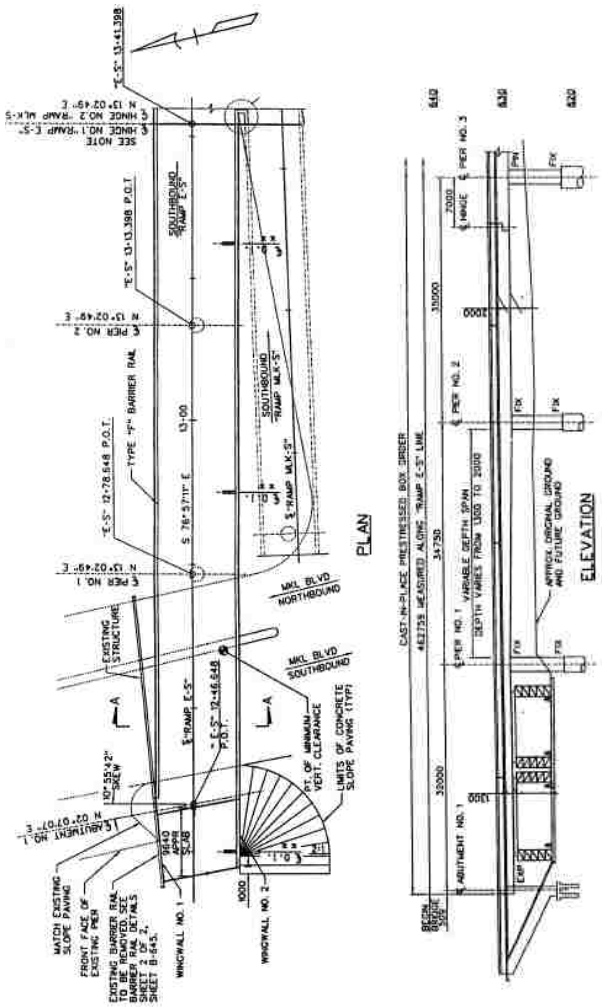

Figure 4.56 Bridge I-2139 - Plan and elevation

The abutment on the west side of the bridge is skewed at 10.93 degrees. On the other side, this bridge ends with an expansion joint to another part of the bridge (not an abutment) that merges to the I-15 interstate highway. The expansion joint on this side (the east side) is not skewed.

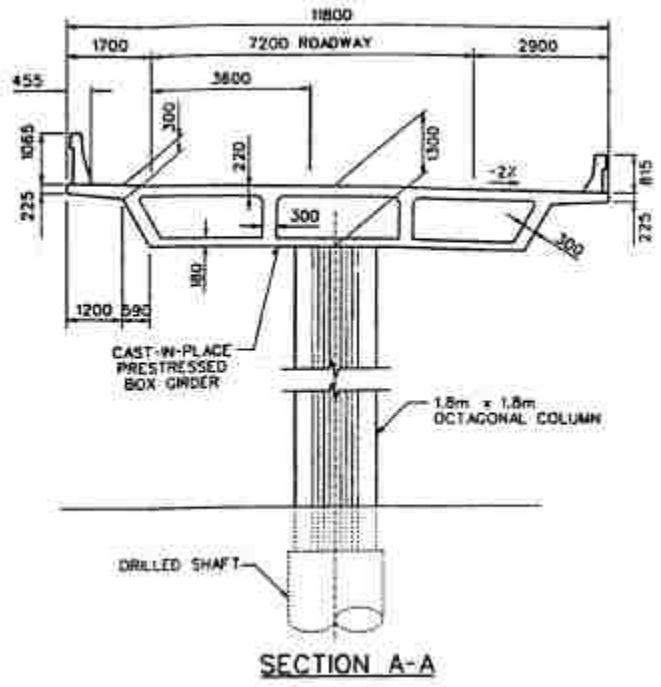

Figure 4.57 Bridge I-2139 - Bridge section

The superstructure of the bridge (shown in Figure 4.57) is a cast-in-place prestressed box girder concrete deck, with two intermediate webs. The total width of the deck is a constant 11.8m width through the entire length of the bridge. The total thickness of the box girder is 1.3 m within the first span on the west side (span 1), 2 m within the span on the east side (span 3), and varies from 1.3 m to 2.0 m in the middle span of the bridge.

The substructure of the bridge is a single column for each pier. The columns have an octagonal shape (shown in Figure 4.58 (a) and (b)), with its longitudinal reinforcement

distributed in a circular configuration. The longitudinal column reinforcement for both piers is 46-D36 (D36 is equivalent to #11 rebars), while the transverse reinforcement value is different in the two piers. Pier 1 has a spiral transverse reinforcement of D19 at 90 mm pitch while pier 2 has a spiral transverse reinforcement of D22 at 75 mm pitch (D19 and D22 are equivalent to #6 and #7 rebars, respectively). The columns in the analysis are considered as circular columns with 1.72 m diameter for simplicity.

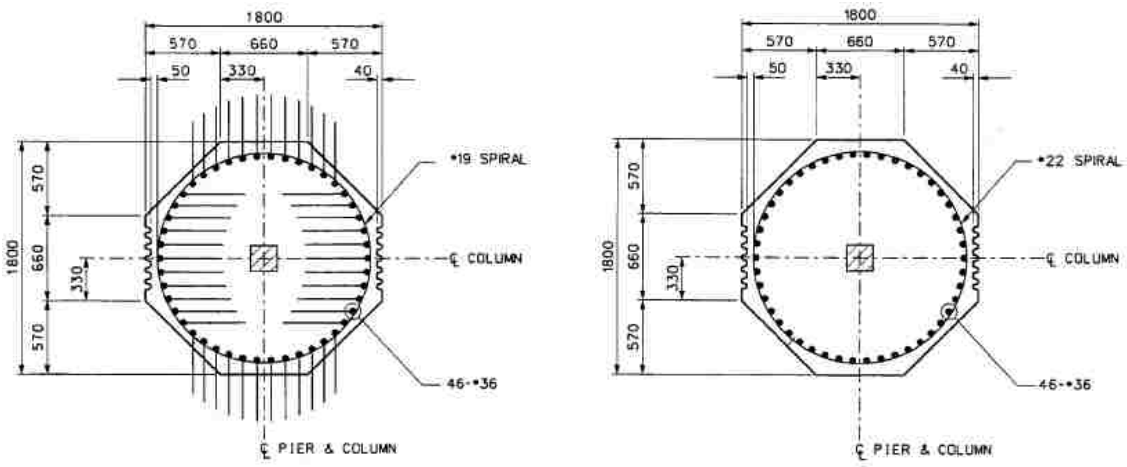

(a) (b)

Figure 4.58 Bridge I-2139 - Bridge column sections at (a) pier 1 and (b) pier 2

The cap beam of the bent has dimensions of 1.3 m depth by 2.1 m width for pier 1 and 2.0 m depth by 2.1 m width as shown in Figure 4.59. Cross diaphragms of 0.2 m thickness are provided at the mid spans, 1 m thickness at the abutment on the west side of the bridge. The concrete compressive strength for this bridge is 28 MPa and the reinforcement yield strength in 414 MPa.

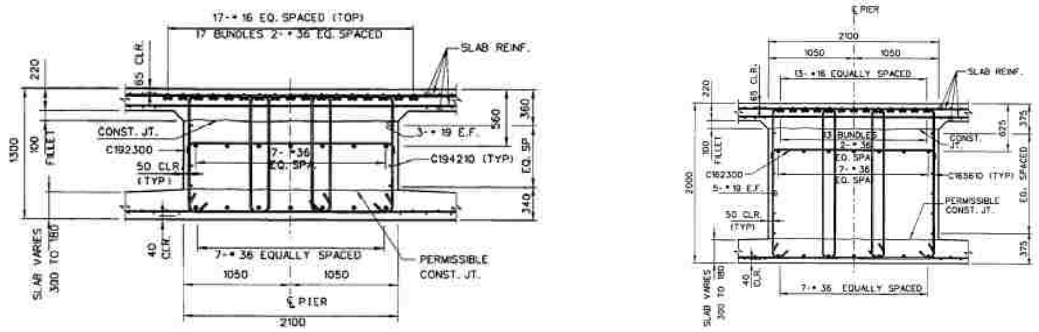

(a) (b)

Figure 4.59 Bridge I-2139 - Bridge cap beam sections at (a) pier 1 and (b) pier 2

4.3.5.2. Bridge model

The structural model for the bridge used for the analysis in both transverse and longitudinal directions in shown in Figure 4.60

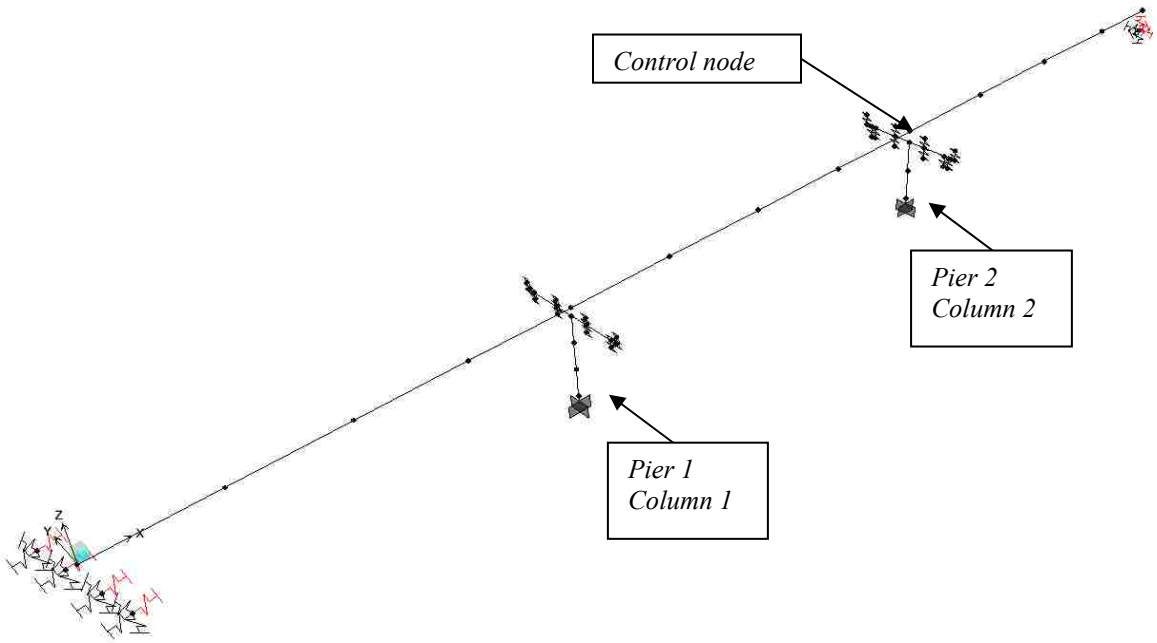

Figure 4.60 Bridge I-2139 - Structural model for both transverse and longitudinal direction

4.3.5.2.1. Superstructure

The superstructure was modeled with four equal elements in each span with a distributed mass along the frame elements. The sectional properties of the bridge decks at the first and the last spans are presented in Table 4.51, the mid span has a variable depth and its properties vary linearly from pier1 to pier 2. An additional load of 39.24 kN/m was added allover the deck to represent the dead load from the concrete barriers, and the wearing surface overlay. An additional load of 18.64 kN/m was added to account for the live load of two lanes.

Table 4.51 Bridge I-2139 - Sectional properties of the bridge deck at spans 1 and 3

Properties	Span 1 (west span)	Span 3 (east span)
Cross sectional area (m^2)	5.399	6.300
Moment of inertia about X-axis (m^4)	1.277	3.662
Moment of inertia about Z-axis (m^4)	54.653	64.257

4.3.5.2.2. Substructure

The columns of the two piers were modeled with their heights starting from the drilled shaft top level (Figure 4.57) to the mid height of the cap beam. Column heights for pier 1 and 2 are 6.58 m and 5.22 m respectively. Plastic hinges were defined at the top and bottom parts of the columns. The columns were modeled with fixed end condition at their lower part. The abutment at the west side of the bridge was modeled as four springs, representing the four seat-type bearings underneath the four girder webs. On the other

side of the bridge (east side), springs with stiffness values representing the existing column were used in all directions.

4.3.5.2.3. Effective moment of inertia for bent columns

The $M-\phi$ relationship for the pier columns of the bridge are presented in Figure 4.61. The axial load used in the sectional analysis is 8212 kN, which is the axial load on the column of pier 2.

For the circular column with 1.72 m diameter

$I_g = 0.4296 \text{ m}^4$

From the $M-\phi$ idealized curve in Figure 4.61:

$M_n = 14500$ kN.m, $\phi_y = 0.00225$ rad/m

and $E_c = 24870062 \text{ kN/m}^2$

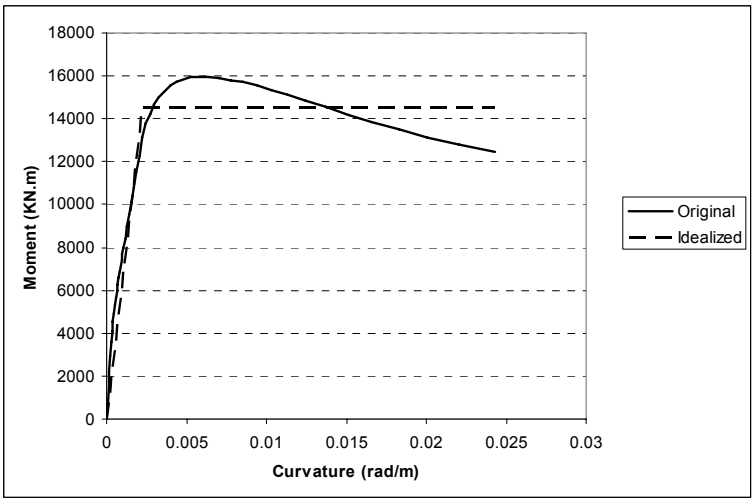

Figure 4.61 Bridge I-2139 - $M-\phi$ curve for the pier columns

since $I_e = \dfrac{M_n}{E_c \phi_y} \rightarrow I_e = 0.25912 \text{ m}^4$

and $\frac{I_e}{I_g} = \frac{0.25912}{0.4296} = 0.60318$

Therefore, Gross flexural rigidity for column sections will be reduced to 60% of its value in the analysis.

4.3.5.2.4. Spectral acceleration curve

Figure 4.62 shows the response spectrum used for the estimation of (S_a) values in the target displacement calculations. From the curve $T_0 = 0.097$ sec and $T_S = 0.483$ sec .

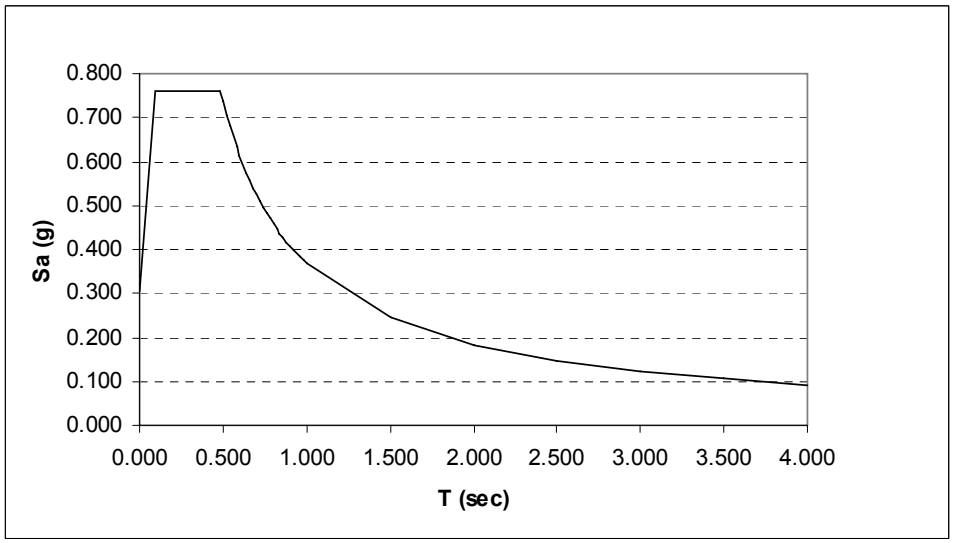

Figure 4.62 Bridge I-2139 - 5% damped response spectrum for BSE-2

4.3.5.3. Acceptance criteria

4.3.5.3.1. Load-deformation curve for plastic hinges

Table 4.52shows the axial loads on the two columns of the bridge in addition to the shear forces used in estimating the load-deformation curves.

Table 4.52 Bridge I-2139 - Applied loads on bridge columns for load-deformation calculations

	Column 1 (pier 1)	**Column 2 (pier 2)**
Axial Load (P)	7497 kN	8212 kN
Shear Force (V)	795 kN	752 kN
$\frac{P}{A_g f_c^{'}}$	0.115 (very close to 0.1)	0.126 (interpolation is requireed)
$\frac{V}{b_w d\sqrt{f_c^{'}}}$	0.063	0.060

The generalized load-deformation relation for each bridge is estimated based on the values calculated in Table 4.52 by using Table 4.2, and the acceptance criteria are presented in Table 4.53. The values of the acceptance criteria are slightly different for the two columns as the axial loads applied on each column is different as shown in Table 4.52.

Table 4.53 Bridge I-2139 - Acceptance criteria for each column of the bridge

Performance level	**Column 1 (pier 1)**	**Column 2 (pier 2)**
IO	0.005	0.00486
LS	0.015	0.0148
CP	0.02	0.0197

4.3.5.3.2. Force-controlled actions

a- Shear capacity:

Shear capacity of the columns are presented in Table 4.54 for the two columns of the bridge. As the columns are circular, the capacities are applicable for the two directions of loading.

Based on Eq. 4.2, Eq. 4.3, and Eq. 4.4 (metric version),

Table 4.54 Bridge I-2139 - Shear capacity calculations for bridge columns

	Column 1 (pier 1)	**Column 2 (pier 2)**
Applied axial load - N_u (kN)	7497	8213
Column diameter - d (mm)	1720	1720
Gross sectional area - A_g (mm^2)	2323521.9	2323521.9
V_c (kN)	**2619.66**	**2666.52**
Area of trans. reinf. - A_v (mm^2)	284 x 2 = 568	387 x 2 = 774
Spacing of trans. reinf. - s (mm)	90	75
V_s (kN)	**3595.21**	**5878.93**
Total shear capacity - V_n (kN)	**6214.88**	**8545.46**

b- Reinforcement development:

Based on Eq. 4.5 and Eq. 4.6 (metric version);

For D36 (#11) rebar,

Development length $l_d = 1.65$ m and the splice length is $1.3 \times l_d = 2.14$ m.

All development, splice, and hook lengths provided in the bridge columns at the two locations are satisfying the codes requirements. These two locations are the splice at the drilled shaft (pile) underneath the column and the B/C joints. At the first location (splice with the drilled shaft), a development length of 3.175 m for both columns is provided. At the second location (the B/C joint), column 1 rebars are hooked in the cap beam as shown in Figure 4.58 as the beam depth is only 1.3 m. while column 2 rebars are extended (straight) inside the cap beam as its depth is 2 m, which is sufficient when compared to the value of l_d.

4.3.5.4. Pushover curves and target displacement

4.3.5.4.1. Transverse direction

The fundamental mode in this direction from the modal analysis was mode-1, which is illustrated in Figure 4.63. The time period for this mode was 0.6325 seconds. The pushover curves for both the uniform and the modal patterns are shown in Figure 4.64 (a) and (b).

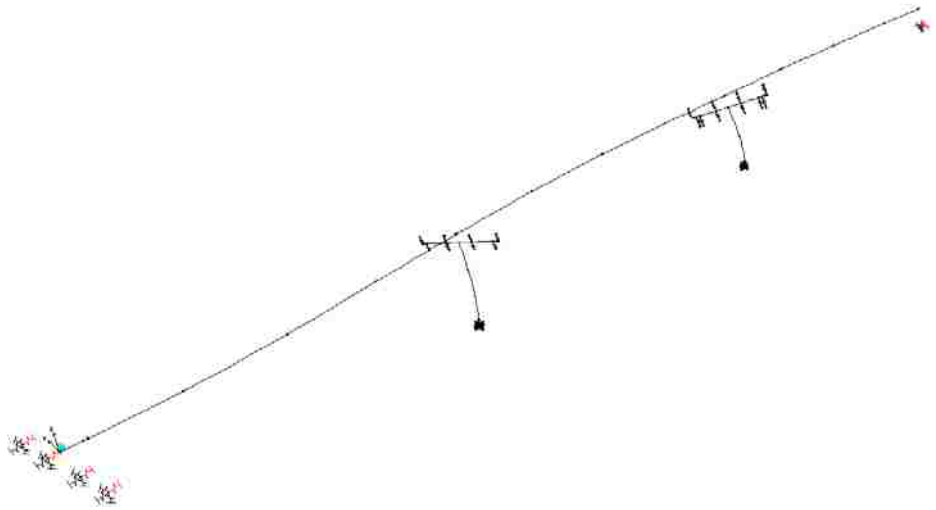

Figure 4.63 Bridge I-2139 - Mode-1, the fundamental mode in the transverse direction

All the parameters used in the target displacement calculation are presented in Table 4.55. The values of K_i and K_e are equal in each case. However, the final target displacement values are identical in both patterns.

Table 4.55 Bridge I-2139 - Target displacement calculations for the transverse direction

Load Pattern	T_i (sec)	K_i	K_e	T_e (sec)	$S_a(g)$	PF	ϕ_{CN} (m)	C_0*	δ_t (m)
Uniform	0.633	207212	207212	0.633	0.596	53.56	0.193	1.03	0.059
Modal	0.633	168717	168717	0.633	0.596	53.56	0.193	1.03	0.059

*Values of C_1, C_2 and C_3 are equal to 1.0

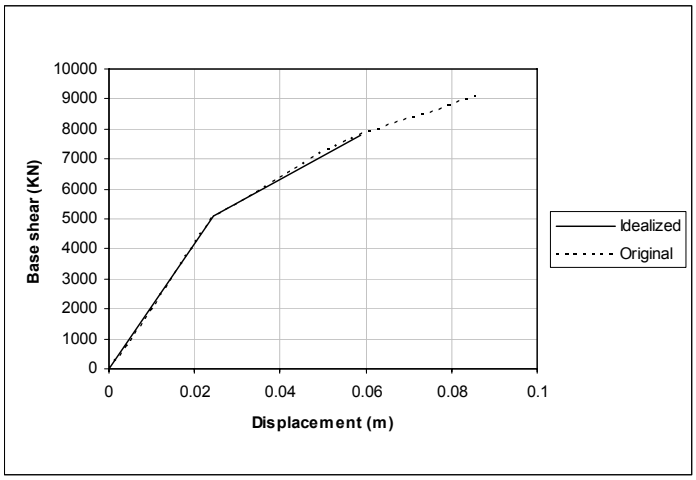

(a)

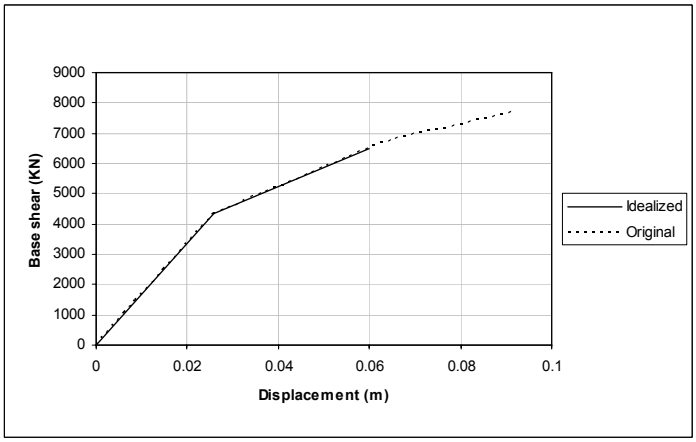

(b)

Figure 4.64 Bridge I-2139 - Pushover curves for the transverse direction using (a) uniform load pattern and (b) modal pattern

4.3.5.4.2. Longitudinal direction

The fundamental mode shape in this direction was mode-7 (shown in Figure 4.65). The time period for this mode was 0.1956 sec. The pushover curves for this direction using the two patterns are illustrated in Figure 4.66 (a) and (b). Parameters used in calculating the target displacement for both patterns are presented in Table 4.56.

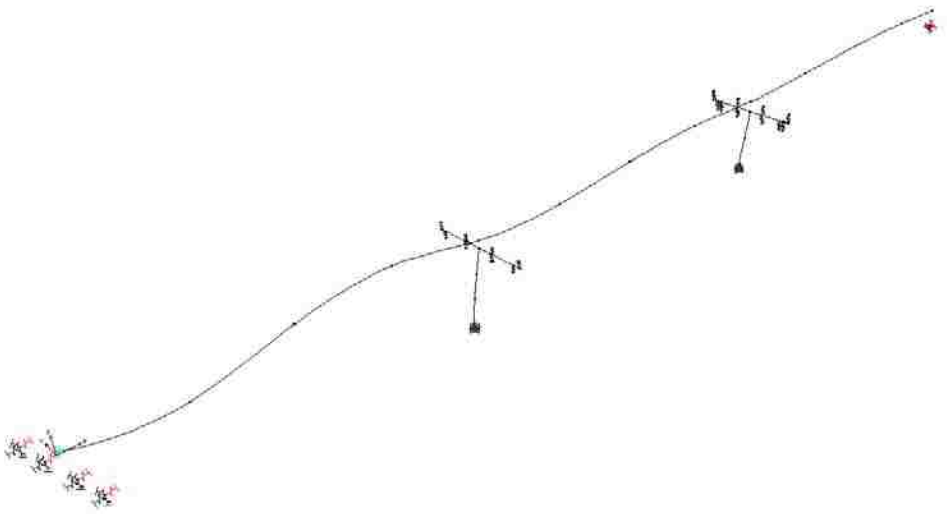

Figure 4.65 Bridge I-2139 - Mode-7, the fundamental mode in the longitudinal direction

In this direction the effective fundamental time period T_e was less that T_s (from the spectrum curve), accordingly the value of C_1 had to be calculated using Eq. 3.8.

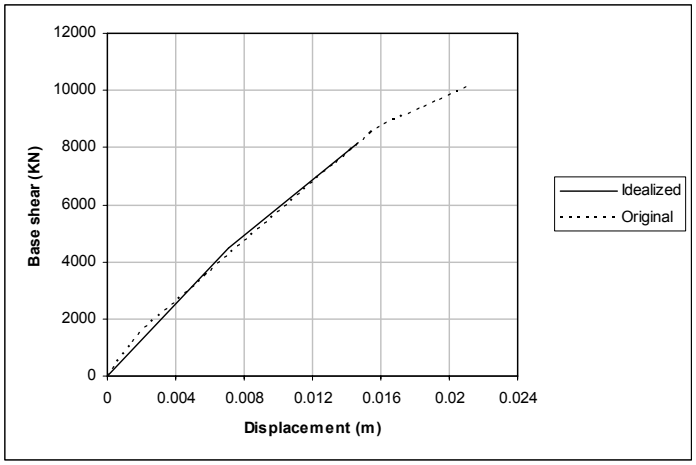

(a)

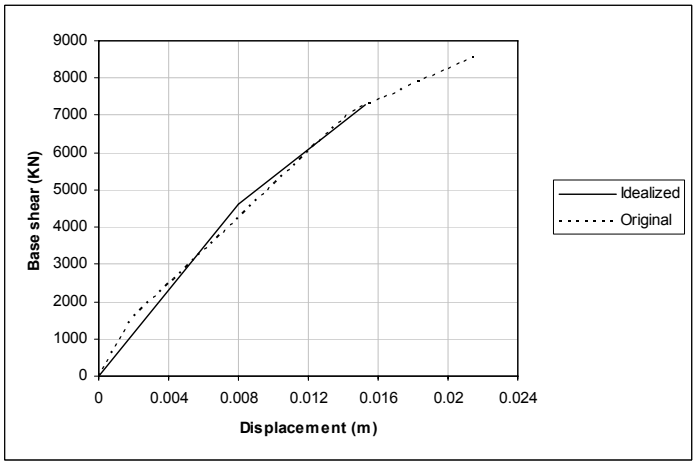

(b)

Figure 4.66 Bridge I-2139 -Pushover curves for the longitudinal direction using (a) uniform load pattern and (b) modal pattern

Table 4.56 Bridge I-2139 - Target displacement calculations for the longitudinal direction

Load Pattern	T_i (sec)	K_i	K_e	T_e (sec)	S_a (g)	PF	ϕ_{CN}, (m)	C_0	C_1*	δ_t (m)
Uniform	0.196	690431	633803	0.205	0.766	55.38	0.018	0.997	1.85	0.0147
Modal	0.196	661813	562500	0.213	0.766	55.38	0.018	0.997	1.79	0.0153

*Values of C_2 and C_3 are equal to 1.0

From the pushover curves:

1- Uniform load pattern

$V_y = 4500$ kN and the effective weight of the bridge $W = 15710$ kN

Based on Eq. 3.8 and Eq. 3.10:

$$R = \frac{0.766}{4500/15710} = 2.6742$$

$$C_1 = \left[1.0 + (R-1)T_s / T_e\right] / R = \left[1.0 + (2.6742-1)0.483/0.205\right] / 2.6742 = 1.85$$

2- Modal Pattern

$V_y = 4600$ kN with the same effective weight,

$$R = \frac{0.766}{4600/15710} = 2.6161$$

$$C_1 = \left[1.0 + (R-1)T_s / T_e\right] / R = \left[1.0 + (2.6161-1)0.483/0.213\right] / 2.6161 = 1.79$$

4.3.5.5. Results

4.3.5.5.1. Deformation-controlled actions

In both directions, none of the columns encountered plastic hinge formation at their top part. However, plastic hinge rotation values at the columns bottom parts in the two directions are presented in Table 4.57, where the underlined values are the values that violated the acceptance criteria for the IO performance level.

Table 4.57 Bridge I-2139 - Plastic hinge rotation values (radians) at target displacement in both directions

	Transverse direction		**Longitudinal direction**	
Column	**1**	**2**	**1**	**2**
Uniform	0.00045	**<u>0.00595</u>**	0.00000	0.00000
Modal	0.00000	**<u>0.00559</u>**	0.00000	0.00029

4.3.5.5.2. Force-controlled actions

The only force-controlled action to be checked in this bridge is the shear force values in the columns at target displacements, as the development, splice and hook lengths are satisfying the code requirement. Table 4.58 presents the shear force values in the columns at the target displacements in both directions.

Table 4.58 Bridge I-2139 - Shear force values (kN) in the bridge columns at target displacement

	Transverse direction		**Longitudinal direction**	
Column	**1**	**2**	**1**	**2**
Uniform	2676.3	5105.1	2988.1	5224.9
Modal	2104.2	4378.9	1756.0	5556.7

For column 2, combining the shear forces (100% of the longitudinal direction and 30% of the transverse direction)

→ $100\% \times 5556.7 = 5556.7\,\text{kN}$ and $30\% \times 4378.9 = 1313.7\ \text{kN}$

$\sqrt{(5556.7)^2 + (1313.7)^2} = 5709.9\ \text{kN} < 8545.56\ \text{kN}$ (from Table 4.54)

Therefore, the columns are safe against shear failure under the MCE level.

4.4. Discussion of the results

4.4.1. Flexural deformation

Figure 4.67 and Figure 4.68 shows the maximum plastic hinge rotation in bridge columns in the transverse and longitudinal directions as a percentage of its acceptance criteria for IO.

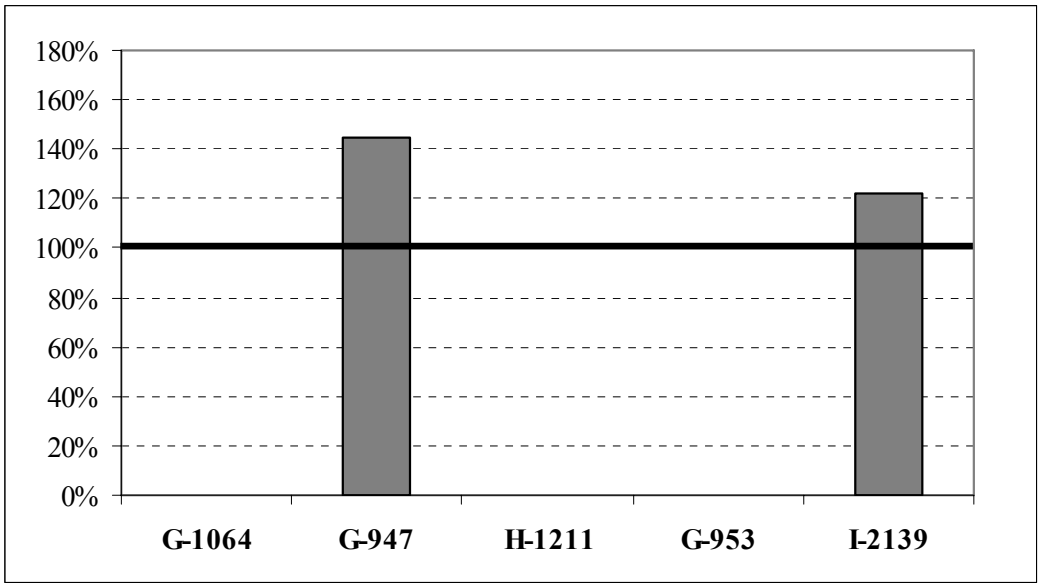

Figure 4.67 Maximum plastic hinge rotation percentage in the transverse direction of the studied bridges

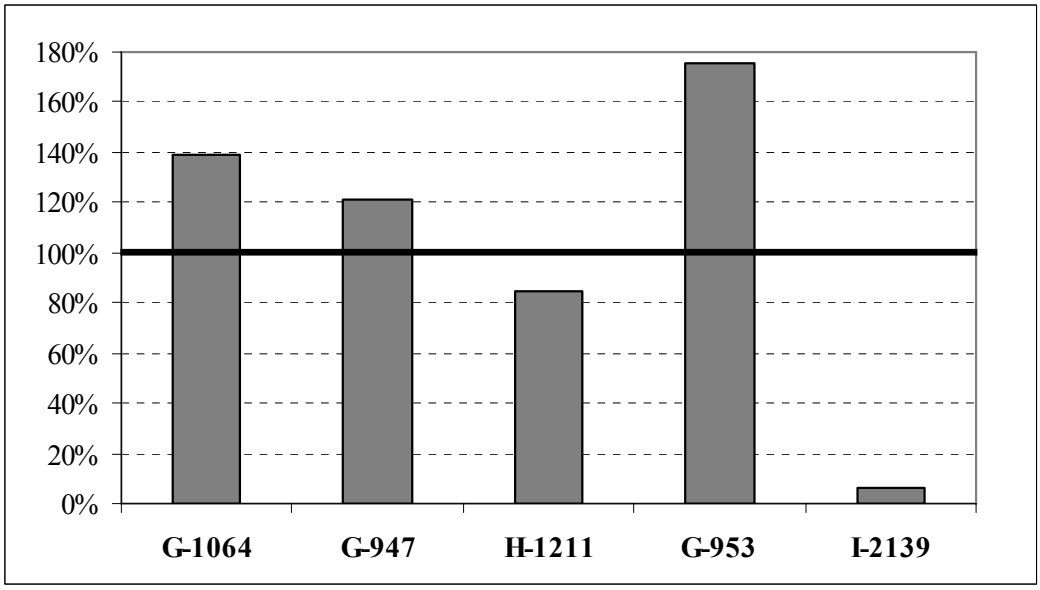

Figure 4.68 Maximum plastic hinge rotation percentage in the longitudinal direction of the studied bridges

The results presented in Figure 4.67 shows that bridges which are restrained by abutments in the two sides (G-1064, H-1211 and G953) did not encounter any plastic deformation in any of their columns in the transverse direction. However, bridges which are considered parts of longer bridges (G-947 and I-2139) encountered extensive plastic hinge rotations that violated the acceptance criteria. These parts of the bridges are not attached to abutments in the two sides, which greatly affected the results compared to other bridges. On the other hand, Figure 4.68 shows that in the longitudinal direction, bridges that were divided into units (to alleviate the thermal expansion overstresses) encountered the highest values of plastic hinge rotations in their columns (Bridges G-1064, G-947 and G-953). Nonetheless, bridges that are not divided into units had better structural integrity and accordingly better performance in the longitudinal direction (e.g. H-1211).

4.4.2. Shear forces

Figure 4.69 shows the percentage of the maximum shear forces in the columns at the target displacements to their shear capacities. The maximum shear force indicated represents the direction with the most critical case (transverse or longitudinal) or by combining the two directions as prescribed in the FEMA-356 (2000) in case of circular columns.

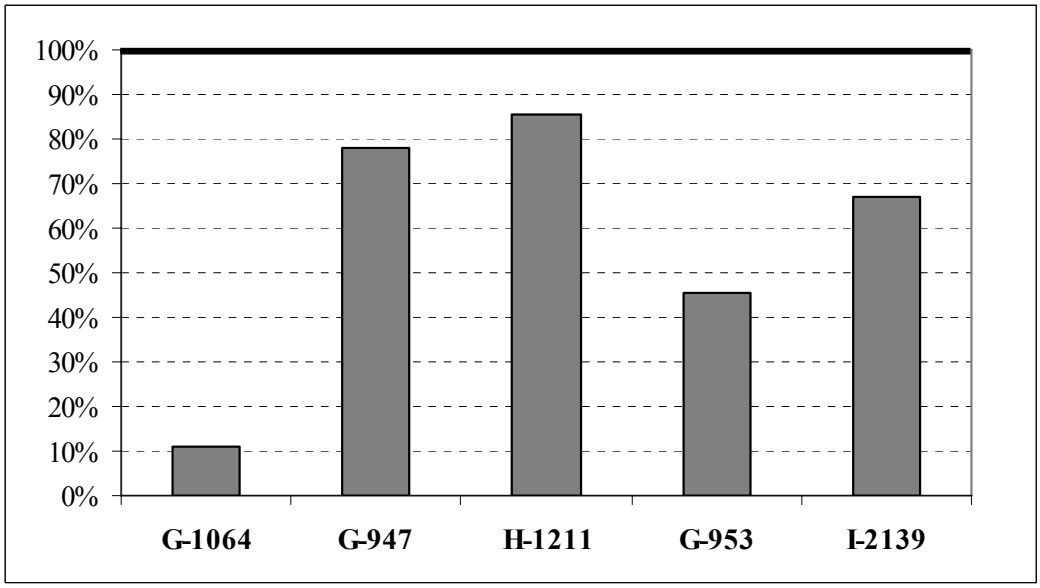

Figure 4.69 Maximum shear force in bridge columns as a percentage of the shear capacity

For the bridges evaluated in this study, shear results in Figure 4.69 demonstrate that the risk of shear failure in the columns due to earthquake loads is low compared to other aspects. And for these bridges, older codes provisions for column shear capacity were sufficient to prevent a shear brittle failure under the MCE level.

4.4.3. Inadequate reinforcement development

Figure 4.70 and Figure 4.71 shows the percentage of the maximum plastic hinge rotation (defined by the inadequate development length of columns longitudinal reinforcement) formed in columns of each bridge in the transverse and longitudinal directions, respectively. Each of the percentages in the tables is related to its acceptance criteria of the IO performance level, which has a value of 0.005 radians for all bridge columns in this study.

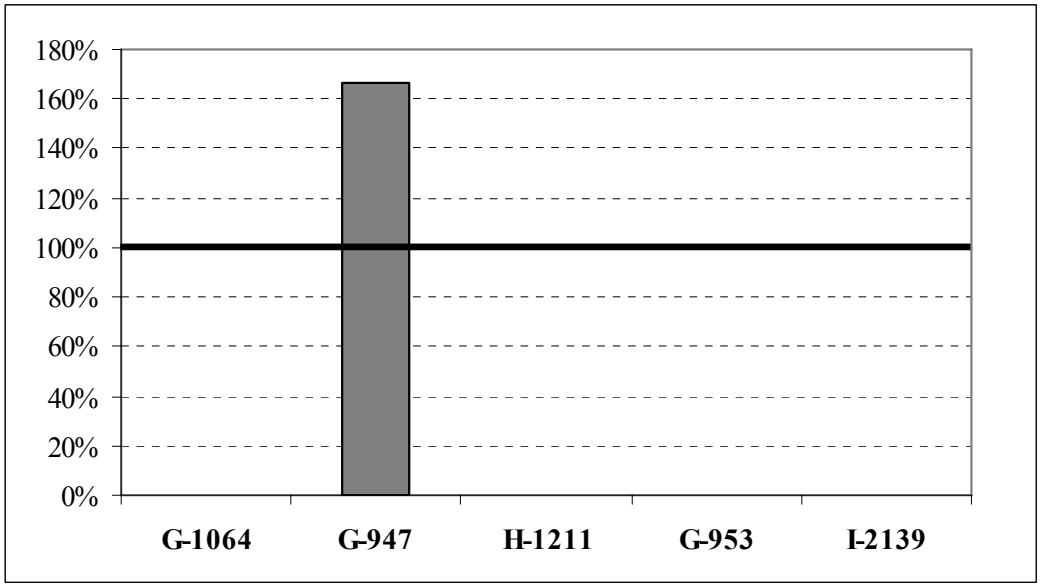

Figure 4.70 Maximum plastic hinge rotation percentage (defined by inadequate development lengths) in the transverse direction of the studied bridges

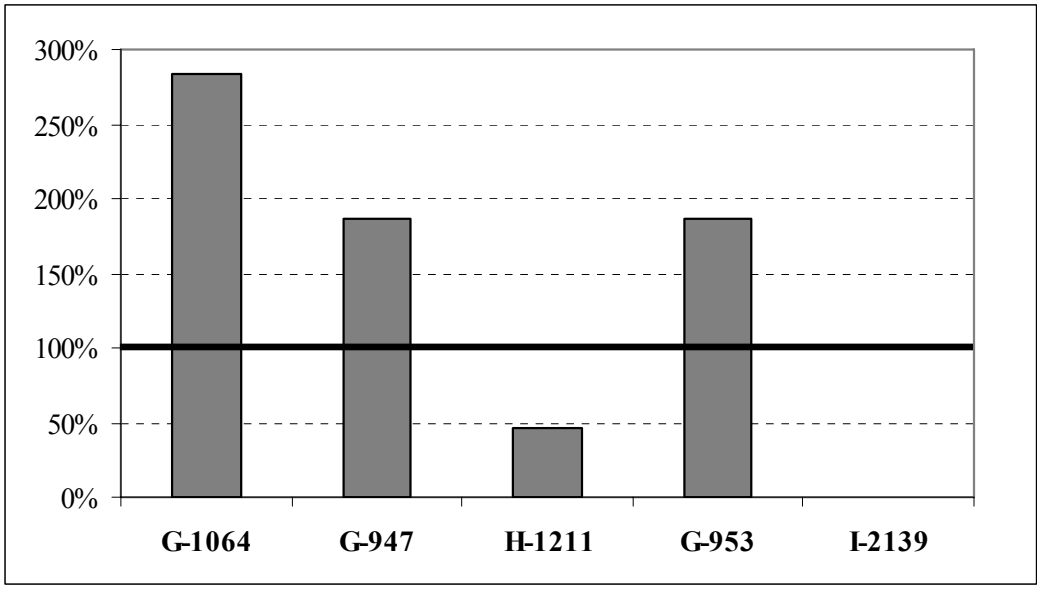

Figure 4.71 Maximum plastic hinge rotation percentage (defined by inadequate development lengths) in the longitudinal direction of the studied bridges

Only bridge I-2139 had its columns reinforcement development in all locations conforming to the current codes provisions. Bridges H-1211 had inadequate development lengths. Despite this fact, at the target displacement, none of the plastic hinge rotations violated the acceptance criteria of the IO performance level. However, Bridges G-1064, G-947 and G-953 had inadequate longitudinal reinforcement development lengths with their plastic hinge rotations violating the acceptance criteria. This violation may put the bridge columns reinforcement at the risk of bond slippage under earthquake loads.

CHAPTER 5

SUMMARY AND CONCLUSIONS

5.1. Summary

A nonlinear static procedure (NSP) was implemented in this study to evaluate five of the most critical bridges in Clark County. These five bridges were chosen out of the 20 bridges that had the highest risk scores which combine both importance and vulnerability scores. The evaluation focused on the performance of the bridge columns in three aspects: (1) flexural deformation; (2) shear forces; and (3) development lengths of the columns' longitudinal reinforcement.

The approach used in this study was introduced by FEMA-356 (2000) for the seismic evaluation of buildings and was evaluated by AlAyed (2002) to be applicable for bridges. It is recognized as the Displacement Coefficient Method (DCM). This approach uses the pushover analysis and a modified version of the equal displacement approximation to estimate the target displacement, which represent the maximum displacement expected by the structure under the given level of earthquake. The three aforementioned aspects were evaluated for all bridge columns at their target displacement.

The earthquake level used for the evaluation is the Maximum Considered Earthquake (MCE). Two different load patterns were used in the analysis in the two horizontal directions of the bridges. The acceptance criteria in this study were set to be the immediate occupancy (IO) performance level. This is because of the high importance of these bridges; this performance level requires full access to normal traffic immediately

following earthquakes events. The computer program SAP2000 nonlinear with bridge module was used in the evaluation of the bridges.

5.2. Conclusions

The following conclusions were made as a result of the work that was completed in this study:

1- The Displacement Coefficient Method (DCM) is a logical method used for evaluation of bridges. It requires reasonable computational efforts compared to other NSP's that involve iterations in their steps.

2- Using different load patterns in bridge seismic analysis, as prescribed by FEMA-356 (2000) for buildings, is an important tool that gives, in certain cases (as in bridge G-947 in this study), different results for different parameters (plastic hinge rotations, shear forces, etc.). Accordingly, it increases the confidence of the results.

3- For flexural deformation and inadequate development length of the columns' longitudinal reinforcement, most of the bridges violated the acceptance criteria in one or more of the analysis cases. This implies that these bridges would not be fully operational after major earthquake events. Thus, they should be considered in rehabilitation plans that include and address deficiencies in the plastic hinge regions in addition to the locations of the reinforcement development and splices.

4- Columns' shear capacities of the five evaluated bridges in this study were sufficient to prevent brittle shear failure of columns under the considered level

of earthquake, even though they were designed and constructed according to older codes.

5- In the transverse direction, short bridges (with abutments considered in the analysis) performed considerably better than long bridges (divided into units) where the abutments had no contribution to the transverse stiffness of the analyzed unit. Thus, it is recommended that special precautions should be taken in the design phase of bents and piers away from the abutments in long bridges.

5.3. Recommendations for future research

The following areas are recommended for future study or additional research:

1- This study was based on the "As Built" structural drawings (blue-prints) for bridges designed and constructed decades ago. An on-site assessment for the bridge different components may increase the confidence in the parameters used in the analysis. This may include non-destructive tests for the concrete elements to obtain the actual compressive strength, evaluation of the longitudinal and transverse reinforcement bars, evaluation of the structural fills used at the abutments to be included in the models in more detail, taking soil-structure interaction into account in modeling the column bases and evaluation of the elastomeric bearings to consider their stiffnesses in the bridge models.

2- Experimental verification of the performance levels and the acceptance criteria given by FEMA-356 (2000) should be done to increase the confidence level in implementing them on bridges.

BIBLIOGRAPHY

AASHTO (2007). "*LRDF Bridge design specifications*" American Association of State Highway and Transportation Officials Inc., Washington, DC.

ACI committee 318, (2008). "*Building code requirement for structural concrete and commentary (ACI 318-08).*" American Concrete Institute, Farmington Hills, MI.

AlAyed, H., (2002). "*Seismic analysis of bridges using nonlinear static procedure*". PhD dissertation, Department of Civil and Environmental Engineering, University of Maryland, College Park, Maryland.

Applied Technology Council (ATC), (1996). "*Seismic evaluation and retrofit of concrete buildings*". Rep. No. SSC 96-01: ATC-40, Redwood City, CA.

Barron, R., (2000). "*Spectral evaluation of seismic fragility of structures*", PhD dissertation, Department of Civil, Structural and Environmental Engineering, State University of New York at Buffalo, Buffalo.

Bentz, E. C., (2000). "*Sectional analysis of reinforced concrete members*". PhD dissertation, Department of Civil Engineering, University of Toronto, Toronto.

Bentz, E. C., Collins, M. P., (2000). "*Response-2000*". Software program for load-deformation response of reinforced concrete sections, http://www.ecf.utoronto.ca/~bentz/inter4/ inter4.shtml

Bracci, J.M., Kunnath, S.K., and Reinhorn, A.M., (1997). "*Seismic performance and retrofit evaluation of RC structures*", ASCE Journal of Structural Engineering, Vol. 123, No. 1, pp. 3-10.

Buckle, I. G., and Friedland, I, M., (1995). "*Seismic retrofitting manual for highway bridges*", (Rep. No. FHWA-RD-94-052), Federal Highway Administration. McLean, Virginia.

Buckle, I. G., Mayes, R. L., and Button, M. R., (1987). "*Seismic design and retrofit manual for highway bridges*", (Rep. No. FHWA-IP-87-6), Federal Highway Administration, McLean, Virginia.

California Department of Transportation (Caltrans), (1999). "*Seismic design methodology*", Memo to designers 20-1, CA.

California Department of Transportation's (Caltrans) Seismic Advisory Board, (2003). "*The Race to Seismic Safety: Protecting California's Transportation System*", CA. http://i80.dot.ca.gov/RaceToSeismicSafetyfinal.pdf.

Chen, W-F., and Duan, L., (2003). "*Bridge engineering seismic design*", CRC Press, Florida.

Chopra, A. K. and Goel, R. K., (2000). "*Evaluation of NSP to estimate seismic deformation: SDF systems*", Journal of Structural Engineering, ASCE 126(4), 482-490.

Chopra, A. K. and Goel, R. K., (2001). "*A Modal Pushover Analysis Procedure to Estimate Seismic Demands for Building: Theory and Preliminary Evaluation*". Tech. Rep. 2001/3, Pacific Earthquake Engineering Research Center, of University of California, Berkeley, CA.

Chopra, A.K., (2007). "*Dynamics of structures: Theory and applications to earthquake engineering*", Third Edition, New Jersey: Prentice Hall.

Chopra, A.K. and Goel, R.K. and Chintanapakdee, C., (2001). "*Statistics of SDF-system estimate of roof displacement for pushover analysis of buildings*". Tech. Rep. 2001/16, Pacific Earthquake Engineering Research Center, of University of California, Berkeley, CA.

City of Los Angeles (COLA), (1995). "*Earthquake hazard reduction in existing reinforced concrete frame buildings with masonry infills*", Tech. Report, Los Angeles.

CSI (2000). SAP2000 Nonlinear Version 11.0.2 with bridge module, Computers and Structures, Inc., Berkelely, CA.

Dutta, A., (1999). "*On energy based seismic analysis and design of highway bridges*". PhD dissertation, Department of Civil, Structural and Environmental Engineering, State University of New York at Buffalo, Buffalo.

Ebrahimpour, A., Porter, D.B., Sack, R.L., and Luke, B., (2007). "*Seismic Risk Assessment of Highway Bridges in Clark County, Nevada*". Proc., Symposium on the Application of Geophysics to Engineering and Environmental Problems, April 1-5, 2007, Denver, CO.

Elnashai, A.S., (2001). "*Advanced inelastic (pushover) analysis for Earthquake applications*". Journal of Structural Engineering and Mechanics in Korea 12(1), 51-69

Fajfar, P., (2000). "*A Nonlinear Analysis Method for Performance-Based Seismic Design*". Earthquake spectra, 16, 573-592.

Federal Emergency Management Agency (FEMA) (1997). "*NEHRP Commentary on the Guidelines for the Seismic Rehabilitation of Buildings*". FEMA-274, Washington, D.C.

Federal Emergency Management Agency (FEMA) (1997). "*NEHRP Guidelines for the Seismic Rehabilitation of Buildings*". FEMA-273, Washington, D.C.

Federal Emergency Management Agency (FEMA) (2000). "*Prestandard and Commentary for the Seismic Rehabilitation of Buildings*". FEMA-356, Washington, D.C.

Federal Highway Administration (FHWA) (1996). "*Seismic Design of Bridges: Design Example No. 4- three-Span Continuous CIP Concrete Bridge*". Publ. No. FHWA-SA-97-009, Springfield, VA.

Fenves, G. L., and Ellery, M., (1998). "*Behavior and failure analysis of a multiple-frame highway bridge in the 1994 Northridge earthquake*". Tech. Report, Pacific Earthquake Engineering Research center, University of California, Berkeley, CA.

Floren, A. and Mohammadi, J., (2001). "*Performance-based design approach in seismic analysis of bridges*". Journal of Bridge Engineering, ASCE 6(1).37-45.

Freeman, S. A., (1978). "*Prediction of response of concrete buildings to severe earthquake motion*". Publ. SP-55, American Concrete Institute. Detroit, 589-605.

Freeman, S. A., Nicoletti, J. P., and Tyrell, J. V., (1975). "*Evaluations of existing buildings for seismic risk - A case study of Puget Sound Naval Shipyard, Bremerton, Washington*". Proceedings of the U.S. National. Conference on earthquake engineering, Berkeley, CA.

Fu, C. and AlAyed, H., (2003). "*Seismic analysis of bridges using Displacement-based Approach*". (03-3175) Transportation Research Board Annual Meeting, January 12-16, Washington, D.C.

Ghobarah, A., (2001), "*Performance based design in earthquake engineering: State of development*". Engineering Structures, Vol. 23, No. 8, pp. 878-884.

Ghobarah, A., Abou-Elfath, H., and Biddah, A., (1999), "*Response-based damage assessment of structures*", Earthquake Engineering & Structural Dynamics, Vol. 28, No. 1, pp. 79-104.

Hwang, H. H. M. and Huo, J., (1998). "*Modeling uncertainty on seismic fragility of structures*". Structural safety and reliability, pp.1721-1724.

Keller, J. R., (2005). "*Seismic vulnerability assessment of essential structures in Clark County, Nevada*". Msc Thesis, Department of Civil Engineering, Idaho State University, Idaho.

Keller, J.R., Ebrahimpour, A., Sack, R.L., and Luke, B.A., (2006) "*The Seismic Vulnerability of Critical Public Buildings in Clark County, Nevada*". Proc., Symposium on the Application of Geophysics to Engineering and Environmental Problems, April 2-6, 2006, Seattle, WA.

Mehta, S., (1999). "*Seismic analysis options for steel truss bridges*". Modern Steel Construction, March 1999.

Nevada Department of Transportation (NDOT) (2007), Personal communications with NDOT.

Porter, D. B., (2006). "*Seismic risk assessment of bridges in Clark County, Nevada*". Msc Thesis, Department of Civil Engineering, Idaho State University, Idaho.

Priestly, M. J. N. and Seible, F., (1991). "*Retrofitting. G. M. Calvi and M. J. N. Preistly*". Proceedings, International Workshop on Seismic Design and Retrofitting of Reinfoced Concrete Bridges, (pp. 529-568). Bormio.

Priestly, M. J. N. and Seible, F., (1994). "*Seismic Assessment of Existing bridges*". Proceedings. 2nd International Workshop on the Seismic Design and Retrofitting of R.C. Bridges, (pp. 46-70). Queenstown, New Zealand.

Priestly, M. J. N., Seible, F., and Calvi, G. M., (1996). *Seismic design and retrofit of bridges.* New York: John Wiley & Sons.

Sack, R.L., Luke, B.A., Ebrahimpour, A., and Keller, J.R., (2006) "Seismic Risk Assessment of Essential Buildings in Clark County, Nevada." Proc., 8th U.S. National Conference on Earthquake Engineering, April 18-22, 2006, San Francisco, CA.

Saiidi, M.S., (1997) "*Working group on bridge design issues*". Conclusions and Recommendations of the Workshop on Seismic Design Methodologies for the Next Generation of codes, Bled, Slovenia.

Sanders, D.H., Douglas, B.M., Martin, T.L., (1993). "*Seismic Retrofit Prioritization of Nevada Bridges" (Report # CCEER-93-3).* Nevada Department of Transportation, Carson City, Nevada.

Shinozuka, M., Feng, M.Q., Kim, H., and Kim, S., (2000) "*Nonlinear static procedure for fragility curve development*" Journal of Structural Engineering, ASCE 126(12), 1287-1295.

Slemmons, D. B.; Bell, J. W., Depolo, C. M.; Ramelli, A. R.; Rasmussen, G. S.; Langenheim, V. E.; Jachens, R. C.; Smith, K.; and O'donnell, J., (2001). "*Earthquake hazard in Las Vegas, Nevada*". Luke, B.; Jacobson, E.; and Werle, J. (Editors), Proceedings of the 36th Engineering Geology and Geotechnical Engineering Symposium, pp. 447–457.

Structural Engineers Association of California (SEAOC), (1995). "*Performance based seismic engineering of buildings – volume I*". Sacramento, CA.

United States Geological Survey (USGS) (2009), *USGS National seismic hazard mapping project*, http://earthquake.usgs.gov/research/hazmaps/pdfs/.

Whittaker, A., Constantinou, M., Tsopelas, P., (1998). "*Displacement estimates for performance-based seismic design*", Journal of Structural Engineering, ASCE 124(8), 905-912.

VITA

Graduate College
University of Nevada, Las Vegas

Ahmad Said Saad

Address:
5400 S. Maryland pkwy, Apt. 110
Las Vegas, Nevada 89119

Degrees:
Bachelor of Civil Engineering, Structural Department, 2004
Ain Shams University, Cairo, Egypt

Master of Science in Engineering, Department of Civil and Environmental Engineering, 2009
University of Nevada, Las Vegas

Publications:
Overview of Progressive Collapse Analysis and Retrofit Techniques.

Comparison of Different Standards for Progressive Collapse Evaluation Procedures at Various Seismic Conditions.

Thesis Title: Seismic Evaluation of Clark County Critical Bridges Using Nonlinear Static Procedures

Thesis Examination Committee:
Chairperson, Aly Said, Ph.D.
Committee Member, Barbara Luke, Ph.D. P.E.
Committee Member, Samaan Ladkany, Ph.D.
Committee Member, Ying Tian, Ph.D.
Graduate Faculty Representative, Wanda Taylor, Ph.D.